Decoding Cobalt's Influence: An Analysis of Environmental Impacts in the Production of NMC Cathode Active Materials for Lithium-Ion Batteries

Master Thesis: Advance Materials Innovative Recycling (AMIR)

Name	Arooba Nazneen	Matrikel Nr. 2848545
Supervisor	Prof. Dr. Anke Weidenkaff	
External Supervisor:	Prof. Dr. Guido Sonnemann	

Arooba Nazneen
Matriculation Number: 2848545
Master Program: Advanced Materials Innovative Recycling

Master Thesis Topic
“Decoding Cobalt’s Influence: An Analysis of Environmental Impacts in the Production of NMC Cathode Active Materials for Lithium-Ion Batteries**”**

Submission Date: 13 March 2025

Supervisor
Prof. Dr. Anke Weidenkaff
Head of the Materials and Resources Group
Department of Materials Science
Professor at Technical University of Darmstadt, Germany

External Supervisor
Prof. Dr. Guido Sonnemann
Head of The Life Cycle Group (CyVi)
Institute of Molecular Sciences (ISM)
Full Professor at University of Bordeaux, France

Erklarung zur Abschlussarbeit gemaß § 22 Abs. 7 APB TU Darmstadt

Hiermit erkläre ich, Vorname Nachname, dass ich die vorliegende Arbeit gemäß § 22 Abs. 7 APB TU Darmstadt selbstständig, ohne Hilfe Dritter und nur mit den angegebenen Quellen und Hilfsmitteln angefertigt habe. Ich habe mit Ausnahme der zitierten Literatur und anderer in der Arbeit genannter Quellen keine fremden Hilfsmittel benutzt. Die von mir bei der Anfertigung dieser wissenschaftlichen Arbeit wörtlich oder inhaltlich benutzte Literatur und alle anderen Quellen habe ich im Text deutlich gekennzeichnet und gesondert aufgeführt. Dies gilt auch für Quellen oder Hilfsmittel aus dem Internet.
Diese Arbeit hat in gleicher oder ähnlicher Form noch keiner Prüfungsbehörde vorgelegen.
Mir ist bekannt, dass im Falle eines Plagiats (§38 Abs.2 APB) ein Täuschungsversuch vorliegt, der dazu führt, dass die Arbeit mit 5,0 bewertet und damit ein Prüfungsversuch verbraucht wird. Abschlussarbeiten dürfen nur einmal wiederholt werden.
Bei einer Thesis des Fachbereichs Architektur entspricht die eingereichte elektronische Fassung dem vorgestellten Modell und den vorgelegten Plänen.

English translation for information purposes only:

Thesis Statement pursuant to § 22 paragraph 7 of APB TU Darmstadt
I herewith formally declare that I, Arooba Nazneen, have written the submitted thesis independently pursuant to § 22 paragraph 7 of APB TU Darmstadt without any outside support and using only the quoted literature and other sources. I did not use any outside support except for the quoted literature and other sources mentioned in the paper. I have clearly marked and separately listed in the text the literature used literally or in terms of content and all other sources I used for the preparation of this academic work. This also applies to sources or aids from the Internet.
This thesis has not been handed in or published before in the same or similar form.
I am aware, that in case of an attempt at deception based on plagiarism (§38 Abs. 2 APB), the thesis would be graded with 5,0 and counted as one failed examination attempt. The thesis may only be repeated once.
For a thesis of the Department of Architecture, the submitted electronic version corresponds to the presented model and the submitted architectural plans.

13 March 2025 Arooba

Datum / Date: Unterschrift/Signature:

Abstract

The increased use of lithium-ion batteries has raised concerns about the sustainability of their usage, prompting the need for an environmental assessment. This study evaluates and compares the environmental impacts of NMC 111 and NMC 811 cathode active materials (CAMs) using Life Cycle Assessment (LCA). To improve the accuracy of the assessment, process simulation with HSC Chemistry was employed to model the production of cobalt sulfate ($CoSO_4$), a key precursor for NMC cathodes. llllllllllllllllllllllllllllllllllllllllllllllllllllllllllllllllllllllllllllll

Using the simulated process data, a custom Life Cycle Inventory (LCI) was generated and the environmental impacts of $CoSO_4$ production were assessed using the ReCiPe 2016, midpoint impact assessment method in OpenLCA were. This custom cobalt sulphate dataset is integrated into the Ecoinvent database by replacing the default CoSO4 input in NMC 111 and NMC 811 inventories, allowing for a comparative LCA of both chemistries

The results indicate that the modelled cobalt sulfate production route has a lower environmental impact than reported literature values, with a GWP of 12.1 kg CO_2-eq per kg of $CoSO_4$. The majority of emissions and resource use were found to stem from extraction and early processing stages, rather than final refining. When applied to NMC 111 and NMC 811, the results highlight key trade-offs: NMC 111 exhibits a higher GWP (22.4 kg CO_2-eq/kg) due to its greater cobalt content, while NMC 811, with lower cobalt dependency, has a slightly reduced footprint (21.8 kg CO_2-eq/kg). However, the increased nickel content in NMC 811 introduces additional environmental burdens, emphasizing the need for a balanced assessment when selecting cathode chemistries.

List of Figures

List of Tables

List of Abbreviations

BTU - British Thermal Units
CAM - Cathode Active Material
CCD - Counter-Current Decantation
CML - Centrum voor Milieuwetenschappen Leiden
DRC - Democratic Republic of Congo
EF - Environmental Footprint
EU - European Commission
EV – Electric Vehicle
FPMF - Fine Particulate Matter Formation
GWP - Global Warming Potential
GREET- Greenhouse gases, Regulated Emissions, and Energy use in Technologies
HCT- Human Carcinogenic Toxicity
HNCT- Human Non-Carcinogenic Toxicity
HPAL - High-Pressure Acid Leaching
LCA - Life Cycle Assessment
LCI - Life Cycle Inventory
LCIA - Life Cycle Impact Assessment
LFP - Lithium Iron Phosphate
LIB - Lithium-Ion Batteries
LME -London Metal Exchange
NCA - Nickel Cobalt Aluminium
NMC - Nickel Manganese Cobalt
PGE - Platinum-Group Elements
PGM - Platinum Group Metals
SAG - Semi-Autogenous Ginding
SX - Solvent Extraction
SIPX - Sodium Isopropyl Xanthate

1 Introduction

There is an energy transition phenomenon taking place worldwide. Most countries are shifting from non-renewable energy sources to renewable energy sources. The ('Paris Agreement', 2016) plays a major role in this trend. It focuses on the "need to limit global warming to 1.5°C by the end of this century." (*The Paris Agreement | UNFCCC*) To achieve this goal, the EU aims to be carbon neutral by 2050. While Germany's goal is to be carbon neutral by 2045. Carbon neutrality requires big changes in the infrastructure of current technology, especially in the energy and transport sector.

The energy sector was responsible for 42% of global CO_2 emissions in 2022 in Germany (*Emissions Factors 2023 - Data product*). Hence, there is a strong need to make developments in the storage of energy to make it carbon neutral. Currently, the primary renewable energy sources are wind, solar, and hydropower, and their share in the energy mix is steadily increasing. However, these sources are not capable of providing a constant voltage to the grid, as they are heavily influenced by weather conditions and other external factors. As a result, energy storage systems are crucial to store excess energy and provide a steady supply, helping to mitigate fluctuations in energy generation and ensure a stable energy grid.

1.1 Role of LIBs in Energy Transition

Different types of energy storage systems include batteries, hydrogen storage mechanisms such as metal hydrides, liquefied hydrogen, and ammonia, metal fuels, supercapacitors, and molten salts for thermal energy storage. Batteries are one of the most used and reliable energy storage systems worldwide. The first battery was invented by Alessandro Volta in 1799 which incorporated different metals separated by paper soaked in a saline solution ('Volta et al.1800). In 1866, Georges-Lionel Leclanché, introduced a battery design using a zinc rod as the anode (negative electrode) and a cathode (positive electrode) made of a mixture of manganese oxide and carbon (Kordesch and Taucher-Mautner, 2009). Gaston Planté invented the first rechargeable lead-acid battery in 1859. In 1901, Swedish engineer Waldmar Jungner developed the rechargeable nickel-cadmium (Ni-Cd) battery, offering a new way to store electrical energy with improved durability and rechargeability.

Initially different types of Li ions batteries were developed using uncommon cathode materials. In the 1970's, they were commercialized as coin cell batteries with manganese dioxide as the cathode to fit into small electronics (Scrosati, Hassoun and Sun, 2011). The first commercial rechargeable lithium batteries were produced by Exxon in the late 1970's, featuring a titanium disulfide (TiS_2) cathode and by Moli Energy in early 1980's which used a molybdenum disulfide (MoS_2) cathode. Both designs employed liquid organic electrolytes to facilitate lithium-ion transfer. In 1991, SONY developed the first Li ion battery in which graphite was the anode and lithium cobalt oxide was the cathode. LiCoO2 was first introduced by Goodenough in 1980 as a cathode material (Mizushima *et al.*, 1980). It was capable of releasing lithium ions during the discharge phase and to reabsorb them during recharging. This reversible movement of ions ensured the ongoing electrochemical reactions necessary for the battery's operation. In the 1990's this cathode chemistry became the standard for consumer electronics due to its high energy density. However, the $LiCoO_2$ battery faced significant drawbacks such as relatively limited cycle life, high costs due to cobalt scarcity, and thermal instability. These limitations drove the development of alternative chemistries such as lithium iron phosphate (LFP), nickel manganese cobalt oxide (NMC) and lithium nickel cobalt aluminum oxide (NCA).

Initially, the LFP gained attention due to its superior thermal stability, longer cycle life, and lower cost, albeit with lower energy density. Later Nickel-based chemistries such as NMC and NCA became dominant, offering higher energy densities, improved power performance, and customizable compositions to balance cost and performance. This evolution made these chemistries especially suitable for applications like electric vehicles (EVs) and grid storage, shifting focus away from $LiCoO_2$ (Rawat *et al.*, 2025). However, LFPs have made a comeback in the market recently because of their lower cost, stability, and safety.

NMC batteries dominate the EV market due to their superior energy density, long lifespan, and enhanced safety, resulting in high-range EVs. (Myung *et al.*, 2017). Initially formulated as NMC-111, research has led to more nickel-rich variants like NMC-532, NMC-622, and NMC-811. These newer chemistries reduce cobalt content, offering higher capacity and lower costs but at the expense of thermal stability and lifespan (Greenwood, Wentker and Leker, 2021). Cobalt is an important component of Li-ion batteries due to its use in NMC batteries, making it an important metal in the energy transition sector. However, there are also significant challenges associated with the use of cobalt, including the environmental and social impact of mining, concerns about supply chain security, and the potential for price volatility as demand for the metal increases.

Thus, lithium-ion batteries, known for their high-capacity storage, are crucial for the energy transition. While currently used in electric vehicles, laptops, and mobile phones, their potential extends to large-scale energy storage. There are numerous Li-ion gigafactory projects for harnessing renewable energy during peak production periods (Fusiek, 2023). This shift highlights the growing importance of lithium-ion batteries in both transportation and energy infrastructure.

1.1.1 Metal Criticality in Lithium-Ion Batteries

Most of the metals used in LIBs are classified as critical materials. Critical materials play a vital role in the economy but face a high supply risk. The European Union (EU) has identified several materials as critical raw materials based on their supply risk and economic significance. Figure 1 presents a graph adapted from the (Blengini *et al.*, 2020), illustrating various critical materials plotted against these two factors. Among them, cobalt and lithium are classified as critical raw materials due to their high supply risk and economic importance. However, the EU's updated 2023 list of CRMs includes copper, nickel and manganese as strategic raw materials, highlighting their economic importance and potential supply risk (*Critical raw materials - European Commission*).

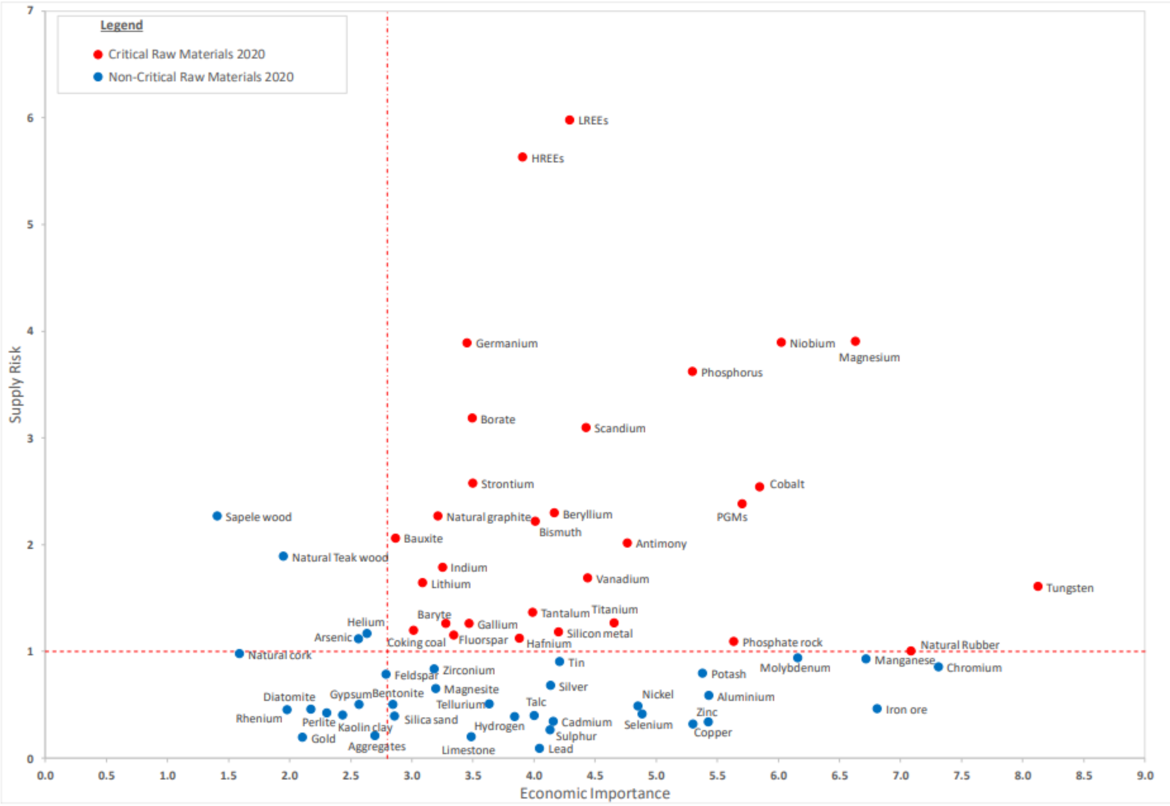

Figure 1: Graph of critical raw materials plotted against supply risk and economic importance reproduced from the European Commission (Blengini *et al.*, 2020)

Cobalt is deemed critical due to its supply chain risks. As a by-product, its availability depends on the economic viability of primary metals, making it scarcer and costlier. Moreover, ethical and political challenges arise from artisanal mining in the Democratic Republic of Congo, where political instability further hampers business and investment (Kapusta, 2006). Artisanal mining in the DRC accounts for 15–30% of cobalt extraction and is often linked to unethical practices, including child labour and unsafe working conditions. Reports by Amnesty International highlight human rights violations in the Katanga region, and the Centre for Research on Multinational Corporations (SOMO) estimates that up to 40,000 children work in underground tunnels without proper safeguards (Gaughran, 2013; Kiezebrink & ten Kate, 2016).

Cobalt is a key material in several energy technologies essential for the transition to a cleaner and more sustainable future. It is used in wind turbines to produce superalloys for high-strength magnets that generate electricity and in thin-film solar cells, which offer higher efficiency than traditional silicon-based cells by absorbing a broader light spectrum. It is also crucial in hydrogen fuel cells, serving as a catalyst to accelerate electrochemical reactions and as a cathode component in proton exchange membrane fuel cells, widely used in transportation. Additionally, cobalt is used in permanent magnets for electric vehicle (EV) motors, enhancing torque and efficiency. However, efforts are underway to reduce cobalt dependency by developing alternative magnet materials and incorporating recycled cobalt to mitigate the demand for newly mined resources.

1.2 Life Cycle Assessment and Process Simulation

Life Cycle Assessment (LCA) is a useful tool to determine the environmental impacts of a product, process or service conducted in accordance with the ISO 14040 and ISO 14044 standards (International Organization for Standardization, 2006). It is also used to improve product design and assist decision makers. (Guinee, 2002). Using this method, environmental impacts can be evaluated throughout the different stages of the life cycle of a product. These stages include the production of raw materials, manufacturing, product use, and its end of life (International Organization for Standardization, 2006). Depending upon the goal and scope of the LCA, a Life Cycle Impact Assessment (LCIA) methodology is chosen that defines the impact categories being considered.

LCA has four stages i.e., goal and scope, life cycle inventory analysis (LCI), life cycle impact assessment (LCIA), and interpretation.

Goal and Scope: Defines the objectives, system boundaries, functional units, and data requirements of the LCA. It establishes the study's purpose, intended application, and target audience, ensuring clarity on its scope and focus.

Inventory Analysis: Involves collecting data on material and energy inputs as well as emissions and waste outputs throughout the product's life cycle. The Life Cycle Inventory (LCI) serves as the foundation for evaluating environmental impacts.

Impact Assessment: This phase processes inventory data to quantify potential environmental impacts across various categories, such as climate change, resource depletion, and toxicity. Different methodologies are used to assess environmental performance, including:

- ReCiPe Method: A comprehensive impact assessment approach that translates environmental data into a wide range of categories, covering climate change, human health, and ecosystem quality. It is distinguished by its dual-level assessment, incorporating both midpoint indicators (specific environmental issues) and endpoint indicators (overall environmental damage) (Huijbregts *et al.*, 2017).
- CML (Centrum voor Milieuwetenschappen Leiden) Method: Developed at Leiden University, this methodology focuses on midpoint categories such as acidification, eutrophication, and ozone layer depletion. Its structured classification and relatively straightforward application make it a widely adopted approach in LCA studies (de Bruijn *et al.*, 2002).
- Environmental Footprint (EF) Method: Established by the European Commission, the EF method provides a robust framework for assessing the environmental impact of products, organizations, and sectors throughout their life cycle. It aligns with key EU sustainability policies, including the European Green Deal and the Circular Economy

Action Plan. Encompassing 16 impact categories, the EF method offers a comprehensive evaluation of environmental effects, covering aspects such as climate change, resource utilization, emissions, and ecosystem degradation (Fazio *et al.*, 2018).

Interpretation: In this final phase, the results are systematically analysed to extract meaningful conclusions and insights. Hotspot identification, uncertainty analysis, and comparative evaluations are conducted to pinpoint key impact areas and potential areas for environmental improvement. The findings inform evidence-based recommendations, facilitating targeted sustainability interventions and strategic decision-making.

Process simulation is a valuable tool for developing comprehensive life cycle inventories (LCIs) within the mineral industry, enhancing data accuracy and consistency by modelling complex production systems (Segura-Salazar, Lima and Tavares, 2019). This method tracks resource flows, emissions, and process dynamics, aiding sustainable practices and environmental assessments. It involves building detailed computer-based models using specialized simulation software, such as HSC Chemistry, to replicate process behaviours, resource usage, and emissions accurately (Metso Outotec). These models provide precise data and insights to improve the environmental and operational performance of mineral industry processes by applying mass and energy balance calculations which allow it to predict how processes will behave under specific conditions. However, variations in real-world conditions can lead to discrepancies in the energy demands of each process step.

Advancements have been made in recent years by combining life cycle assessment (LCA) with process simulation in metal production (Reuter, van Schaik and Gediga, 2015; Rinne, Elomaa and Lundström, 2021, 2023; Mas-Fons *et al.*, 2024). This integration allows for accurate modelling and assessment of environmental impacts throughout the entire production process by combining LCA's environmental analysis with process simulation's detailed operational modelling.

Consistent LCI data remains scarce, making data collection one of the most time-consuming steps. To address this, process simulation, experimental data, and LCA are used in combination, filling in important data gaps for LCA (Morales-Mendoza and Azzaro-Pantel, 2017). Process simulation provides accurate, system-based insights that might be unavailable or difficult to obtain through traditional data collection. This integration enhances LCA accuracy, particularly in complex or novel systems, by offering reliable estimates of process flows. Figure 2, adapted from (Mas-Fons *et al.*, 2024), illustrates the interconnection between data collection, process simulation, and life cycle inventory (LCI) generation. Parameters sourced from reports, industry data, and literature are integrated into process simulation software, where system-specific controls are applied to model real-world operations accurately. This simulation enables the generation of an LCI that reflects the current system’s performance, facilitating a data-driven approach to environmental impact assessment.

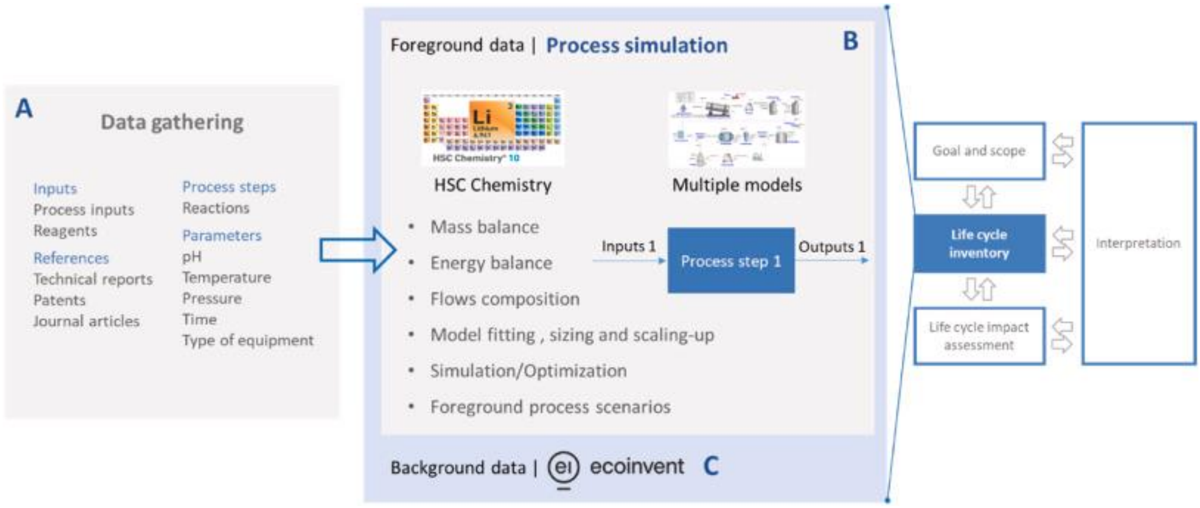

Figure 2: Stages of methodical approach for the Process simulation based LCI reproduced from Mas-Fons et al., (2024)

1.3 Research Objective

As the demand for cobalt rises for use in production of LIBs, understanding and managing its environmental impacts becomes imperative. Cobalt sulphate heptahydrate is precursor used in the production of cathode active material of lithium-ion batteries which has high environmental impacts and supply risks associated with it. Despite region-specific LCI datasets on cobalt sulfate production (Rinne, Elomaa and Lundström, 2021), a comprehensive dataset for assessing environmental impacts across defined production processes and representative sources is missing.

This study aims to perform a comprehensive Life Cycle Assessment of NMC 111 and NMC 811 cathode active material chemistries, utilizing a self-generated cobalt sulfate dataset for enhanced accuracy and reliability. Initially, a literature review of the production processes and available LCI datasets on battery-grade cobalt sulfate is conducted. The objective is to simulate the production process of cobalt sulfate using process simulation. Initially, a representative process flow is defined for the production of battery grade cobalt sulfate. Then, a thorough study of numerous literature sources is done to collect data for this process flow. Reasonable assumptions have been made regarding certain parameters where data was missing. Based on various literature sources that provide information on the identified process flow, battery-grade cobalt sulfate is modelled in HSC Chemistry, a process simulation software. The cobalt sulfate model in HSC Chemistry provides comprehensive data for the LCA of battery grade cobalt sulfate and assists in filling data gaps where consistent information cannot be found in literature sources. Additionally, the custom cobalt sulphate dataset generated via process simulation is used in pre-existing NMC oxide datasets to determine the environmental impacts of lithium-ion battery cathode active material with different concentrations of cobalt in their cathode chemistries. Moreover, the research discusses potential mitigation options, and process optimizations based on relevant literature with the aim of reducing impacts.

2 Literature Review

2.1 Overview of Cobalt

2.1.1 Types of Cobalt Deposits

In most cases, cobalt is either a co-product of mining for other metals such as copper or nickel. Approximately, 68% of the time it is a by-product of copper and the other 38% it is a by-product of nickel. While 2% of the time it is a by-product of other PGMs (Cobalt institute market report, 2022). Cobalt has been categorized according to various types of deposits via information from the cobalt institute (‘Types of Deposits - Cobalt Institute’, 2023).

- **Sediment Hosted:** Sediment Hosted deposits mainly consist of copper and have cobalt as a by-product. They include more than 50% of the world's cobalt-mined production. These deposits are characterized by organic-rich pyritic shales and sandstones. Two of the largest well-known deposits of this type are the European Kupferschiefer and the Central African Copperbelt.

- **Magmatic Nickel Sulphide Deposits:** Nickel, cobalt and platinum-group elements (PGE) are present in the form of sulphur rich layers in this type of deposit. These elements are then extracted from the residual magma. These deposits are found at e.g., Sudbury, Canada, and Norilsk, Russia and comprise a major part of the cobalt extraction, especially for the USA (Bleiwas, 2012).

- **Nickel laterite deposits:** These deposits are more commonly mined for their high nickel concentration where cobalt is a by-product. They are found in tropical regions such as New Caledonia, Western Australia, Indonesia, and South America.

- **Manganese Nodules and Cobalt-rich Crusts:** Cobalt is also found in these deposits, but they are not currently being mined. They are found in proximity to mid-ocean ridges. They are not economically viable yet. Advanced technology in the future may make it possible to mine these deposits.

In 2016, stratiform sediment-hosted Cu-Co deposits accounted for the majority of the world's mined cobalt production (67%) followed by Ni-Co laterite deposits (21%) and magmatic Ni-Cu sulphide deposits (10%), and polymetallic (Ag-Ni-Co-As-Bi) cobalt-rich veins (2%) (van den Brink *et al.*, 2020).

2.1.2 Cobalt Supply Chain and Value Chain

Global cobalt mine production reached approximately 232,000 metric tons in 2023, with the Democratic Republic of Congo (DRC) contributing about 74% of this total (‘Cobalt-Market-

Report-2023'). Refined cobalt production grew by 9% in 2023, totalling 179,000 metric tons, with China producing approximately 140,000 metric tons, accounting for 78.5% of the global refined cobalt supply ('Cobalt-Market-Report-2023'). DRC and China dominate the cobalt industry worldwide. Figure 3 shows the share of countries in cobalt mining and figure 4 shows the share of countries in cobalt refining across the world.

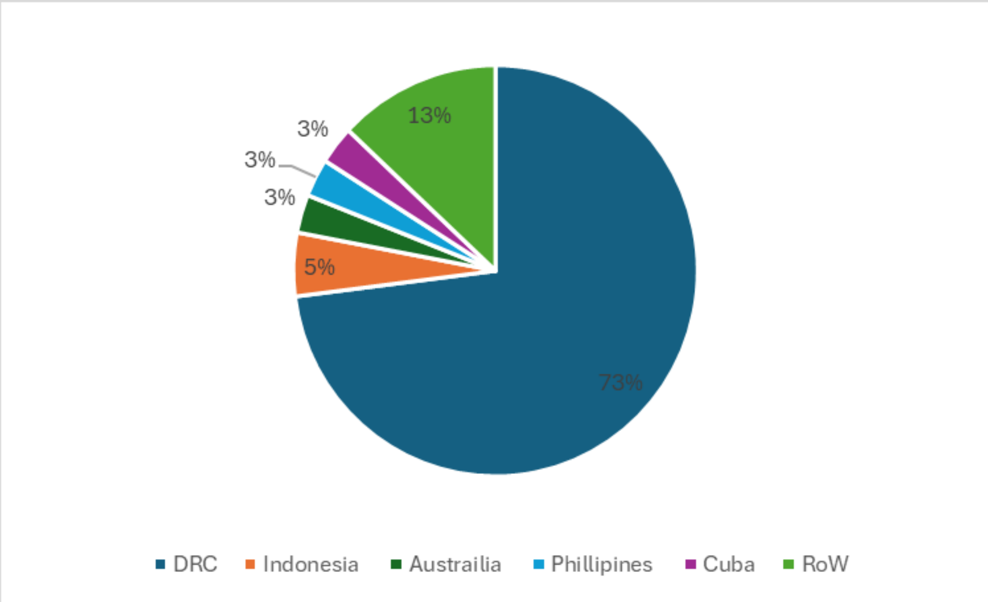

Figure 3: Pie chart showing share of countries in cobalt mining, adapted from Cobalt ('Cobalt-Market-Report-2023', no date)

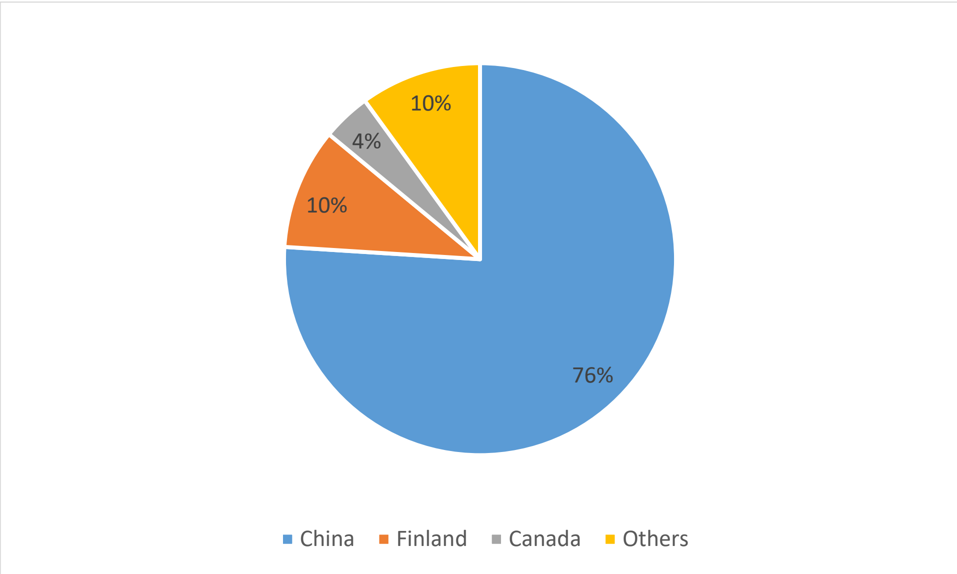

Figure 4: Pie chart showing share of countries in cobalt refining, data from ('Cobalt-Market-Report-2023', no date).

As cobalt is mined as a by-product, after the initial extraction and processing steps which usually occur within the vicinity of the mine site, a cobalt intermediate is usually shipped to another location for the final refining steps. These intermediate compounds usually consist of alliage blanc, crude cobalt hydroxides, mixed sulphide precipitates, mixed hydroxide precipitates, nickel matte, and PGM-cobalt matte. These compounds undergo a refining step to form a variety of commercially available refined cobalt chemicals in the market. Figure 5. illustrates the distribution of refined cobalt forms obtained throughout its value chain. Cobalt sulphate and cobalt tetroxide are both used in the battery industry for the manufacturing of NMC or NCA cathodes. Together they comprise more than fifty percent of the refined cobalt product. While fifteen percent of cobalt is refined to be used in CAMs. Other refined forms of cobalt are used in the chemical industry.

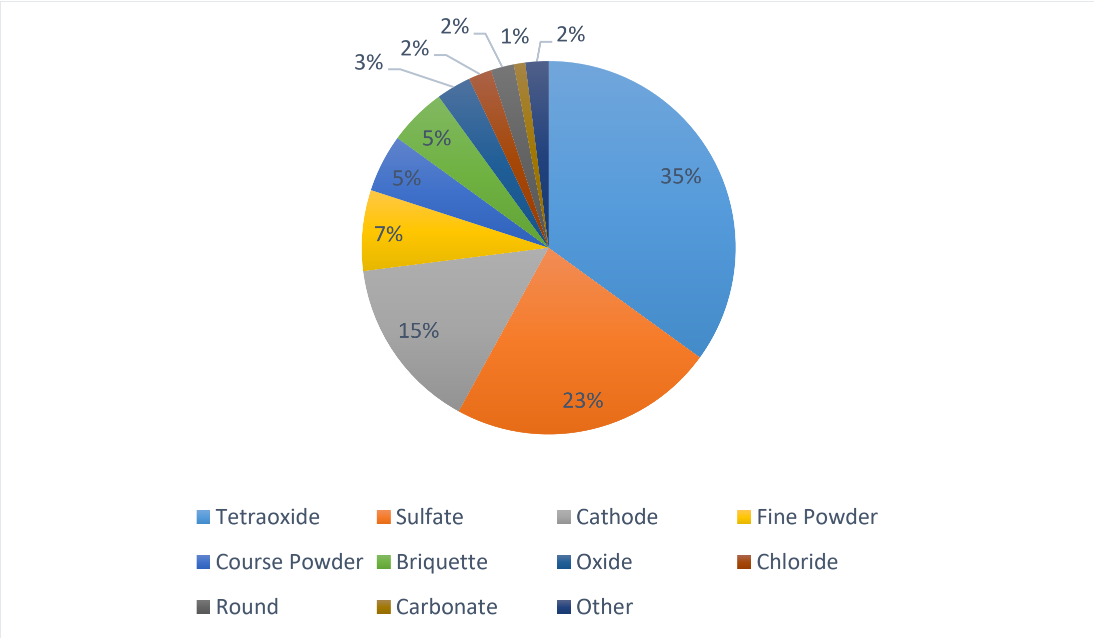

Figure 5: Pie Chart showing the forms of refined cobalt obtained throughout its value chain, data obtained from ('Cobalt Value Chain Mapping | Cobalt Institute', 2022).

Global cobalt production has seen substantial growth, reaching 170 kt/year in 2021. Despite geopolitical and economic challenges, production has consistently increased by more than 5 kt/year since 1994, with forecasts suggesting it could rise to 250 kt/year by 2040 if this trend continues, as shown in Figure 6 (Savinova *et al.*, 2023). The primary driver of this growth is the increasing demand for LIBs, particularly for electric vehicles, as global policies such as the COP26 declaration promote zero-emission transportation. The Glassgow climate pact aim is to have "all sales of new cars and vans being zero emission globally by 2040, and by no later than 2035 in leading markets" (Lennan and Morgera, 2022). Although the cobalt content in EV batteries is expected to decline, the increasing number of EVs and expanding energy storage needs could significantly increase global cobalt consumption. In 2020, the cobalt content in electric vehicle batteries was estimated to range between 130 and 240 g/kWh. However, projections indicate a decline to 30–120 g/kWh by 2030, with some battery technologies already eliminating cobalt entirely (*Electric Vehicle Batteries.Pdf* ; *Mathieu Lucien & Mattea Cecilia*, 2021). Meeting projected EV demand alone would necessitate a 50% boost in current cobalt production, while additional demand from other battery applications could push requirements even higher (Savinova *et al.*, 2023). Another study by (Zeng *et al.*, 2022) states that future cobalt demand could be three to five times greater than EV-related projections based on the increase in a linear trend calculated by (Savinova *et al.*, 2023) shown in Figure 6. According to

(Zeng *et al.*, 2022), advancements in cobalt-free battery technologies and improvements in recycling efforts can substantially mitigate long-term cobalt supply risks. However, despite these developments, a cobalt supply shortage remains unavoidable in the short to medium term (2028–2033), even under the most technologically optimistic scenario.

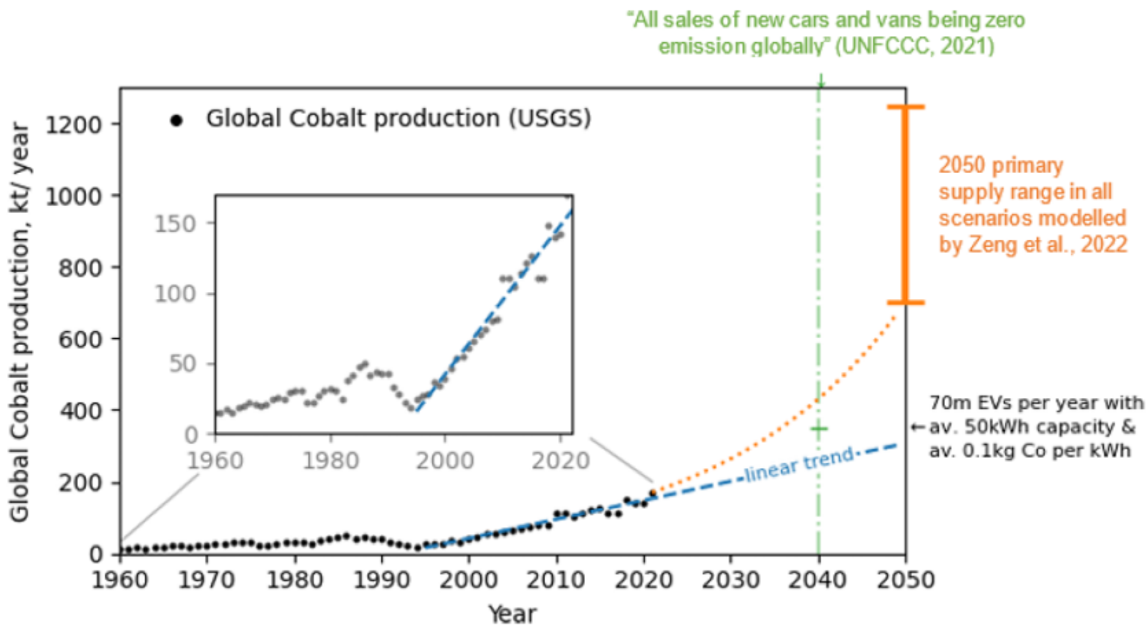

Figure 6: Historical global cobalt production in the context of possible future demand from electric vehicle production, reproduced from (Savinova *et al.*, 2023)

2.2 Global Battery Grade Cobalt Sulphate Production

Depending upon the cobalt ore deposit, ore concentration method and primary metal extraction process, various cobalt intermediates are formed which undergo further refining and finishing processes to form cobalt sulphate heptahydrate as the final product. These can result in various routes or process flows to form cobalt sulphate heptahydrate or battery grade cobalt sulfate. Figure 7, reproduced from the cobalt institute, gives a comprehensive overview of the possible production routes for cobalt sulphate.

Copper cobalt and nickel cobalt ores are processed using different methods depending on their mineral composition. Copper cobalt sulphide ores are typically concentrated and then smelted to extract copper. Alternatively, a sulphatising roast can be employed to convert sulphides into soluble sulphates, which are then leached. Copper cobalt oxide ores, on the other hand, can be directly leached after concentration, eliminating the need for smelting. Nickel cobalt lateritic and sulfidic ores often undergo energy-intensive pyrometallurgical processes such as roasting and smelting. However, nickel cobalt lateritic ores can also be processed using High-Pressure Acid Leaching (HPAL), a hydrometallurgical method that has gained popularity as a more efficient and environmentally friendly alternative.

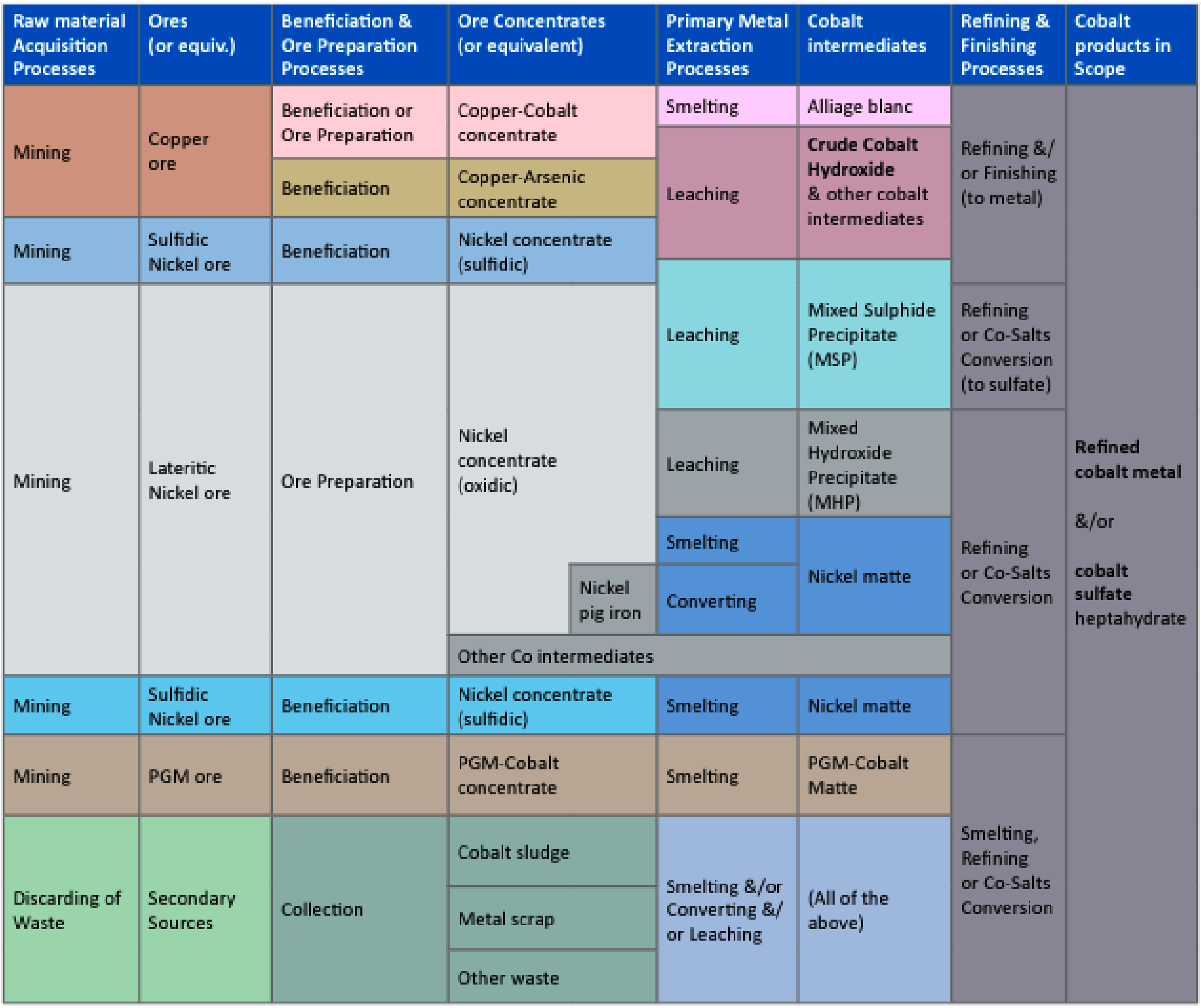

Figure 7: The value chain of cobalt, reproduced from the cobalt institute, cobalt value chain

Battery-grade cobalt sulfate is a high-purity crystalline material essential for lithium-ion battery production. It is crystallized as cobalt sulfate heptahydrate ($CoSO_4.7H2O$). It contains a cobalt content of 21%, with strict limits on impurities such as manganese, iron, nickel, zinc, and copper (Crundwell, du Preez and Knights, 2020). These specifications ensure optimal performance of batteries by minimizing potential negative effects from contaminants. Cobalt sulphate heptahydrate appears as pink-red, odourless crystals and is suitable for use as a raw material for precursor cathode active materials in battery manufacturing. Adhering to these stringent purity standards is crucial for the use of cobalt sulphate crystals as a precursor in lithium-ion batteries cathode active material. Table 1, adapted from (Crundwell, du Preez and Knights, 2020), specifies the permissible levels of impurities in cobalt sulfate heptahydrate required for it to be classified as battery grade. These impurity limits ensure the material meets the high-purity standards necessary for lithium-ion battery applications, minimizing the risk of performance degradation caused by contaminants.

Table 1: Specification of metal impurities in battery grade cobalt sulphate. adapted from (Crundwell, du Preez and Knights, 2020)

Specifications of metal	**Amount Required**
Cobalt	More than 21%
Nickel	Less than 80 ppm
Iron	Less than 3 ppm
Copper	Less than 3 ppm
Zinc	Less than 3 ppm
Manganese	Less than 3 ppm
Magnesium	Less than 10 ppm
Sodium	Less than 10 ppm
Lead	Less than 3 ppm
Quartz	Less than 10 ppm
Calcium	Less than 10 ppm
Cadmium	Less than 3 ppm

2.3 LCA Studies on Cobalt sulfate and NMC batteries

LCA has been widely used to evaluate the environmental implications of cobalt sulfate production and Nickel-Manganese-Cobalt (NMC) cathodes production. The Cobalt Institute performed a comprehensive LCA in 2020, updating their 2015 study, to assess the cradle-to-gate environmental impacts of cobalt and its compounds, including cobalt sulfate heptahydrate. This study adhered to ISO standards and provided industry-average datasets for various cobalt products such as cobalt metal, crude cobalt hydroxide, cobalt oxide and cobalt sulphate (Cobalt Institute, 2020). However, the geographical representativeness of the study was quite limited when it came to cobalt sulfate heptahydrate and tri cobalt tetroxide production. It accounted for 55% (26,818 tonnes) of the globally produced refined cobalt metal, 37% (39,797 tonnes) of the cobalt contained in global crude cobalt hydroxide production, 8% (4,439 tonnes) of the cobalt contained in global tri-cobalt tetroxide production and 9% (2,751 tonnes) of the cobalt contained in global cobalt sulfate heptahydrate production. The relatively lower representativeness of tri-cobalt tetroxide and cobalt sulphate heptahydrate reflect the fact that more than 70% of cobalt refining takes place in China, and Chinese refiners were not included in the study. The GWP of 1 kg of cobalt sulphate heptahydrate found in this study was 4.0 kg CO_2 Eq. First Cobalt released a gate-to-gate LCA in 2020, focusing on the production of cobalt sulfate heptahydrate from crude cobalt hydroxide. The study, conducted by Minviro, compared the environmental impacts of First Cobalt's refinery in Canada with a benchmark refinery in China, highlighting areas for potential environmental improvements (Minviro, 2020). In First Cobalt’s production process, the carbon footprint generated through the production of one kilogram of cobalt sulfate from crude cobalt hydroxide is 1.58 kg CO_2 eq compared to 3.25 kg CO_2 eq for a benchmark refinery in Tongxiang, China. However, this study does not provide a cradle to gate analysis and has a limited representativeness as global refining of cobalt in Canada is four percent as compared to seventy six percent in China.

T. Zhang et al., 2021 conducted a cradle-to-gate LCA of cobalt sulfate production derived from a nickel–copper–cobalt mine in China. Their study identified that the beneficiation stage, due to the low-grade cobalt ore, and the refining stage were significant contributors to environmental impacts, particularly in fossil depletion and freshwater ecotoxicity categories. The GWP was approximately found to be 35.6 kg of CO_2 Eq. The study uses operational data from Chinese refineries and mining site. The mine site in China used for the analysis is a nickel–copper–cobalt mine with 0.04% cobalt content. While mines in Congo can have ten times higher cobalt concentration. Rinne et al., (2021) performed an LCA combined with process simulation for battery-grade cobalt sulfate production from cobalt–gold ores in Finland. They reported a global warming potential (GWP) of approximately 20.9 kg CO_2-equivalent per kilogram of cobalt sulfate produced, with the hydrometallurgical process being a major contributor. Their study integrated process simulation with life cycle assessment to evaluate environmental impacts. They utilized process simulation to model the hydrometallurgical processes involved in cobalt sulfate production, allowing for a detailed analysis of material and energy flows. This approach enabled the identification of major contributors to environmental impacts, such as global warming potential (GWP), and facilitated the exploration of process optimization strategies to enhance cobalt recovery and reduce their impacts.

Das et al., 2024 performed a cradle to gate LCA analysis to quantify the environmental impacts of cobalt along its supply chain with a functional unit of 1 MWh of LIB storage capacity. The analysis examines three refinery locations (China, Canada, and Finland), different ore grades, and five battery chemistries (NMC111, NMC532, NMC622, NMC811, and NCA) to evaluate their influence on environmental impacts. Their findings indicate that impacts increase inversely with ore grade, refining outside of China can lower global warming potential (GWP) by over 12%, and cobalt use in NCA and advanced NMC chemistries results in 45–74% lower GWP compared to NMC111. Statistical analysis identifies cobalt content in the battery as the strongest predictor of environmental impact, followed by ore grade and refining location.

Farjana et al., (2019) used data from the Australian life cycle assessment database and ecoinvent to do a comprehensive analysis of the environmental impacts associated with cobalt extraction. The research examines various stages of cobalt mining and processing to identify key contributors to environmental burdens. The findings indicate that the beneficiation and refining stages are significant contributors to environmental impacts, particularly in categories such as fossil depletion and freshwater ecotoxicity. The study also highlights that the environmental impacts are inversely related to ore grade; lower-grade ore results in higher environmental burdens. They obtained a GWP potential of 11.73 kg CO_2 eq for a functional unit of 1 kg of cobalt. Table 2 summarizes the key points in the studies, along with their GWP results and scope.

Table 2: Summary of various literature sources study, scope, key findings and GWP LCA on cobalt, cobalt sulfate and NMC

Study	Scope	Key Findings	GWP (kg CO_2-eq)
Cobalt Institute (2020)	Cradle-to-gate LCA of cobalt products, limited geographical coverage (excludes China)	Industry-average datasets for cobalt sulfate heptahydrate	4
First Cobalt (Minviro, 2020)	Gate-to-gate LCA for cobalt sulfate production from crude cobalt hydroxide	Canada refinery GWP lower than China refinery	1.58 (Canada), 3.25 (China)
Zhang et al. (2021)	Cradle-to-gate LCA for cobalt sulfate from a nickel–copper–cobalt mine in China (low ore grade)	Beneficiation and refining stages are major contributors	35.6
Rinne et al. (2021)	LCA with process simulation for cobalt sulfate from cobalt–gold ores in Finland	Hydrometallurgical process identified as a key contributor	20.9
Das et al. (2024)	Cradle-to-gate LCA for cobalt refining across three locations (China, Canada, Finland)	Refining outside China reduces GWP by over 12%	Varies based on location and ore grade
Farjana et al. (2019)	LCA for cobalt extraction using Australian and ecoinvent databases	Environmental impacts inversely related to ore grade	11.73 (for 1 kg of cobalt)

2.4 Novel Contributions and Improvements

Most existing studies regarding cobalt sulphate (Rinne, Elomaa and Lundström, 2021; Zhang *et al.*, 2021) focus on China, Canada, and Finland, while the current research highlights primary mining steps from the DRC, where more than 70 percent of cobalt is sourced. This is crucial because the DRC's mining conditions, energy sources, and supply chain dynamics differ significantly from those in industrialized countries. Additionally, the refining step is modelled in China where more than seventy percent of the cobalt is refined. The research focuses on one of the most representative routes for cobalt production globally. Whereas prior research regarding cobalt sulfate production does not have a high representativeness of global cobalt sulfate production.

Additionally, this research simulates the production of battery-grade cobalt sulfate using process modelling in HSC Chemistry. This allows for a more accurate representation of process efficiencies, emissions, and material flows, filling data gaps where literature shows discrepancies. If data is collected from various literature sources to perform an LCA, the material or energy flows are not uniform with other literature sources due to variations in process conditions, scale, and measurement methods. This results in inconsistencies in data collection for the LCA. Additionally, some values of material or energy flows may not be found in literature at all.

HSC Chemistry uses rigorous thermodynamic calculations to resolve the mass and energy balances of the flowsheets based on well-established chemical and physical principles. This not only ensures that all inputs and outputs are accounted for consistently but also produces reproducible and reliable data Process models in HSC sim generate data by resolving the mass and energy balances of the flowsheets, providing estimations based on chemical and physical principles and generating reliable LCI data. For example, while literature sources might simply report a pH value for a leaching reactor, In HSC Sim, a precise pH can be set by adjusting the acid inputs and the composition of the leach solution. This means that the material flow is calculated based on current plant conditions, rather than relying solely on static values. Consequently, HSC Simulation effectively resolves the inconsistencies often encountered in literature.

The approach of using process simulation for generating LCI, ensures that all parameters, processes, and materials are clearly outlined, enabling a transparent comparison and enables the identification of hotspots. In LCA studies, data is often aggregated, making it challenging to pinpoint the exact process step responsible for specific emissions. This lack of transparency complicates the identification of environmental hotspots.

The current model for the production of battery grade cobalt sulphate uses process simulation and provides detailed insights into extraction processes, location specifics, and modelling parameters. Furthermore, the current research defines a representative process flow for cobalt sulfate production and uses data from various sources to model this process accurately. This contrasts with other studies that rely on single datasets or assume standard industrial conditions without validating the robustness of process flows.

Following the process simulation, a Life Cycle Assessment (LCA) of cobalt sulfate is conducted, which identifies the specific energy and material flows within each process step, pinpointing the hotspots in the corresponding impact categories responsible for emissions. By highlighting these hotspots, the study provides valuable insights for process optimization, enabling targeted improvements to reduce environmental impacts and enhance the overall sustainability of cobalt sulfate production.

Cobalt sulfate is a critical precursor in the production of NMC CAMs due to its ability to provide a stable and controlled source of cobalt for the synthesis of cathode materials. The precise control of cobalt content and its interactions with nickel and manganese are crucial for optimizing the electrochemical properties and performance of the battery. Cobalt sulfate allows for better homogeneity and uniformity in the synthesis process, leading to improved energy density, stability, and cycle life of the resulting NMC cathodes. Therefore, understanding the environmental impacts and production process of cobalt sulfate production is imperative, as it directly impacts the overall sustainability of NMC-based cathodes used in lithium-ion batteries.

The custom cobalt sulphate dataset produced from process simulation is then used in NMC 111 and NMC 811 CAM chemistries for a targeted approach, offering insights into the trade-offs between older and newer NMC compositions in terms of environmental impact. By comparing the environmental impacts associated with different cobalt concentrations in LIB cathodes, the current research provides practical insights for industry and policymakers. Moreover, the research allows for a more in-depth evaluation of lithium-ion battery cathode active materials as previous LCAs isolate cobalt sulfate without considering its interactions with other battery precursors, limiting their applicability.

3 Process Simulation of Battery Grade Cobalt Sulphate

3.1 Process Flow for Simulation of Battery Grade Cobalt Sulphate

In order to use process simulation to model multiple processes, parameters such as pH, additives, feed rate, concentrations, densities, reagents, chemical equations, temperature, rate of reactions, and reaction kinetics need to be known. Although in some cases, if certain parameters are not known, process simulation software can use controls to set the value of a parameter by changing the value of another parameter. This can assist in identifying material flows used in a process.

Multiple process flows were initially considered for modelling process simulation of battery grade cobalt sulfate which were derived from patents. As patents have detailed information regarding parameters to be used in process simulation. A patent by (Lantto *et al.*, 2022) for preparing battery grade metal sulphate solutions and another patent by (Fraser *et al.*, 2021) for producing crystallized metal sulphates was considered. The starting material of the initial patent was impure pieces of cobalt. This would not be possible to use this for a cradle to gate LCA analysis. The starting material of the second patent was impure cobalt chloride. On performing value chain analysis of cobalt, it was found that only two percent of cobalt is processed into cobalt chloride which may or may not be further processed into battery grade cobalt sulfate. This would also not result in a cradle to gate LCA analysis of battery grade cobalt sulfate.

To achieve a highly representative process simulation, the process flow from the Argonne National Laboratory's Greenhouse gases, Regulated Emissions, and Energy use in Technologies (GREET) model was selected (Dai, Kelly and Elgowainy, 2018). The processing steps outlined in this report have served as the foundation for the cobalt sulfate process simulation. This model accounts for the concentration and hydrometallurgical processing of both copper-cobalt sulphide and oxide ores in the Democratic Republic of Congo, leading to the production of crude cobalt hydroxide, which is then refined in China into battery-grade cobalt sulfate and other cobalt products. After production of crude cobalt hydroxide, the refining steps include re-leaching, solvent extraction and evaporation and crystallization. While the report defines the overall process flow, it lacks detailed process parameters. Additionally, it provides a life cycle inventory (LCI) but does not include a life cycle impact assessment (LCIA). Figure 8 illustrates the key processing steps involved in the manufacturing of cobalt sulfate, as described in the Cobalt Life Cycle Analysis Update for the GREET Model.

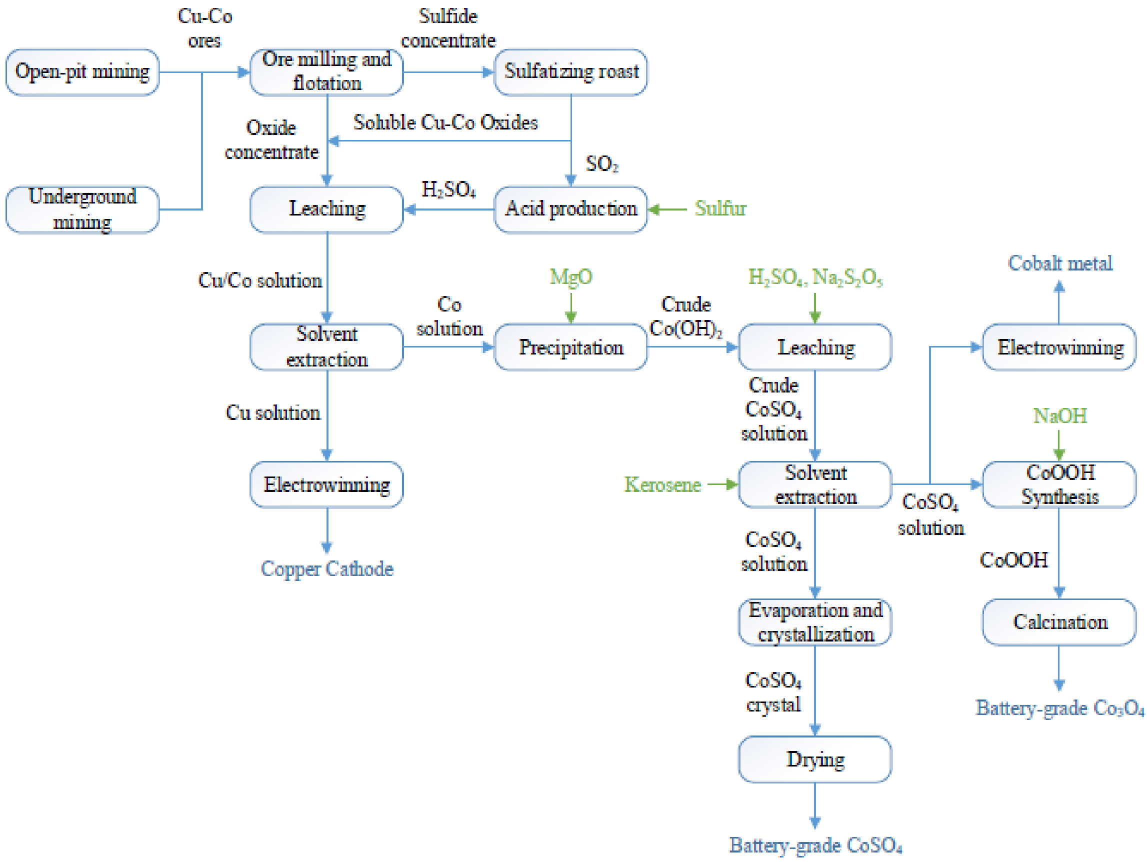

Figure 8: Process Flow of production of battery grade cobalt sulfate, reproduced from Cobalt Life Cycle Analysis Update for the GREET Model (Dai, Kelly and Elgowainy, 2018).

To obtain detailed process parameters, information was primarily sourced from metallurgy books and academic journals relevant to copper processing as cobalt is processed as a by-product of copper mining and refining. The data used for process simulation is largely derived from publicly available literature, as it was not possible to acquire industry-specific data. Consequently, the process simulation was constructed by piecing together information from various sources, much like assembling a puzzle, to create a comprehensive representation of the processing steps within the HSC model. Over 20 literature sources have been used for various steps of the process simulation model. Most of the information used for the flow sheets has been obtained from (Crundwell, 2011; Crundwell, du Preez and Knights, 2020).

However, there was not sufficient data in literature sources regarding the solvent extraction of cobalt and crystallization and drying of cobalt sulfate crystals to model these steps in HSC chemistry. Critical process parameters, including the type of extractant and diluent used, solvent concentrations, reaction pH, and process yields, are missing for the cobalt solvent extraction steps. Solvent extraction is employed in the production of cobalt sulfate when directly processed from cobalt hydroxide (Dai, Kelly and Elgowainy, 2018; Zhang *et al.*, 2021).

To address these data gaps, the model was adapted based on information from Crundwell et al. (2011), where the final product following the re-leaching of cobalt is cobalt metal. Prior to cobalt electrowinning, the electrolyte consists of a cobalt sulfate solution. It is assumed that this intermediary cobalt sulfate electrolyte, formed before electrowinning, undergoes crystallization to produce the final cobalt sulfate product. For the crystallization of cobalt sulphate crystals, the parameters for temperature conditions and yield of crystallization of cobalt sulphate crystals are taken from Xhang, J. et al. (2022).

Another process flow was developed by integrating information from (Crundwell, 2011; Crundwell, du Preez and Knights, 2020),(Dai, Kelly and Elgowainy, 2018), and (Zhang *et al.*, 2022). The simulation follows the same overall process from mining to the re-leaching of cobalt hydroxide as described by (Dai, Kelly and Elgowainy, 2018), while most process parameters are derived from (Crundwell, 2011; Crundwell, du Preez and Knights, 2020). The crystallization stage is modelled based on the information provided by (Zhang *et al.*, 2022). Figure 9 shows the overall adapted process model derived from modelling the process simulation of cobalt sulfate in HSC Chemistry Sim.

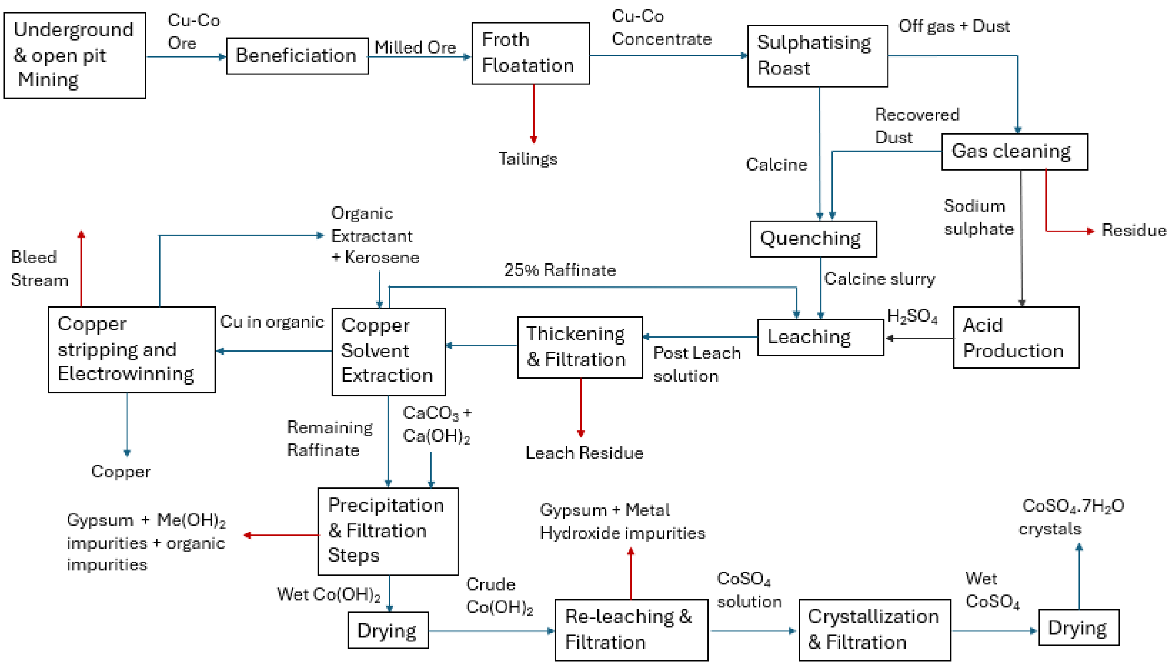

Figure 9: Block diagram of adapted process model derived from modelling the process simulation of cobalt sulfate in HSC Chemistry Sim

3.2 Selection of Ore Composition

Ore composition plays a crucial role in determining the environmental impacts of the process. To input ore composition into the HSC model, it was essential to account for 100% of the minerals or compounds present in the deposit. Various literature sources, including (Crundwell, 2011; Crundwell, du Preez and Knights, 2020),(Broughton, 2014),(Mambwe *et al.*, 2022a),(Mambwe *et al.*, 2022b), and (Dehaine *et al.*, 2021), provide data on the percentages of copper and cobalt in the ore, along with ranges for other compounds. However, none of these sources offer a complete 100% weight composition of the deposit. In contrast, (Dehaine *et al.*, 2024) presents a study on the flotation characteristics of copper-cobalt sulphide ore, which includes a detailed mineralogical composition reaching 100 weight percent. Sulphide ores have been used for this study as over the years sulphide ores will become predominant after the upper oxide ore layer has been mostly mined (Crundwell, 2011). Table 3 displays the composition of a sample taken from a copper-cobalt sulphide deposit.

The mineral content of carrolite and bornite in this deposit is higher than what is typically found in the African Copper Belt. This results in a higher copper and cobalt weight percentage as input for the HSC model, potentially leading to a lower environmental footprint compared to ores with lower copper and cobalt grades.(Dehaine *et al.*, 2024) provides the most comprehensive mineralogical composition available, offering valuable insights not only into the ore composition but also into the characteristics of the copper-cobalt concentrate obtained after froth flotation. Therefore, this data has been used as the input for the run-of-mine ore in the model. To ensure consistency, minerals with the closest compositions to those listed in the table were selected from the HSC mineral database. Additionally, since (Dehaine *et al.*, 2024) explores the flotation behaviour of copper-cobalt sulphide ore, the post-flotation composition was derived using the results from this study.

Table 3: The mineralogical composition of a sample from copper cobalt deposit adapted from Flotation of a copper-cobalt sulphide ore: Quantitative insights into the role of mineralogy. (Dehaine *et al.*, 2024)

Mineral	**Chem. Formula**	**Abundance (wt%)**	**content in mineral (wt%)**	
			Cu	**Co**
Carrollite	$CuCo_2S_4$	8.5	18.96	38.36
Chalcopyrite	$CuFeS_2$	0.7	34.36	-
Bornite	Cu_5FeS_4	32.6	62.95	-
Chalcocite	Cu_2S	0.5	79.33	-
Pyrite	FeS_2	0.1	–	–
Chrysocolla	$(Cu,Al)_2H_2Si_2O_5(OH)_4 \cdot nH_2O$	0.1	33.86	–
Heterogenite	$Co^{3+}O(OH)$	0.1	–	66.85
Goethite	$FeO(OH)$	0.8	–	–
Rutile	TiO_2	0.2	–	–
Dolomite	$CaMg(CO_3)_2$	16.7	–	–
Apatite	$Ca_5(PO_4)_3(F,Cl,OH)$	0.6	–	–
Magnesite	$MgCO_3$	2	–	–
Quartz	SiO_2	28	–	–
Magnesiochlorite	$(Fe,Mg,Al)_6(Si,Al)_4O_{10}(OH)_8$	7.7	–	–
Mg silicates	$Mg_3Si_4O_{10}(OH)_2$	1.3	–	–
Others	–	0.1	–	–
Total		100	22.80	3.332

3.3 HSC Modelling Steps

The production of battery-grade cobalt sulfate takes place across three distinct processing plants. The first is the mineral processing or concentrator plant, where mining, beneficiation, and froth flotation are carried out to produce a copper-cobalt concentrate. This concentrate is then transferred to the hydrometallurgical plant, where it undergoes a series of processes, including roasting, leaching, solvent extraction, electrowinning, and precipitation. These steps result in the production of copper cathode and cobalt hydroxide. The roasting process is included in the hydrometallurgical plant as the primary purpose of the roasting is to convert the copper sulphides into more leachable forms such as copper oxides or sulphates which can then be effectively dissolved in an aqueous medium during the leaching stage. Since the recovery of copper and cobalt ultimately rely on solution-based techniques (leaching, solvent extraction, electrowinning, and precipitation), the overall process is classified as hydrometallurgical. The cobalt hydroxide is then transferred to refining plant where it undergoes leaching, solvent extraction and crystallization to form battery grade cobalt sulphate.

3.3.1 Beneficiation

The initial ore input for the concentrator plant is set at 1,000 tons. The ore undergoes a series of grinding and resizing steps before being processed via froth flotation. After primary and secondary crushing, water is introduced into the system to facilitate further fine crushing. Oversized particles are separated using screens and sent back for additional crushing. The ore size is progressively reduced from 250 mm to 3 mm by the time it reaches the semi-autogenous grinding (SAG) mill. The ball mill then further reduces the ore size to 85 micrometres. The hydrocyclone directs the underflow back to the ball mill for further grinding, reducing particle size to approximately 80 micrometres. The details of the parameters, along with their sources, are provided in the Appendices. Figure 10 shows the beneficiation of cobalt copper ore modelled in HSC Sim.

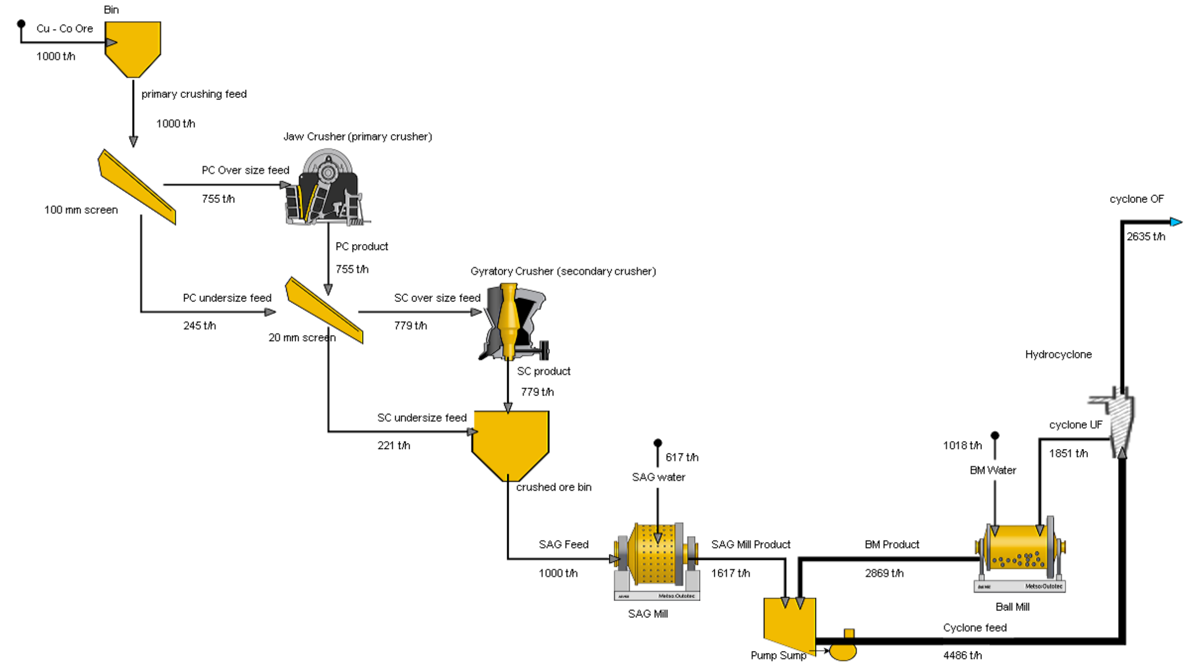

Figure 10: Process flow of ore beneficiation modelled in HSC Sim. PC denotes primary crushing, SC represents secondary crushing, SAG refers to semi-autogenous grinding, BM stands for ball mill, and cyclone UF and OF correspond to cyclone underflow and overflow, respectively.

3.3.2 Froth Floatation

During froth flotation, the crushed ore first enters a conditioner, where reagents are added along with additional water to achieve a solid weight percentage of 31%. There are the three floatation circuits, rougher floatation, cleaner floatation and scavenger floatation. The flotation process is carried out in six flotation cells in rougher floatation. In the initial stage, gangue minerals are separated and removed from the flotation cell, while the remaining pulp proceeds to cleaner flotation. The cleaner and scavenger stages play a crucial role in maximizing mineral recovery by further separating valuable minerals from gangue, which is sent back to the tailings. After the scavenger stage, the enriched pulp is directed to a concentrator, followed by a filtration step for dewatering the concentrate, where the final sulphide concentrate is separated and collected.

The concept of flowsheet design was based on (Crundwell, du Preez and Knights, 2020) and (Moats, Alagha and Awuah-Offei, 2021). Additionally, parameters related to solid percentages were sourced from (Bleiwas, 2012). A detailed list of parameters and their sources can be found in the Appendices. Figure 11 depicts the froth floatation process in HSC Sim module.

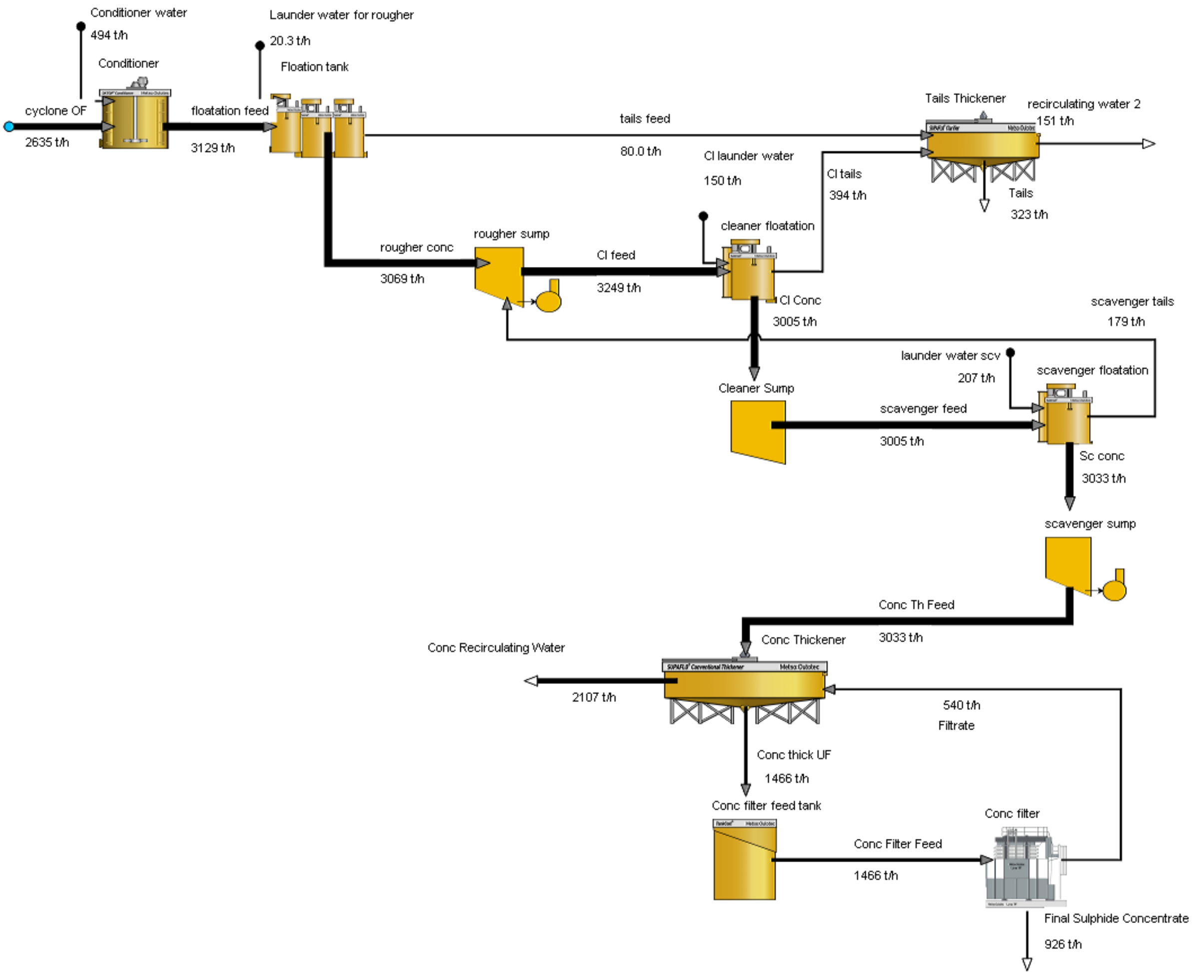

Figure 11: Froth flotation of milled ore modelled in HSC Sim. Cyclone OF refers to cyclone overflow, Cl feed and Cl conc represent cleaner feed and concentrate obtained from cleaner, respectively. Launder water scv indicates launder water for scavenger, Sc conc refers to concentrate obtained from scavenger, Conc Th feed refers to concentrate thickener feed, Conc thick UF refers to concentrate thickener underflow, Conc filter feed represents concentrate filter feed, Conc filter refers to filter for dewatering concentrate, and Conc recirculating water signifies concentrate recirculating water which is treated before being reintroduced in the system.

3.3.3 Roasting and Gas Cleaning

The concentrate obtained from froth flotation was used as the feed material for the roasting process. The mineralogical composition was converted into chemical compounds using the HSC Species Converter module. Any compounds not available in the HSC database were manually added. Table 4 presents the composition of the compounds introduced into the roasting system. The initial feed rate of 500 tons for the roasting plant was based on values reported by (Crundwell, 2011). Since roasting plants are typically separate from concentrator plants, a feed rate representative of industrial roasting operations was adopted.

Using the Gibbs equilibrium module in the roasting reactor, the amounts and ratios of roasted species were determined. This module uses thermodynamic data to determine the quantities of various products produced during roasting. The roasting process operates at approximately

700°C, at which insoluble copper and cobalt sulphides are converted into soluble sulphates. This reaction is highly exothermic, requiring the addition of water to regulate the temperature. The furnace is initially preheated using natural gas to reach the reaction temperature. However, once the roasting reaction begins, it becomes self-sustaining and does not require additional external heating as the reaction is highly exothermic. Nevertheless, the furnace continues to consume electricity for auxiliary systems, including pumps, blowers, and temperature control mechanisms. The following chemical reaction takes place during the sulphatising roast (Thoumsin and Coussement, 1964).

$$2\ CuFeS_{2(s)} + 5\ O_{2(g)} + S_{(s)} \rightarrow CuO.CuSO_{4(s)} + Fe_2O_{3(S)} + SO_{2(g)} \quad (1)$$

$$2\ Cu5FeS_{4(S)} + 12\ O_{2(g)} + S_{(s)} \rightarrow CuO.CuSO_{4(S)} + Fe_2O_{3(S)} + 8SO_{2(g)} \quad (2)$$

$$Cu2S_{(s)} + 5O_{2(g)} + S_{(s)} \rightarrow CuO.CuSO_{4(S)} \quad (3)$$

$$CuCo_2S_4 + O_{2(g)} + S_{(s)} \rightarrow CuO.CuSO_{4(S)} + CoO_{(S)} + SO_{2(g)} \quad (4)$$

A distributor unit was modelled to account for dust expelled during the process, which is directed to the gas cleaning system. The dust and off-gas are first sent to a cyclone separator for initial gas cleaning, where 90% of the dust is recovered as coarse particles. Following this, 90% of the sulphur dioxide (SO_2) gas produced is captured using Venturi scrubbers. In the scrubbers, sodium hydroxide (NaOH) is dissolved in water and reacts with SO_2 to form sodium sulfate (Na_2SO_4). The resulting dissolved sodium sulfate is then sent to an acid production plant for further processing.

$$SO_{2(g)} + O_{2(g)} + 2NaOH_{(aq)} \rightarrow Na_2SO_{4(aq)} + H_2O_{(l)} \quad (5)$$

The recovered coarse dust and calcine from the roasting process are quenched in water, reducing their temperature from 700°C to 70°C, before being sent to the leaching plant for further processing. The entire process for the modelling of roasting, gas cleaning and quenching in HSC sim is shown in figure 12. Additional parameters used in roasting can be found in appendices.

Table 4: Compounds used as roasting input derived from minerals used

Mineral	**Chemical Formula for compound**	**Final Concentrate (wt%)**
Chalcopyrite	$CuFeS_2$	1.108
Bornite	Cu_5FeS_4	62.700
Chalcocite	Cu_2S	0.554
Carrollite	$CuCo_2S4$	12.983
Goethite	Fe_2O_3	0.079
Magnesiochlorite	$MgAl_2SiO_5(OH)_2$	5.383

Dolomite	$CaMg(CO_3)_2$	1.583
Quartz	SiO_2	9.920
Magnesite	$MgCO_3$	0.688
Moisture	H_2O	5.000
total		100.00

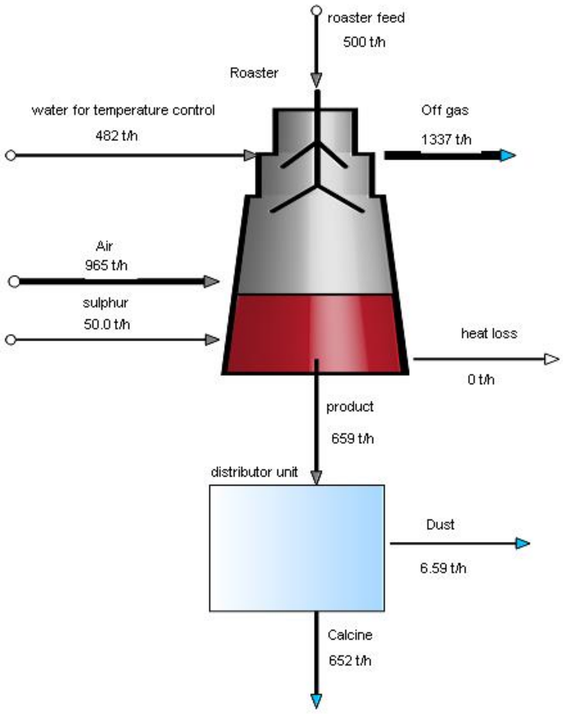

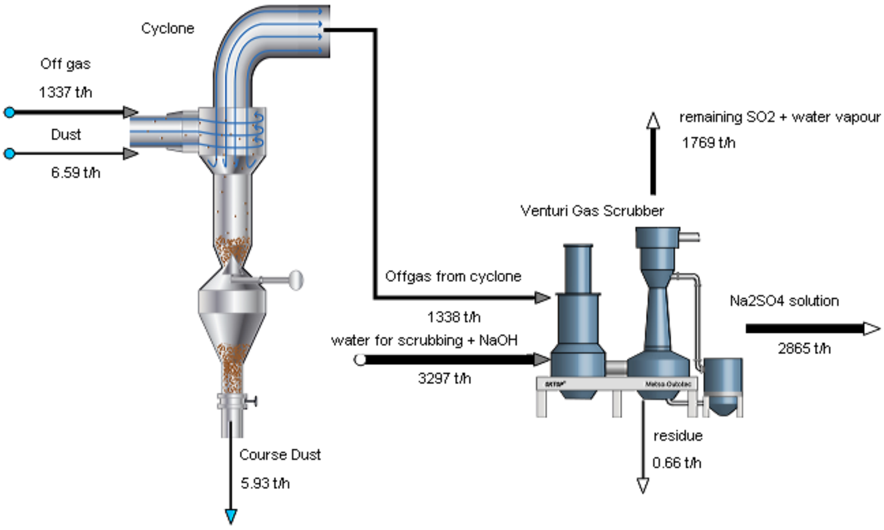

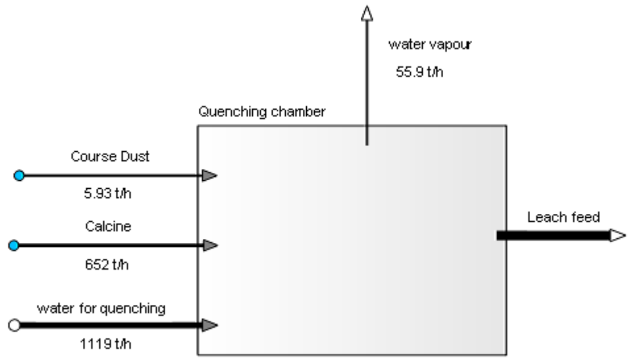

Figure 12: Roasting, gas cleaning, and quenching processes modelled in HSC Sim. The top represents the roasting process, the middle represents gas cleaning, and the bottom represents quenching.

Preheating of Roasting Furnace

An additional process was modelled to determine the natural gas consumption required for preheating the fluidized bed roasting furnace to 700 °C. In this model, natural gas is burned in a blast furnace, generating hot air that is then introduced into the fluidized bed furnace. This hot air raises the temperature of the roasting feed to 700 °C. By incorporating this step, the model provides a more accurate representation of fuel usage within the roasting process. Figure 13 represents the model for the preheating of roasting furnace.

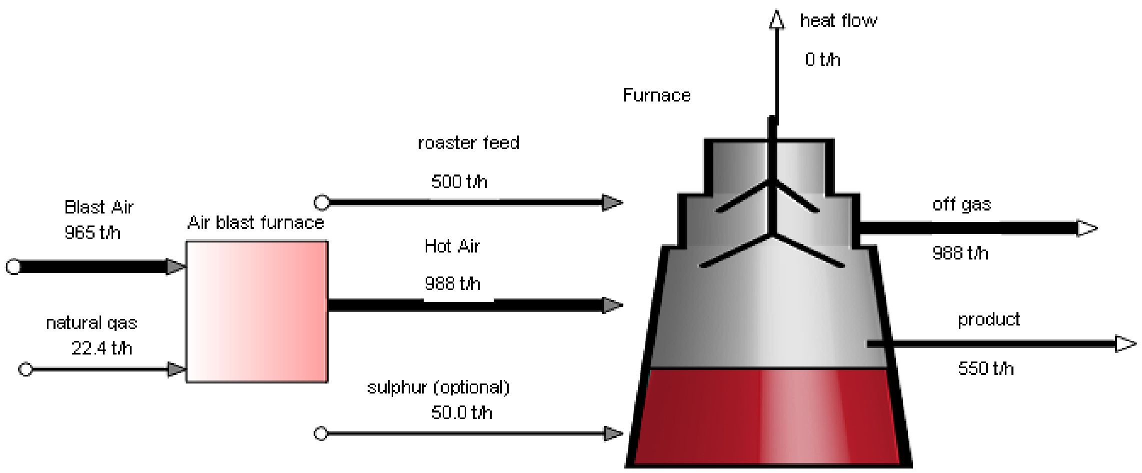

Figure 13: HSC Sim model of preheating of roasting furnace

3.3.4 Leaching

During the leaching process, the leach feed from the roasting plant is introduced to the leaching reactor for further processing. In copper-cobalt processing, once copper and cobalt are separated from the leach solution via solvent extraction, the remaining liquid, containing unextracted elements, residual acid, and impurities, is referred to as raffinate. A portion of this raffinate is recycled back into the leaching process to optimize resource utilization.

To maintain the required leaching conditions, diluted sulfuric acid (H_2SO_4) in water is introduced into the system, ensuring a solids density of 25 g/L in the leaching tank. The leaching reaction occurs at a pH of 1.5, allowing the copper and cobalt oxides and sulphates to dissolve. Additionally, impurity metals such as calcium, magnesium, iron, and aluminium are also leached out to varying degrees. Table 5 shows the chemical reactions that have been modelled to take place in the leaching reactant.

After leaching, the slurry enters a thickener, where solid particles settle through gravitational separation. The thickener divides the slurry into two streams: the high-grade copper solvent extraction (SX) feed, containing approximately 60% of the metallic ions, which proceed to the SX process for further purification, and the mixer feed, which receives the settled solids along with water and other dissolved ions that are evenly distributed between the streams. Following thickening, the low-grade solvent extraction feed is obtained through filtration and counter-current decantation (CCD), where the filtration process separates solid residues. Additional parameters regarding leaching can be found in Appendices. Figure 14 illustrates the modelling of leaching in HSC Sim.

Table 5: Chemical Reaction taking place in leaching reactant

Substance	**Yield %**	**Reason**	**Reaction**	**Equation number**	**Reference**
CuO	90	overall highest Cu yield is 90%	$CuO_{(s)} + 2H^{+1}_{(aq)} \rightarrow Cu^{+2}_{(aq)} + H_2O_{(aq)}$	(6)	(Dai, Kelly and Elgowainy, 2018) (Davenport *et al.*, 2002)
CoO	75	overall highest Co yield is 80%	$CoO_{(s)} + 2H^{+1}_{(aq)} \rightarrow Co^{+2}_{(aq)} + H_2O_{(l)}$	(7)	(Dai, Kelly and Elgowainy, 2018)
$CuSO_4$	95	It is completely soluble and breaks into ions	$CuSO_{4(s)} \rightarrow Cu^{+2}_{(aq)} + SO^{-2}_{4(aq)}$	(8)	
$CoSO_4$	95	It is completely soluble and breaks into ions	$CoSO_{4(s)} \rightarrow Cu^{+2}_{(aq)} + SO^{-2}_{4(aq)}$	(9)	
H_2SO_4	99.99	At very low pH, due to high concentration of hydroxyl ions, sulfuric acid does not completely dissociate	$H_2SO_{4(aq)} \rightarrow H^{+1}_{(aq)} + HSO^{-1}_{4(aq)}$	(10)	

Fe_2O_3	10	Fe_2O_3 reacts with sulfuric acid to form $Fe_2(SO_4)_3$, but the reaction can slow as a passivating layer forms. Fe2SO4 is soluble so it would form ions.	$Fe_2O_{3(s)} + 6H^{+1}_{(aq)} \rightarrow 2Fe^{+3}_{(aq)} + 3H_2O_{(l)}$	(11)	Free, 2021
MgO	80	**MgO** reacts readily with sulfuric acid to form **$MgSO_4$** (magnesium sulfate), which is highly soluble in water. Therefore remains in ionic state.	$MgO_{(s)} + 2H^{+1}_{(aq)} \rightarrow Mg^{+2}_{(aq)} + H_2O_{(l)}$	(12)	assumption for yield
CaO	95	Dissociates into ions after hydration	$CaO_{(s)} + H_2O_{(l)} \rightarrow Ca(OH)_{2(aq)}$	(13)	(Balladares *et al.*, 2018)
$Ca(OH)_2$	95	Ca(OH)2 can be dissolved in such low concentration and does not reaction with sulphate ions yet, thus remaining in ionic form	$Ca(OH)_{2(aq)} + 2\,H^{+1}_{(aq)} \rightarrow Ca^{+2}_{(aq)} + 2H_2O_{(l)}$	(14)	
Al_2O_3	1%	Forms a strong passivating layer resulting in negligible leaching of Al	$Al_2O_3 + 6\,H^{+1}_{(aq)} \rightarrow 2\,Al^{+3}_{(aq)} + 3\,H_2O_{(L)}$	(15)	
FeO	90%	Does not form a passivating layer and can easily dissociate into ions	$FeO_{(s)} + 2\,H^{+1}_{(aq)} \rightarrow Fe^{+2}_{(aq)} + H_2O_{(l)}$	(16)	assumption for yield

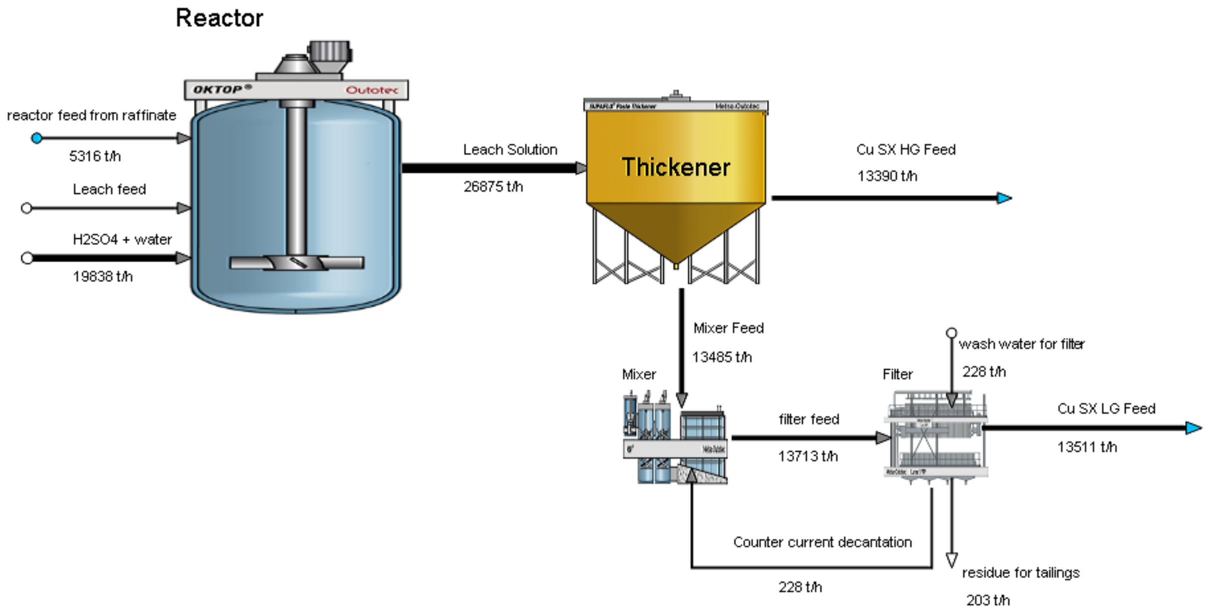

Figure 14: Modelling of leaching in HSC Sim. The leach solution undergoes thickening where it is distributed into high grade and low grade solvent extraction feed.

3.3.5 Solvent Extraction

The solvent extraction process has been modelled primarily using process parameters from the study by Devi et al. (2014). The extractant employed for solvent extraction is LIX 984N, which has been added to the HSC database. For the diluent, kerosene was used in the study; however, since kerosene is not available in the HSC database, decane which is a major component of kerosene, was used as a substitute. The extractant-to-diluent ratio is set at 0.20, and the copper removal efficiency is 93%. The organic solution, composed of 20% LIX 984N and 80% decane, is has approximately the same volume as the aqueous copper-containing aqueous phase. The following chemical reaction takes places during solvent extraction.

$$Cu^{2+}_{(aq)} + 2C_{16}H_{26}NO_{2(l)} \rightarrow Cu(C_{16}H_{25}NO_2)_{2(l)} + H^+_{(aq)} \quad (17)$$

This equation represents the extraction of Cu^{2+} by the organic extractant LIX 984N ($C_{16}H_{26}NO_2$) in the solvent extraction process Devi et al. (2014).

The high-grade copper solvent extraction feed has a copper concentration of 11.65 g/L, which is higher than the 10 g/L typically reported by (Mambwe *et al.*, 2022a) and (Crundwell, 2011). In contrast, the low-grade copper solvent extraction feed contains 7.60 g/L of copper, while literature values from the same sources range between 4 and 6 g/L. For cobalt, the concentration in the high-grade solvent extraction feed is 1.77 g/L, whereas the low-grade feed contains 1.16 g/L. According to Crundwell et al. (2011), cobalt concentrations in solvent extraction feeds generally fall between 2 and 4 g/L for high-grade feeds and 1.0 to 1.7 g/L for low-grade feeds. This can be attributed to the high difference in concentrations between copper and cobalt from the ore onwards.

The solvent extraction of high-grade and low-grade feeds takes place in separate tanks, as a portion of the high-grade raffinate is recycled back into the leaching process. The remaining high-grade raffinate, along with the low-grade raffinate, is sent to precipitation. The organic copper-containing solution from both extraction tanks is directed to the copper electrowinning process. Due to the inherent limitations of phase separation in solvent extraction, 0.25% of the organic phase remains in the raffinate, while 0.01% of the aqueous phase transfers into the organic phase. Figure 15 depicts the HSC sim model of solvent extraction of copper.

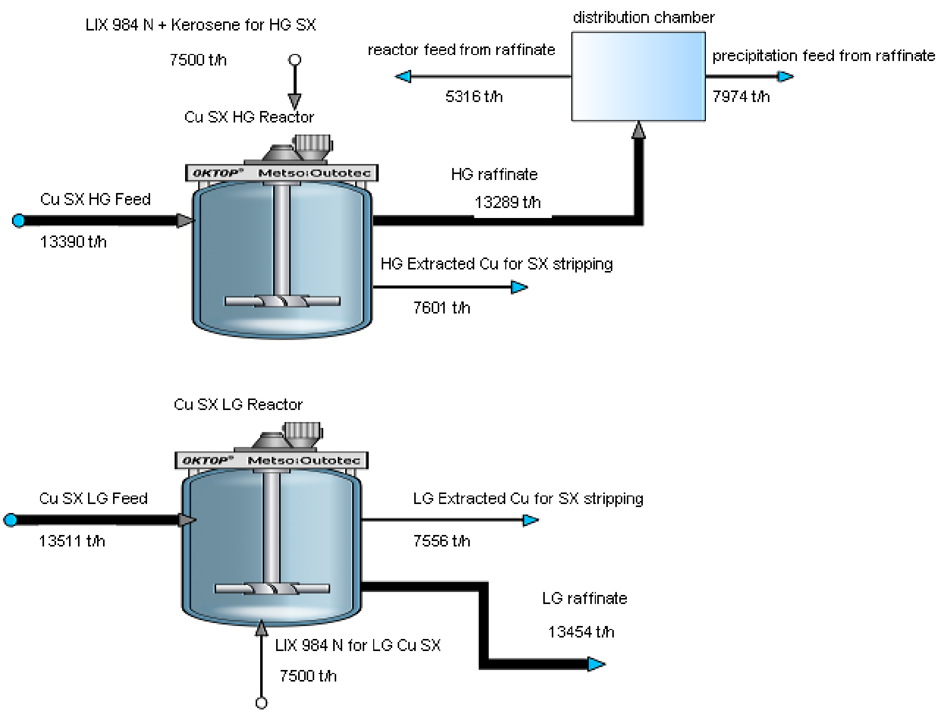

Figure 15: Modelling of solvent extraction of Copper in HSC Sim

3.3.6 Copper Electrowinning

The copper-laden organic solution from the solvent extraction process is directed to a copper stripping plant, where water is added to maintain a copper concentration of 40 g/L in the output stream ('Roasting Copper Sulfides Chemistry - 911Metallurgist', 2021). Sulfuric acid is introduced to achieve an acid concentration of 175 g/L, creating a highly acidic medium necessary for the efficient back-extraction of copper into the aqueous phase ('Copper Recovery by Solvent Extraction Techniques - 911Metallurgist', 2017). The stripped organic phase is then recycled back into the system for further copper solvent extraction. A phase crossover has also been accounted for in this step, with 0.01% of the aqueous phase remaining in the stripped organic and 0.05% of the organic phase transferring to the rich electrolyte. The rich electrolyte is then sent to copper electrowinning. On applying an electric current, water undergoes oxidation, releasing oxygen gas (O_2) and protons. Copper ions (Cu^{2+}) gain electrons and deposit as pure copper metal. The overall chemical equations are as follows.

$$2\ Cu^{2+}_{(aq)} \ + \ 2\ H_2O_{(l)} \ \rightarrow \ 2\ Cu_{(s)} \ + \ 4H^{+}_{(aq)} \ + \ O_{2(g)} \tag{18}$$

The copper concentration in the lean electrolyte after electrowinning is 25 g/L ('Electrowinning - 911Metallurgist', 2020). The rate of copper electrowinning is determined by the concentration difference between the rich and lean electrolytes. The depleted electrolyte is recirculated, with adjustments made to maintain the copper concentration and acidity. A bleed stream is introduced to remove impurities, and after the split, the remaining electrolyte is recirculated to the copper stripping plant. Figure 16 depicts the solvent extraction process modelled in HSC Sim.

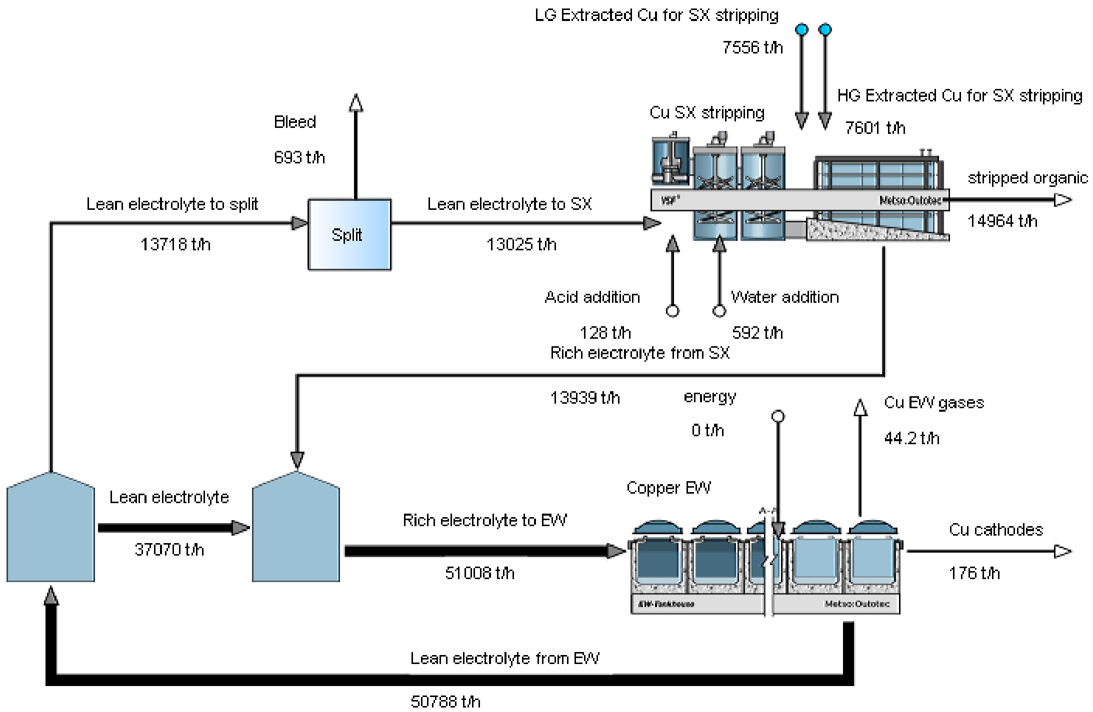

Figure 16: Modelling of Copper Electrowinning in HSC Sim. Copper is tripped from organic solution and introduced to rich electrolyte where it undergoes electrowinning.

3.3.7 Precipitation

The parameters of precipitation were adopted from (Crundwell, 2011). The remaining portions of high-grade and low-grade raffinate undergo a series of precipitation steps to produce impure cobalt hydroxide. In the first precipitation step, the pH is raised to 3.5 by adding limestone and lime. Due to the limited solubility of hydrated lime, it is first dissolved in a dissolution reactor to prevent excessive use before being introduced into the precipitation reactor for neutralization, while limestone is added directly to the reactor. Although both lime and limestone have limited solubility in water, approximately 0.17 g per 100 g of water (Dean and Lange, 1999), their reaction yield in the model exceeds 90%. This high yield is achieved by ensuring that only an amount within the defined solubility range is added. However, at a pH of 3.5, their solubility is slightly higher. The use of limestone results in the release of carbon dioxide gas. At this pH, some iron and aluminium precipitate as hydroxides, while the primary product of the neutralization reaction between lime (calcium hydroxide) and sulfuric acid is gypsum, which predominantly precipitates. The slurry then undergoes a filtration step after each precipitation stage to remove solid waste.

In the second precipitation reactor, additional lime is directly added to the reactor as it is within the solubility limit. The pH of the solution in reactor is raised to 6.7. At this pH most of the aluminium, iron and copper precipitates out in the form of hydroxides along with gypsum. After a second filtration step, the remaining solution goes to the third precipitation tank where the pH is increased to 8.8. Here cobalt precipitates out in the form of hydroxides while additional impurities and gypsum precipitate out as well. The chemical reactions that take place in the precipitation reactors have been shown in table 7 along with their yields. Some of the yields of the reactions have been taken from literature sources while other yields have been estimated based on scientific reasoning. Figure 17 shows the HSC Sim model of the precipitation process.

Table 6: List of Chemical Reaction taking place during the precipitation step

Yield	**Reaction**	**Reason**	**Reference**	**Equation number**
	First Precipitation			
100.0 %	$OH^{-1}_{(aq)} + H^{+1}_{(aq)} \rightarrow H_2O_{(l)}$	All of the hydroxyl ions would neutralize the solution		(19)
90.0%	$HSO_4{}^{-1}_{(aq)} \rightarrow H^{+1}_{(aq)} + SO_4{}^{-2}_{(aq)}$	Since the pH is increased to more than 1.5, lesser Hydrogen ions concentration in solution so HSO4 ions start dissociating		(20)
99.9%	$CaCO_{3(s)} + 2\,H^{+1}_{(aq)} \rightarrow Ca^{+2}_{(aq)} + CO_{2(g)} + H_2O_{(l)}$	High yield as only the amount of limestone which falls under the solubility limit is added		(21)
99.9%	$CaO_{(s)} + H_2O_{(l)} \rightarrow Ca(OH)_{2(aq)}$		(Balladares *et al.*, 2018)	(22)
99.9%	$Ca(OH)_{2(aq)} \rightarrow Ca^{+2}_{(aq)} + 2\,OH^{-1}_{(aq)}$	High yield as only the amount of hydrated lime which falls under the solubility limit is added	(Balladares *et al.*, 2018)	(23)
10.0%	$Fe^{+3}_{(aq)} + 3\,OH^{-1}_{(aq)} \rightarrow Fe(OH)_{3(aq)}$		(Balladares *et al.*, 2018)	(24)

10.0%	$Al^{+3}_{(aq)} + 3\ OH^{-1}_{(aq)} \rightarrow Al(OH)_{3\,(aq)}$		(Balladares *et al.*, 2018)	(25)
95.0%	$CaSO_{4\,(s)} \rightarrow Ca^{+2}_{(aq)} + SO_{4\,(aq)}^{-2}$		(Balladares *et al.*, 2018)	(26)
100.0 %	$CaSO_{4\,(aq)} + 2\ H_2O_{(l)} \rightarrow CaSO_{4\,(s)} \cdot 2H_2O_{(l)}$	All the CaSO4 is precipitated as gypsum	(Balladares *et al.*, 2018)	(27)
Second Precipitation				
100.0 %	$OH^{-1}_{(aq)} + H^{+1}_{(aq)} \rightarrow H_2O_{(l)}$	All of the hydroxyl ions would neutralize the solution		(19)
100.0 %	$HSO_{4\,(aq)}^{-1} \rightarrow H^{+1}_{(aq)} + SO_{4\,(aq)}^{-2}$	Since is higher, lesser Hydrogen ions concentration in solution so HSO4 ions start dissociating		(20)
95.0%	$Al^{+3}_{(aq)} + 3\ OH^{-1}_{(aq)} \rightarrow Al(OH)_{3\,(aq)}$		(Balladares *et al.*, 2018)	(28)
95.0%	$Ca^{+2}_{(s)} + 2\ OH^{-1}_{(aq)} \rightarrow Ca(OH)_{2\,(aq)}$		(Balladares *et al.*, 2018)	(29)
99.9%	$CaO_{(s)} + H_2O_{(l)} \rightarrow Ca(OH)_{2\,(aq)}$		(Balladares *et al.*, 2018)	(30)
98.0%	$Ca^{+2}{}_{(aq)} + SO_{4\,(aq)}^{-2} \rightarrow CaSO_{4\,(s)}$	Even though Calcium reacts instantly with sulphate to form gypsum, gypsum keeps on precipitating at high pH which implies that not 100% of the gypsum is precipitated out but still a very high amount	(Balladares *et al.*, 2018)	(31)
99.9%	$Ca(OH)_{2\,(aq)} \rightarrow Ca^{+2}_{(aq)} + 2OH^{-1}_{(aq)}$			(32)
100.0 %	$CaSO_{4\,(aq)} + 2\ H_2O_{(l)} \rightarrow CaSO_{4\,(s)} \cdot 2H_2O_{(l)}$	All the CaSO4 is precipitated as gypsum	(Balladares *et al.*, 2018)	(27)
Third Precipitation				
100.0 %	$OH^{-1}_{(aq)} + H^{+1}_{(aq)} \rightarrow H_2O_{(l)}$	Remaining H+ ions would be neutralized		(19)

99.5%	$Fe^{+3}_{(aq)} + 3\ OH^{-1}_{(aq)} \rightarrow Fe(OH)_{3(aq)}$		(Balladares *et al.*, 2018)	(24)
99.5%	$Al^{+3}_{(aq)} + 3\ OH^{-1}_{(aq)} \rightarrow Al(OH)_{3(aq)}$		(Balladares *et al.*, 2018)	(25)
99.5%	$Cu^{+2}_{(aq)} + 2\ OH^{-1}_{(aq)} \rightarrow Cu(OH)_{2(aq)}$		(Balladares *et al.*, 2018)	(33)
99.9%	$CaO_{(s)} + H_2O_{(l)} \rightarrow Ca(OH)_{2(aq)}$		(Balladares *et al.*, 2018)	(30)
99.9%	$Ca(OH)_{2(aq)} \rightarrow Ca^{+2}_{(aq)} + 2OH^{-1}_{(aq)}$			(32)
100.0 %	$CaSO_{4(aq)} + 2\ H_2O_{(l)} \rightarrow CaSO_{4(s)} \cdot 2H_2O_{(l)}$	All the CaSO4 is precipitated as gypsum	(Balladares *et al.*, 2018)	(27)
99.9%	$Ca^{+2}_{(aq)} + SO_{4(aq)}^{-2} \rightarrow CaSO_{4(aq)}$			(34)
99.5%.	$Co^{+2}_{(aq)} + 2\ OH^{-1}_{(aq)} \rightarrow Co(OH)_{2(aq)}$	Almost all the cobalt is precipitated out, so high yield chosen	(Crundwell, du Preez and Knights, 2020)	(35)

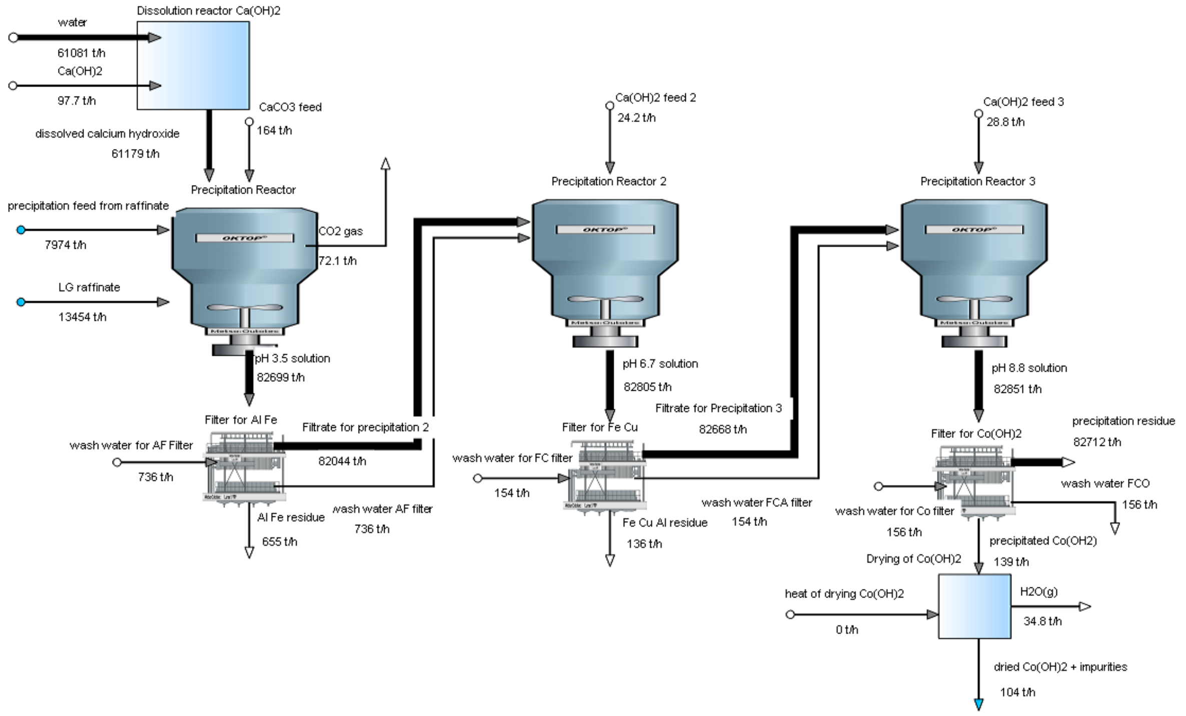

Figure 17: Modelling of the Precipitation process in HSC Sim. Calcium hydroxide is initially dissolved in a precipitation reactor and introduced into precipitation reactor to increase the pH. Limestone and lime are subsequently also added to the reactor. There is a filtration step after each precipitation step to remove solid waste.

3.3.8 Re-leaching and Crystallization

The step in which impure cobalt hydroxide is refined into battery-grade cobalt sulfate is referred to as "refining" in literature. However, since the current HSC model does not incorporate all the steps typically included in the refining process, this step is referred to as re-leaching and crystallization here. In this stage, impure cobalt hydroxide is re-leached in a leaching reactor, with water and sulfuric acid added to control the pH and solids percentage. The pH of the re-leaching reactor is maintained between 6.2 and 6.3, and water is introduced to achieve a solid concentration of 25 g/L (Crundwell, 2011). At this pH, cobalt dissolves into the solution, while impurities remain as solids, allowing for their removal during filtration. These impurities primarily consist of gypsum and minor amounts of metal hydroxides. The main chemical reactions occurring in the re-leaching tank are as follows.

$$Co(OH)_2 + 2H^+ \rightarrow Co^{2+} + 2H_2O \tag{36}$$

$$H_2SO_4 \rightarrow 2H^+ + SO_4^{2-} \tag{37}$$

For the crystallization of cobalt sulfate crystals, the temperature conditions and crystallization yield are adapted from (Zhang *et al.*, 2022). At 30°C, approximately 60% of cobalt sulfate crystallizes into cobalt sulfate heptahydrate. In the reaction chamber, the temperature is maintained at 29°C to optimize crystallization efficiency. The crystallized cobalt sulfate heptahydrate is separated using a filtration process, while the uncrystallized portion is recirculated back into the reaction chamber for further crystallization. After filtration, heat is applied to dry the crystals. Figure 18 illustrates the re-leaching and crystallization process in HSC Sim to make cobalt sulfate heptahydrate. The following reaction occurs in the reaction chamber.

$$Co^{2+} + SO_4^{2-} + 7\,H_2O \rightarrow CoSO_4 \cdot 7H_2O \quad (38)$$

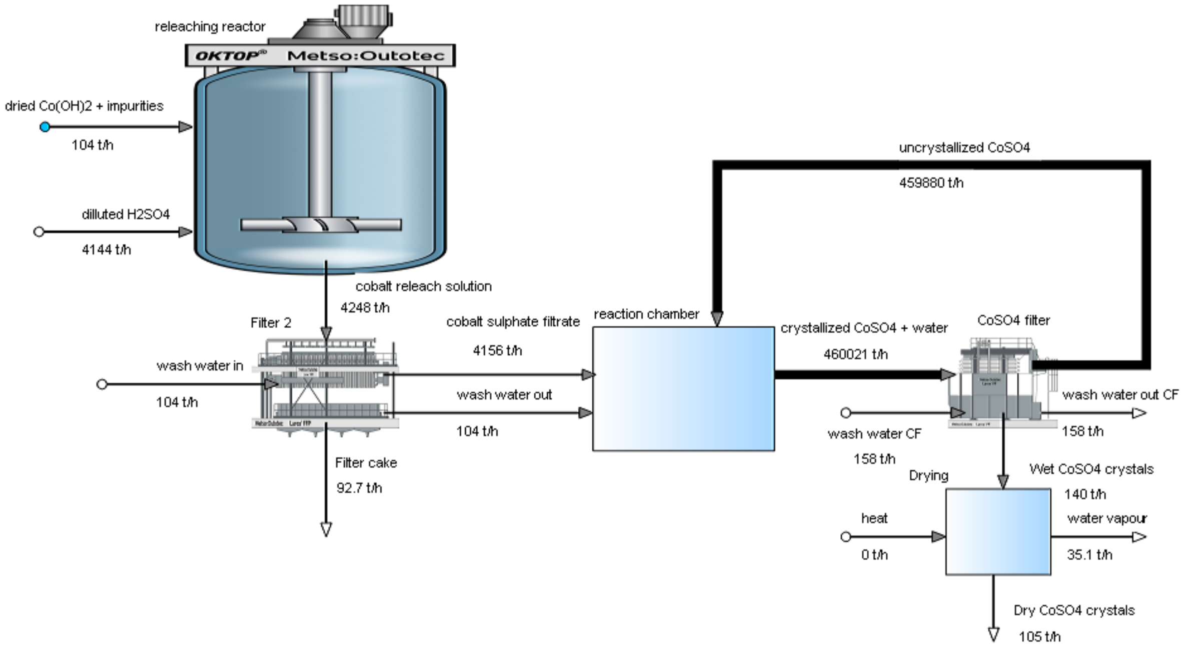

Figure 18: Modelling of Re-leaching and Crystallization in HSC Sim. Cobalt dissolves in leach reactor while impurities are separated by filtration. Then cobalt is crystallized in a reaction chamber.

3.4 Limitations of the HSC Model

3.4.1 Mining

The mining process has not been modelled in HSC Chemistry, as it focuses on thermodynamic and process simulations rather than mechanical excavation and ore extraction. It excels in modelling chemical and metallurgical processes, such as leaching, flotation, and refining, but lacks capabilities for geological modelling, rock mechanics, and mine design. Mining-specific factors like drilling methods, and equipment logistics are not considered in HSC.

3.4.2 Froth Floatation

HSC Sim requires flotation kinetics data for various minerals to accurately model the composition and quantity of the tails and concentrate. However, kinetics data was only available for three minerals in the ore-grade composition used. As a result, the concentrate composition obtained from the HSC model was not used in the roasting model. In the floatation model, HSC was only used to calculate the material and energy flows. Instead, the flotation composition was derived from (Dehaine *et al.*, 2024), which also examines the flotation characteristics of copper-cobalt sulphide ore. R1 to R6 refer floatation cells in rougher floatation, while S1 and S2 refers to two scavengers in the floatation circuit. The composition was derived by taking an average of R1, R3 and S1. Figure 19 shows, reproduced from (Dehaine *et al.*, 2024) shows the outputs of various gangue minerals and ore minerals in various stages of froth floatation. Table 8 shows the composition of concentrate obtained after froth floatation based on the paper of (Dehaine *et al.*, 2024).

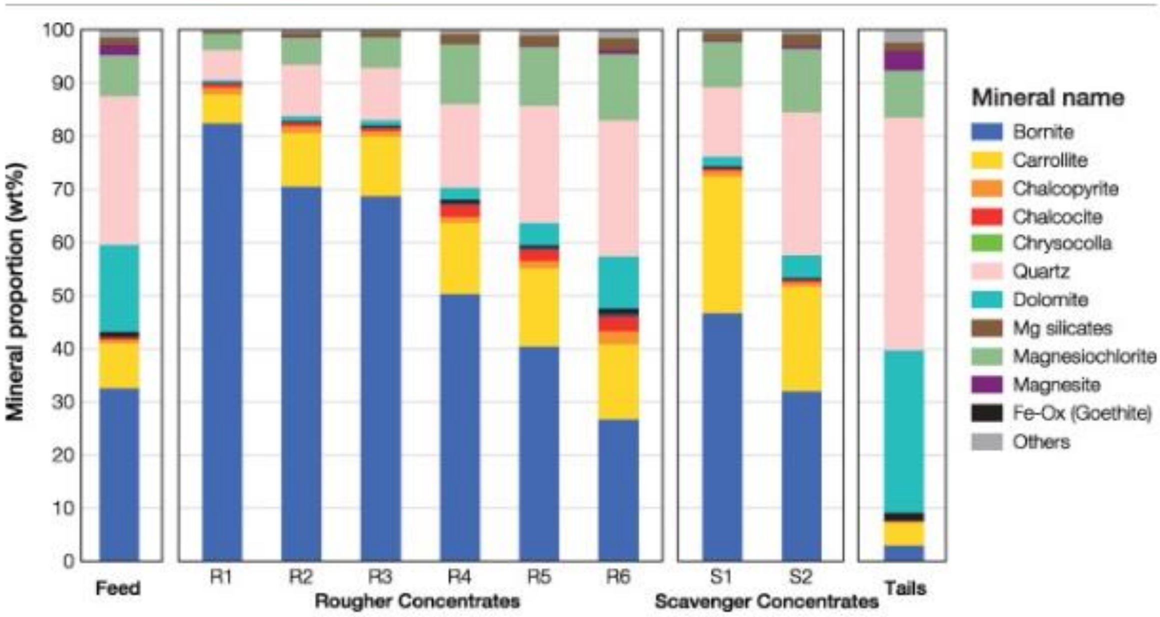

Figure 19: Composition of concentrates obtained during various stages of froth floatation from Flotation of a copper-cobalt sulphide ore: Quantitative insights into the role of mineralogy. (Dehaine *et al.*, 2024)

Table 7: Composition of the Cu Co concentrate obtained after Froth Floatation based on the results in the paper by (Dehaine *et al.*, 2024).

Mineral	Final Concentrate (wt%)
Chalcopyrite	1.17
Bornite	66.00
Chalcocite	0.58
Carrollite	13.67
Chrysocolla	0.00
Heterogenite	0.00
Goethite	0.08
Rutile	0.00
Apatite	0.00
Magnesiochlorite	5.67
dolomite	1.67
Quartz	10.44

Magnesite	0.72
Pyrite	0.00
total	100.00

By using the flotation-based composition from (Dehaine *et al.*, 2024), the percentages of copper, cobalt, and sulphur obtained remain comparable to Cu-Co concentrates and roasting feed compositions reported in other literature sources. This ensures consistency with existing data and improves the reliability of the modelled process. Table 9 shows the comparison of copper, cobalt and sulphur weight percent obtained in concentrates from other literature sources.

Table 8: Comparison of weight percentages of copper cobalt and sulphur found in concentrates

Cu weight %	**Co weight %**	**Sulphur weight %**	**Reference**	**Scenario**
45%	4%	-	Crundwell, 2011	concentrate obtained after floatation
31%		28%	Crundwell, 2020	feed for roasting (Extra sulphur has been added to aid in roasting process)
9%	1.60%	21%	Crundwell, 2020	concentrate obtained after selective floating of cobalt minerals from mixed sulphide oxide ore (Some sulphur is added in floatation of oxide minerals to aid in floatation via sulphidization process.)
16%	4%	-	Crundwell, 2020	concentrate obtained after selective floating of cobalt minerals
12%	2%	21%	Crundwell, 2011	feed for roasting (Extra sulphur has been added to aid in roasting process)
45%	5%	23%	own model	concentrate obtained after froth floatation

Calculations were performed to determine the amount of concentrate produced from froth flotation based on the given ore composition. The ore grade consists of 22.8% copper and 3.2% cobalt, while the resulting concentrate contains 45% copper and 5% cobalt.

Let:

X be the tons of ore processed

Y be the tons of concentrate produced

The mass balance equations are as follows:

$$X * 0.228 = Y * 0.45$$

$$X * 0.032 = Y * 0.05$$

Solving these simultaneous equations, the ore-to-concentrate ratio is determined to be 3.51. Therefore, processing 1,000 tons of ore yields approximately 285 tons of sulphide concentrate. Using mass balance principles, the mass of tailings produced is calculated to be 850 tons. However, due to moisture content in both the concentrate and tailings, the total mass exceeds the initial 1,000 tons of ore.

3.4.3 Roasting and Leaching

In the roasting process, the captured sulphur dioxide (SO_2) gas is processed in an acid production plant, where it reacts with elemental sulphur to produce sulfuric acid (H_2SO_4). This sulfuric acid is then used in subsequent leaching and electrowinning processes. However, due to data limitations and time constraints, the acid production process has not been modelled in HSC Sim. This limitation has been addressed in the LCA modelling of cobalt sulfate.

3.4.4 Precipitation

The precipitation process varies across literature sources, with some studies describing up to five precipitation steps before the re-leaching of cobalt hydroxide. The simplest approach, outlined in Crundwell et al. (2011), was adopted for this study. During HSC modelling, the Gibbs equilibrium mode could not be applied to precipitation reactions while maintaining pH controls, so it was not used. Instead, reaction yield estimates based on literature sources were incorporated into the HSC Sim model. Additionally, in Crundwell et al., (2011 & 2020), there is zinc solvent extraction step or zinc precipitation step. However, since the current ore composition does not have zinc in it, this process was not modelled.

In the GREET model by (Dai, Kelly and Elgowainy, 2018), magnesium oxide (MgO) is used as the primary precipitant instead of lime. However, due to a lack of detailed parameters on how MgO reacts within the system and its precipitation behaviour, it was not included in the HSC model. Additionally, the GREET model employs sodium bisulphate as a reductant during precipitation, but this reagent was not used in the HSC model.

3.4.5 Refining

During the refining step, cobalt is extracted through two solvent extraction stages, followed by back-extraction in sulfuric acid. However, due to the lack of data on process parameters, these steps were not included in the HSC model. The solvent extraction process facilitates the selective separation of cobalt from organic impurities and nickel, ensuring a higher purity of cobalt for subsequent processing. Since nickel was not present in the composition, an additional step to remove nickel did not require modelling.

3.5 Data obtained from HSC Sim

From a LCA perspective, HSC Chemistry provides valuable thermodynamic and process simulation data that is used to model and analyse the environmental impacts of various metallurgical and chemical processes. HSC models track the inputs and outputs of materials (e.g., ores, reagents, and by-products) in different unit operations. The software calculates heat requirements and reaction enthalpies in high-temperature processes such as roasting. HSC simulates the formation and capture of SO_2 and CO_2, which are important for Life Cycle Impact Analysis. It estimates slag, tailings, and wastewater compositions, helping quantify waste flows for impact assessment. HSC provides Gibbs free energy calculations to determine equilibrium product distributions, helping estimate process efficiencies and unreacted waste materials. The software helps quantify acid, lime, and solvent usage, based on information such as pH and concentration. It can also perform power calculations for equipment used in mineral processing such as crushers, grinders, and floatation cells. It can also determine the energy required for the heating or drying of systems to a certain temperature using enthalpy calculations.

However, HSC Sim has limitations in predicting the total energy consumption of certain systems. Mineral processing plants rely on pumps and conveyor belts to transport ore and slurry, but these energy demands are not accounted for in the software. Similarly, fluidized bed furnaces used for roasting require auxiliary systems such as temperature control units, blowers, exhausts, and scrubbers, none of which are included in the energy calculations. Additionally, mixers, thickeners, filters, and other unit operations are modelled without considering their actual power consumption. Leaching reactors require electricity, but HSC Sim does not factor in this energy usage. Likewise, in precipitation, a large volume of solution is pumped through multiple reaction tanks, yet the energy for mixing and pumping is not considered in the model. The power required for pumping, leaching, thickeners, scrubbers etc, has been calculated using the information obtained from the HSC model for the current models which can be found in the Appendices.

4 Life Cycle Assessment of Battery Grade Cobalt Sulfate

4.1 Goal and Scope

4.1.1 Goal

The goal of the study is to evaluate the environmental impacts of the production of battery grade cobalt sulphate heptahydrate and to identify the hotspots in its production from copper cobalt sulfidic ore originating from the African copper belt. Additionally, it can support the development of environmental policies and regulations related to critical raw materials, supply chain transparency, and sustainable battery production. The study can help companies assess the environmental footprint of cobalt sulfate sourcing, compare different supply chain options, and make informed sustainability decisions. Since the data is sourced from process simulation, the study can highlight inefficiencies in cobalt processing and refining, providing a basis for improving energy use, waste management, and overall environmental performance.

This LCA study is designed to provide valuable insights for a range of stakeholders involved in the cobalt supply chain, battery manufacturing, and sustainability assessment, including policymakers, battery & EV manufacturers, cobalt and copper mining and refining companies, LCA practitioners and researchers, investors, and recycling and circular economy stakeholders.

4.1.2 Scope of the Study

The scope of the study gives information on the choices of functional unit, system boundaries, allocation, impact methodology and categories, made to define the study.

Functional Unit

The functional unit serves as the reference basis for quantifying environmental impacts, ensuring consistency in system boundary definition and comparability of results (ISO 14040, 2006). The functional unit of the study is defined as "The primary production of 1kg of battery grade cobalt sulphate heptahydrate with a cobalt content of 21% from a Cu-Co sulfidic ore mined in the African Copperbelt and refined in China." These environmental impacts are calculated based on the declared unit wherein each flow related to material consumption, energy consumption, emissions, effluent and waste is scaled to the reference flow.

System Boundaries

The LCA studies follows a cradle to gate approach, covering all stages from resource extraction to production of cobalt sulfate heptahydrate. The system includes three key processing stages, the first one is the mining and concentration named grouped under the concentration plant, which involves underground and open-pit mining of Cu-Co sulfidic ore, followed by beneficiation and froth flotation at a concentrator plant (near mine site) to produce a Cu-Co concentrate. After concentration, the Cu-Co concentrate is transported to a hydrometallurgical plant, where it undergoes further processing. The second stage, Hydrometallurgical Processing, begins with roasting and gas cleaning, followed by leaching, solvent extraction, copper electrowinning, and cobalt precipitation to obtain crude cobalt hydroxide. This stage also includes the management of process emissions, such as sulphur dioxide (SO_2), which is captured and directed to an acid plant for sulfuric acid production. However, the acid plant itself is excluded from the system boundaries of this LCA model. Finally, in the Refining stage, which is assumed to take place in China, the crude cobalt hydroxide is subjected to re-leaching, filtration, and crystallization to obtain battery-grade cobalt sulfate heptahydrate. Figure 20 depicts the system boundaries of the study.

Although HSC Sim enables the analysis of energy and material flows for individual processes such as froth flotation and beneficiation, the results for processes occurring within the same plant have been aggregated. Results are grouped into three categories: processes within the concentrator plant, the hydrometallurgical plant, and the refining plant. This aggregation is necessary because various processes within the same plant are highly interconnected.

During LCA modelling, discrepancies in mass balances can lead to skewed results. For instance, in the concentrator plant, the water used in beneficiation is subsequently treated in froth flotation. Similarly, sulphur dioxide gas captured during roasting is utilized to produce sulfuric acid, which is then used in leaching and electrowinning. Additionally, raffinate from solvent extraction is recycled back to the leaching plant, and the extractant and diluent used in solvent extraction are recovered during the copper electrowinning process. Due to these interdependencies, results are aggregated at the plant level to ensure consistency and accuracy in the LCA model.

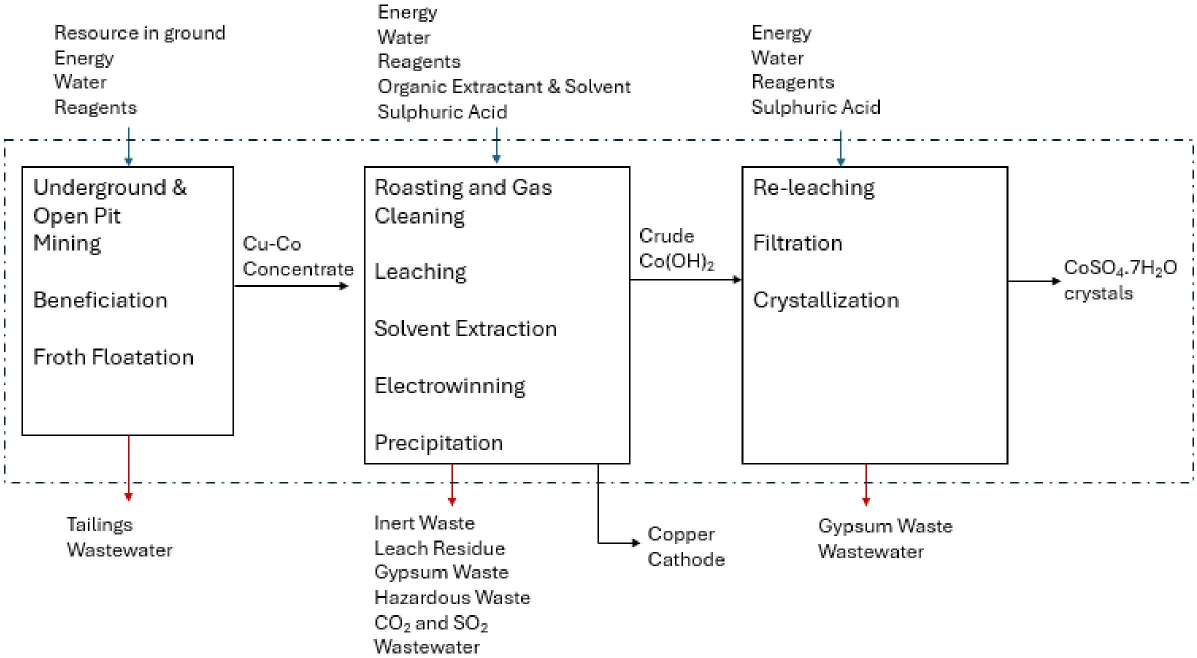

Figure 20: System Boundaries of the LCA of Battery Grade Cobalt Sulphate

Allocation

According to ISO 14044, allocation should be avoided where possible by subdividing processes or expanding system boundaries; when this is not feasible, impacts should be allocated based on physical relationships like mass or economic value.

In this study, economic allocation is applied because copper and cobalt are co-extracted and processed together up to the precipitation stage. Among different allocation methods, economic allocation is the most appropriate as both copper cathode and impure cobalt hydroxide are globally traded commodities with well-defined market values. Mass-based allocation was not selected, as it does not account for the significant economic disparity between copper and cobalt, which would lead to an inaccurate distribution of environmental burdens.
Economic allocation has been applied from mining to precipitation, covering both the concentrator and hydrometallurgical plants, as copper and cobalt remain interlinked throughout these stages. After precipitation, the refining of cobalt hydroxide into cobalt sulfate heptahydrate is attributed solely to cobalt, as copper is no longer part of the process. Detailed data for the economic allocation has been provided in the Appendices.

Within the solvent extraction step, copper in the organic phase and cobalt in the raffinate do not hold direct monetary value and are not considered sellable products at this stage. Additionally, a portion of the copper extractant and diluent is recovered during electrowinning and reused in solvent extraction, further complicating allocation at this step. Consequently, allocation is only applied once marketable products, copper cathode and cobalt hydroxide, are obtained. This approach aligns with the GREET model developed by (Dai, Kelly and Elgowainy, 2018), where economic allocation is applied from ore processing through hydrometallurgical processing. By following ISO 14044 principles, this study ensures a transparent and justifiable allocation of environmental burdens, reflecting the economic significance of both metals.

Selection of Impact Assessment Method and Categories

The ReCiPe 2016 v1.03 method has been chosen for this study to evaluate the potential environmental impacts associated with the production of battery-grade cobalt sulfate heptahydrate. ReCiPe 2016 is one of the most widely used Life Cycle Impact Assessment (LCIA) methods, providing a comprehensive framework to quantify environmental burdens across multiple impact categories (Huijbregts *et al.*, 2017). It translates emissions and resource extractions into quantifiable midpoint and endpoint impact indicators, allowing for a detailed evaluation of environmental trade-offs. For this study ReCiPe impact assessment method was applied at the midpoint level. Table 10 presents the impact categories included in ReCiPe 2016 v1.03, along with their corresponding descriptions and units of measurement. These categories cover a wide range of environmental concerns, enabling a holistic assessment of the life cycle impacts of the studied process.

Table 9: Impact Categories associated with the ReCiPe 2016 v1.03

Impact Category	Indicator Unit	Unit
Global Warming	Measures the potential contribution of greenhouse gas emissions to climate change by trapping heat in the atmosphere.	kg CO2 Eq
Fine Particulate Matter Formation	Assesses the potential for emissions to form fine particulate matter, which can adversely affect human respiratory health.	kg PM 2.5 eq
Terrestrial Acidification	Evaluates the potential of emissions, such as sulphur dioxide (SO_2) and nitrogen oxides (NO_x), to cause acidification of soil and terrestrial ecosystems, leading to harmful effects on vegetation and soil quality.	kg SO2 Eq
Fresh Water Ecotoxicity	Measures the potential toxic effects of chemical emissions on freshwater aquatic ecosystems.	kg 1,4 DCB eq
Terrestrial Ecotoxicity	Assesses the potential toxic effects of chemical emissions on terrestrial ecosystems.	kg 1,4 DCB eq
Marine Ecotoxicity	Evaluates the potential toxic effects of chemical emissions on marine ecosystems.	kg 1,4 DCB eq
Fresh water Eutrophication	Measures the potential for nutrient enrichment (primarily phosphorus) in freshwater bodies, leading to excessive algal growth and oxygen depletion.	kg P eq
Marine Eutrophication	Assesses the potential for nutrient enrichment (primarily nitrogen) in marine environments, causing harmful algal blooms and hypoxia.	kg N eq
Human Carcinogenic Toxicity	Evaluates the potential impact of chemical emissions that can cause cancer in humans.	kg 1,4 DCB
Human Non-Carcinogenic Toxicity	Assesses the potential impact of chemical emissions that can cause non-cancer health effects in humans.	kg 1,4 DCB
Mineral Resource Scarcity	Measures the potential impact of resource extraction on the scarcity of mineral resources, indicating the	kg Cu eq

	depletion of mineral and metal resources.	
Fossil Resource Scarcity	Assesses the potential impact of fossil fuel extraction on the scarcity of fossil resources, indicating the depletion of fossil fuels like oil and coal.	kg Oil Eq
Land Use	Examines the impact of land occupation and transformation on soil quality, biodiversity, and ecosystem services.	m2a crop Eq
Water Consumption	Measures the potential impact of water use on water scarcity, considering the consumption of freshwater resources.	m3
Ionizing Radiation	Assesses the potential human health effects due to exposure to ionizing radiation, often associated with radioactive materials or energy production.	kBq Co-60-eq
Ozone Depletion	Quantifies the potential of emissions to deplete the stratospheric ozone layer, which protects the Earth from harmful ultraviolet radiation.	kg CFC Eq
Ozone Formation, Human Health	Measures the potential of emissions to form ground-level ozone (smog), which can adversely affect human respiratory health.	kg NOx Eq
Ozone Formation Terrestrial Ecosystems	Evaluates the potential of emissions to form ground-level ozone, which can harm terrestrial ecosystems and vegetation.	kg NOx Eq

Software and Database

The LCA model is conducted using OpenLCA 2.3.0 software. The software supports various LCIA methods, including ReCiPe 2016 v1.03, allowing for a comprehensive assessment of environmental impacts. For the background data, ecoinvent 3.8 cutoff is being used, as ecoinvent provides high-quality, peer-reviewed inventory data covering a broad range of sectors, including energy, materials, chemicals, transportation, and industrial processes.

4.2 Life Cycle Inventory

A process simulation-based life cycle inventory (LCI) has been developed for this LCA study. In the initial data collection phase, process parameters and variables for each stage of cobalt sulfate production were established through a comprehensive literature review. This data served as the foundation for constructing process simulation models using the HSC Sim module of

HSC Chemistry software (version 10.5.7) by (*HSC Chemistry*, no date). The simulation covered key processing steps, including beneficiation, froth flotation, roasting, leaching, solvent extraction, electrowinning, precipitation, re-leaching, and crystallization. Material and energy flows for the mining stage were obtained from literature sources.

The resulting HSC Sim models provide essential foreground data for the LCI. Background processes were modelled using the ecoinvent 3.8 database, which also facilitated the integration of foreground data into the LCA framework. Details of the HSC Sim models are presented in Section 3 of this report. While the models provide material and some energy flows, they do not account for the energy consumption of equipment such as pumps, filters, mixing reactors, auxiliary systems, and leaching reactors. However, based on process-specific outputs from HSC Sim, energy consumption estimates have been derived through additional literature sources and relevant calculations. Calculations for the power consumption of auxiliary systems are provided in the appendices. Using the mass flow rates from HSC Sim, energy values can be derived from power calculations.

4.2.1 Data Collection

Concentration Plant

The mining data has been sourced from the GREET model (Dai, Q. et al., 2018), as the mining process could not be modelled in HSC Sim. The GREET model provides data on the energy consumption for extracting one ton of ore, which has been incorporated into the LCA modelling of battery-grade cobalt sulfate. The mining energy and water flows adopted from the GREET model are shown in table 11. Since mining is primarily a mechanical process, the ore’s chemical composition has minimal impact on its overall energy consumption. The energy consumption in mining operations is predominantly influenced by mechanical processes such as drilling, blasting, and hauling. These activities are largely dependent on factors like rock hardness and the physical properties of the ore body, rather than its chemical composition (Norgate and Haque, 2010).

Mining data from the GREET model was collected under the assumption of an equal split between underground and open-pit mining (50% each). To model the extraction of one ton of ore, an average of both mining methods was used. The mining infrastructure was modelled using ecoinvent 3.8 flows, with allocation based on the concentrate output from the concentration plant. While the GREET model provided data on energy consumption and water use, it did not account for explosives used in blasting. To address this, the ecoinvent dataset "Copper mine operation and beneficiation, sulfide ore | Copper concentrate, sulfide ore | Cutoff, U – ZM" was used to determine the quantity of explosives required per kilogram of concentrate, which was then integrated into the model. Additionally, the infrastructure for the concentrate plant was modelled using the ecoinvent flow "Market for aluminium hydroxide factory | Aluminium hydroxide factory | Cutoff, S – GLO," as it is also referenced in the infrastructure modelling of the copper mine operation and beneficiation dataset. The quantity was allocated based on the concentrate output from the concentration plant.

Table 10: Material and Energy Flows for mining 1 ton of copper cobalt ore reproduced from the GREET model (Dai, Q. et al., 2018)

	TFM (Open pit mine)	Kamoto (Open pit/ Underground mine)
Energy Consumption (kWh/t ore mined)		
Diesel	163	0
Electricity	0	61.7
Water Consumption (gal/t ore mined)	45.3	725
Emissions (Kg/t ore mined)		
PM10	1.44	N/A
PM2.5	0.148	N/A

The material and energy flows obtained from HSC Sim for the beneficiation and froth flotation processes are shown in Table 12. The quantity of tailings and concentrate produced from froth flotation has been determined by calculations outlined in Section 3.4.2. To account for in-facility transport, transport via conveyor belts has been incorporated into the model. A distance of 100 meters between different dry grinding machines has been assumed. Using the mass flow data, calculations for the transport of solid ore via conveyor belts were made by multiplying tons by kilometres, and this data was then incorporated into the LCA model. The provider for water in the concentrate plant was chosen as water, unspecified natural source as concentrate plants usually use natural sources of water from rivers, dams, wells etc.

The reagent Sodium Isopropyl Xanthate (SIPX) was modelled using background data from Kunene, M. C. (2014), since an appropriate dataset could not be found in the ecoinvent database for its modelling. The power calculations for pumping, hydrocyclone, and conveyor belt transport can be found in the appendices. Since the concentrate obtained after flotation is 285 tons and the roasting feed concentrate is 500 tons, the material and energy flows from the concentrate plant were upscaled in the LCA model to align with the input requirements of the roasting plant.

Table 11: Material and Energy Flows Obtained from HSC Sim for concentrator plant

Flows	**Quantity**	**Unit**
Jaw Crusher Power	340.97	kW
Gyratory Crusher Power	156.74	kW
SAG Mill	7094.52	kW
Ball Mill	19,715.97	kW
Water for Ball Mill	617	ton
Water for SAG Mill	1018	ton

Ball Mill media	2.43	ton
Ball Mill liners	0.19	ton
Sodium Isopropyl Xanthate (SIPX)	0.2	ton
1,1,3-triethoxybutane (TEB)	0.02	ton
Conditioner water	494.17	ton
Rougher launder water	20.32	ton
Cleaner launder water	149.91	ton
scavenger launder water	207.22	ton
Power Floatation tank electricity	494.77	kW
Scavenger tank electricity	501.21	kW
Cleaner tank electricity	488.08	kW
Water from tails	322.88	m^3
Water from concentrate	2107	m^3

Hydrometallurgical plant

To model the transport impacts of concentrate to the hydrometallurgical plant, a distance of 50m was considered. For the infacility transport of copper-cobalt concentrate, sulphur, and calcine, the mass flows were multiplied by a distance of 0.1 km to determine the ton-kilometre value to model it as conveyor belt transport. Oxygen-enriched gas is used in the roasting process. Since there is no direct flow dataset for oxygen-enriched gas, the additional oxygen content compared to normal air is calculated and converted into a flow. The oxygen concentration in the process gas is 9% higher by volume than in normal air. Therefore, 9% of the total gas volume of 750,000 m^3 (total volume of gas) corresponds to 67,500 m^3 of O_2 gas, which is sourced from liquid oxygen. Given that 1 kg of liquid O_2 expands to 764 L or 0.764 Nm^3 of O_2, the amount of liquid oxygen required to obtain 67,500 Nm^3 of O_2 is 88.35 ton.

Since the energy required by the auxiliary systems used in the fluidized bed furnace for roasting cannot be calculated directly by HSC Sim, literature values were utilized to estimate the energy consumption. According to Pitt and Wadsworth (1980), the energy required for smelting is reported to be between 6.2 and 22.7 million British Thermal Units (BTU) per ton of copper produced. In the case of an electric furnace used for heating in smelting, it is assumed that 80% of the electricity is used for heating, while 20% is allocated to powering auxiliary systems such as temperature control, blowers, exhausts, and scrubbers. For the purpose of this study, an average value of 10 million BTU per ton of copper produced was used for smelting. The lower end of the reported range is chosen due to the use of an old literature source, which reflects less efficient systems. It is assumed that 20% of the electricity used an electric smelting furnace would be used by the fluidized bed reactor's control systems, pumps, exhausts, and other auxiliaries. This equates to an energy consumption of 2 million BTU per ton of copper produced. Given that 175.69 tons of copper are produced during electrowinning, the total energy required for the roasting furnace is estimated to be 102,566.92 kWh. This value is supported by another statement within the same literature source that states electrowinning consumes 73.6% of the energy used in roasting, leaching, electrowinning circuits. The energy value of 102,566.92 kWh is consistent with this claim.

The Life Cycle Inventory (LCI) model also accounts for the preheating of the roasting furnace. Since the roasting reaction is exothermic, natural gas is used to heat the furnace when it is initially started up. The preheating of the roasting furnace was modelled in HSC Sim, which estimates that 22.37 tons of natural gas are required for one preheating cycle. Assuming the furnace is shut down twice a year for maintenance, and with a feed rate of 500 tons per day, the natural gas required for preheating 500 tons of concentrate over the course of a year amounts to 122.9 kg. This value was then converted to the ecoinvent flow "heat, district or industrial, from natural gas," which corresponds to approximately 6,500 MJ.

The sodium sulfate used for gas cleaning is sent to the acid production plant, where it is used to produce sulfuric acid for the leaching and electrowinning processes. Molar calculations were performed based on the Hargreaves process, in which sodium sulfate reacts with carbon and sulphur dioxide to form sodium sulphide, which subsequently reacts with oxygen and water to produce sulfuric acid. To generate 1 kg of sulfuric acid, approximately 1.5 kg of sodium sulfate is required. The amount of sodium sulfate was divided by 1.5 and modelled as the "market for sulfuric acid" flow as an avoided product, recognizing the contribution of sodium sulfate to sulfuric acid production. For modelling the infrastructure, the "market for copper smelting facility" flow was selected and scaled relative to the amount of calcine produced.

HSC Sim provides both the chemical composition and quantity of waste streams. Each waste stream is assigned an appropriate treatment process; otherwise, it is considered an elementary flow. Depending on its composition, a waste stream may be divided into fractions, each undergoing a different treatment method. The scrubber residue contains a mixture of compounds from both the concentrate and calcine. Since it also contains cobalt, it is classified as hazardous waste and is treated through residual material landfill. Similarly, leach residue obtained after filtration in the leaching process is modelled under ‘market for leach residue from copper production’.

In the solvent extraction process, a significant amount of kerosene and organic solvent is used. However, a large portion of these solvents is recovered during the electrowinning step when copper is stripped from the organic phase. Only the portion of the organic phase that is not recovered is reported in the table. Additionally, the organic and aqueous components in the bleed stream and stripped organic stream are presented separately, as they undergo different treatment processes. The organic phase in the waste stream is classified as hazardous waste and is treated through incineration. Meanwhile, the aqueous phase, which contains metal ions and is acidic, is modelled as leach residue.

For a copper electrowinning plant, the energy used per Kg of copper produced is between 1.8 and 2.2 kWh (Forner, Scheepers and Du Toit, 2024). Since 175.69 tons of copper is produced during electrowinning, the energy use for the electrowinning plant is calculated as 386518 kWh.

Similarly, the residues generated during precipitation are treated based on their composition. In HSC Sim, these residues are represented as slurries. The solid fraction of the slurries undergoes appropriate waste treatment processes, while the liquid phase is modelled as wastewater. In the solid fraction of the waste stream, the Al-Fe residue consists of 99% gypsum, with minor amounts of iron and aluminium hydroxide. Therefore, it is modelled as waste gypsum treatment and disposed of in an inert material landfill. However, the Fe-Cu residue from the second precipitation step contains a higher proportion of metal hydroxides, including gypsum, iron hydroxide, aluminium hydroxide, and copper hydroxide. Given that copper hydroxide is classified as toxic, this residue is treated as hazardous waste in the model.

The water used for cooling in the roasting process is assumed to come from natural sources. However, in the hydrometallurgical plant, where multiple chemical processes take place, water purity and composition are crucial. To prevent unwanted carbonate reactions, decarbonized water has been used for gas cleaning and precipitation. For leaching and electrowinning, deionized water has been selected for modelling. The power calculations for cyclone, venturi gas scrubber, leaching reactor, and pumping can be found in Appendices. The flows obtained from HSC Sim from the hydrometallurgical plant are shown in table 13.

Table 12: Material and Energy Flows Obtained from HSC Sim for hydrometallurgical plant

Flows	**Quantity**	**Unit**
Sulphur	50	ton
Water for temperature control	482	ton
Water for scrubbing	3140	ton
Sodium Hydroxide	157	ton
Water for quenching	1119	ton
Sulphuric acid	122.4	ton
Water added in leaching reactor	19717	ton
Wash water for filter	196.63	ton
Kerosene	44.99	ton
LIX 984 N	11.25	ton
Water Addition in copper electrowinning	610.08	ton
Sulfuric Acid in copper electrowinning	131.52	ton
Calcium carbonate (CaCO3)	164.12	ton
Calcium Hydroxide (Ca(OH)2)	150.64	ton

Water for Ca(OH)2 dissolution	61081.28	ton
Wash Water for AF Filter	738.8	ton
Wash Water FC Filter	154.45	ton
Wash Water Co Filter	171.31	ton
Heat for Drying Co(OH)2	24806	kWh
SO2 gas	13.91	ton
CO2 gas	5.57	ton
Water vapour	1755	ton
Scrubber residue	0.65	ton
Sodium Sulphate	277.65	ton
Water in Sodium sulphate solution	2587.64	ton
Leach residue for tailings	202.8	ton
Organic phase in bleed stream	7.48	ton
Aqueous phase in bleed stream	705.96	ton
Aqueous phase in stripped organic	1.43	ton
Al Fe residue solid phase	490.88	ton
Fe Cu residue solid phase	103.00	ton
Water phase in Al Fe residue	163.64	ton
Water phases in Fe Cu residue	33.33	ton
Aqueous phase in precipitation residue	82680	ton
Organic phase in precipitation residue	30.37	ton
Wash Water FCO	171.31	ton

Refining Plant

The transport from the African Copperbelt to China has been modelled by calculating the distance between Durban Port and Shanghai Port (approximately 10,500 nautical miles), with an assumed round-trip road transport distance of four thousand kilometres between the plant and the port. Similar to the precipitation process, the solid and liquid phases of the waste are treated separately and are therefore presented individually. The solid phase of the filter cake has a high content of gypsum. The power calculations for the leaching reactor and pumping can be found in the appendices. The flows obtained from HSC Sim for the refining plant are shown in Table 14.

Table 13: Table 10: Material and Energy Flows Obtained from HSC Sim for refining plant

Flows	Quantity	Unit
Sulphuric Acid	40.36	ton
Water added with sulphuric acid	4107.38	ton
Wash water for filter 2	113.97	ton
Wash water filter CF	173.41	ton
Heat for Drying CoSO4.7H2O	25024.40	kWh
Solid phase in filter cake	75.99	ton
Liquid phase in filter cake	25.3	ton
Wash water out CF	173.41	ton
CoSO4.7H2O Crystals	105.19	ton

4.2.2 Data Normalization

Appropriate datasets from the ecoinvent database were selected to align with the material and energy flows obtained from HSC Sim. Water flows were modelled based on their sources and the required purity levels for different processes. Power calculations were incorporated to determine energy flows, while transportation and infrastructure were also accounted for in the model. Economic allocation was applied from ore processing till hydrometallurgical processing. The entire model was then downscaled to establish the life cycle inventory (LCI) for 1 kg of cobalt sulfate. Table 15 presents the LCI results for 1 kg of battery-grade cobalt sulfate with economic allocation.

Table 14: LCI of 1Kg of Cobalt sulfate heptahydrate

Concentrator plant (Mining + Beneficiation + Froth floatation)			
Input Flows	**Amount**	**Unit**	**Provider**
Explosives used for blasting	1.95E-01	kg	market for blasting | blasting | Cutoff, S - GLO
Energy	4.89E+00	MJ	diesel, burned in building machine | diesel, burned in building machine | Cutoff, S - GLO
Water	3.88E-02	m3	water, unspecified natural origin, ZM
Infrastructure for Concentrate plant	7.79E-11	Item(s)	market for aluminium hydroxide factory | aluminium hydroxide factory | Cutoff, S - GLO
Mine Infrastructure	4.17E-10	Item(s)	market for mine infrastructure, open cast, non-ferrous metal | mine infrastructure, open cast, non-ferrous metal | Cutoff, S - GLO
Mine Infrastructure	4.17E-10	Item(s)	market for mine infrastructure, underground, non-ferrous metal | mine infrastructure,

			underground, non-ferrous metal | Cutoff, S - GLO
Transport	8.34E-02	t*km	market for transport, freight, lorry 16-32 metric ton, EURO4 | transport, freight, lorry 16-32 metric ton, EURO4 | Cutoff, S - RoW
Aluminium	3.19E-01	kg	Elementary flows/Resource/in ground
Calcium	6.45E-01	kg	Elementary flows/Resource/in ground
Carbon	4.22E-01	kg	Elementary flows/Resource/in ground
Cobalt	5.40E-01	kg	Elementary flows/Resource/in ground
Copper	3.87E+00	kg	Elementary flows/Resource/in ground
Iron	7.33E-01	kg	Elementary flows/Resource/in ground
Magnesium	6.29E-01	kg	Elementary flows/Resource/in ground
Phosphorus	1.85E-02	kg	Elementary flows/Resource/in ground
Silicon	2.41E+00	kg	Elementary flows/Resource/in ground
Sulfur	2.04E+00	kg	Elementary flows/Resource/in ground
Titanium	2.00E-02	kg	Elementary flows/Resource/in ground
Electricity	4.12E+00	MJ	market for electricity, medium voltage | electricity, medium voltage | Cutoff, S - ZM
Steel Liners	4.05E-02	kg	market for steel, chromium steel 18/8 | steel, chromium steel 18/8 | Cutoff, S - GLO
Nickel Chrome Ball Mill Media	3.17E-03	kg	market for iron-nickel-chromium alloy | iron-nickel-chromium alloy | Cutoff, S - GLO
Conveyor Belts (Infrastructure)	3.53E-09	m	market for conveyor belt | conveyor belt | Cutoff, S - GLO
In facility transport	1.02E-02	t*km	market for transport, freight, conveyor belt | transport, freight, conveyor belt | Cutoff, S - GLO
Sodium Isopropyl Xanthate (SIPX)	3.34E-03	kg	Background modelling from Kunene, M. C. (2014).
1,1,3-triethoxybutane (TEB)	3.34E-04	kg	market for chemical, organic | chemical, organic | Cutoff, S - GLO
Output Flows	**Amount**	**Unit**	**Provider**
Wastewater	4.05E-02	m3	market for wastewater, average | wastewater, average | Cutoff, S - RoW
Tails	1.33E+01	kg	treatment of sulfidic tailings, from copper mine operation | sulfidic tailings, from copper mine operation | Cutoff, U - ZM
Particulates, < 10 um	2.40E-02	kg	Elementary flows/Emission to air/unspecified
Particulates, < 2.5 um	2.47E-03	kg	Elementary flows/Emission to air/unspecified

Hydrometallurgical Processing plant (Roasting, leaching, solvent extraction, electrowinning and precipitation)			
Input Flows	**Amount**	**Unit**	**Provider**
Sodium Hydroxide	1.49E+00	kg	market for sodium hydroxide, without water, in 50% solution state | sodium hydroxide, without water, in 50% solution state | Cutoff, S - GLO
Electricity	2.22E+01	MJ	market for electricity, medium voltage | electricity, medium voltage | Cutoff, S - ZM
Oxygen	8.40E-01	kg	market for oxygen, liquid | oxygen, liquid | Cutoff, S - RoW
Transport	2.38E-01	t*km	market for transport, freight, lorry 16-32 metric ton, EURO4 | transport, freight, lorry 16-32 metric ton, EURO4 | Cutoff, S - RoW
Sulphur	4.75E-01	kg	market for sulfur | sulfur | Cutoff, S - GLO
Decarbonised Water	6.31E+02	kg	market for water, decarbonised | water, decarbonised | Cutoff, S - ZA
Copper smelting facility	5.01E-10	Item(s)	market for copper smelting facility | copper smelting facility | Cutoff, S - GLO
Infacility Transport	1.05E-03	t*km	market for transport, freight, conveyor belt | transport, freight, conveyor belt | Cutoff, S - GLO
Roasting residue	6.18E-03	kg	market for process-specific burdens, residual material landfill | process-specific burdens, residual material landfill | Cutoff, S - RoW
Water	4.58E-03	m3	water, unspecified natural origin, ZM
Heat from natural gas	6.18E-02	MJ	heat production, natural gas, at industrial furnace >100kW | heat, district or industrial, natural gas | Cutoff, S - RoW
Sulfuric acid	2.41E+00	kg	sulfuric acid production | sulfuric acid |Cuttoff, S-Row
Deionised Water	1.97E+02	kg	market for water, deionised | water, deionised | Cutoff, S - RoW
Kerosene	4.28E-01	kg	market for kerosene | kerosene | Cutoff, S - CH
Limestone	1.56E+00	kg	market for calcium carbonate, precipitated | calcium carbonate, precipitated | Cutoff, S - RoW
Lime	1.43E+00	kg	market for lime, hydrated, loose weight | lime, hydrated, loose weight | Cutoff, S - RoW
Heat	8.49E-01	MJ	market for heat, district or industrial, natural gas | heat, district or industrial, natural gas | Cutoff, S - RoW

Organic Extractant	1.07E-01	kg	market for solvent, organic | solvent, organic | Cutoff, S - GLO
Output Flows	**Amount**	**Unit**	**Provider**
Sulfuric acid	1.76E+00	kg	sulfuric acid production | sulfuric acid |Cuttoff, S-Row (avoided product from sodium sulphate)
Carbon dioxide	5.46E-02	Kg	Emission to air/unspecified
Sulfur dioxide	1.57E-01	Kg	Emission to air/unspecified
Leach Residue	8.64E+00	kg	market for leach residue from copper production | leach residue from copper production | Cutoff, S - GLO
Organic Hazardous Waste	3.60E-01	kg	market for hazardous waste, for incineration | hazardous waste, for incineration | Cutoff, S - RoW
Wastewater	8.14E-01	m3	market for wastewater, average | wastewater, average | Cutoff, S - RoW
Inorganic Hazardous waste	9.79E-01	kg	treatment of hazardous waste, underground deposit | hazardous waste, for underground deposit | Cutoff, S - RoW
Waste gypsum	4.68E+00	kg	treatment of waste gypsum, inert material landfill | waste gypsum | Cutoff, S - RoW
Carbon dioxide	6.85E-01	kg	Emission to air/unspecified
Refining Plant (Re-leaching and Crystallization)			
Input Flows	**Amount**	**Unit**	**Provider**
Electricity	1.36E+01	MJ	market for electricity, medium voltage | electricity, medium voltage | Cutoff, S - CH
Transport	3.96654	t*km	market for transport, freight, lorry 16-32 metric ton, EURO4 | transport, freight, lorry 16-32 metric ton, EURO4 | Cutoff, S - RoW
Transport	19.28728	t*km	market for transport, freight, sea, bulk carrier for dry goods | transport, freight, sea, bulk carrier for dry goods | Cutoff, S - GLO
Sulfuric acid	0.38369	kg	market for sulfuric acid | sulfuric acid | Cutoff, S - RoW
Heat	0.85643	MJ	market for heat, district or industrial, natural gas | heat, district or industrial, natural gas | Cutoff, S - CH
Deionised Water	41.779	kg	market for water, deionised | water, deionised | Cutoff, S - CH
Output Flows	**Amount**	**Unit**	**Provider**
Waste Gypsum	0.7225	kg	market for waste gypsum | waste gypsum | Cutoff, S - CH

Wastewater	0.00189	m3	market for wastewater, average | wastewater, average | Cutoff, S - CH

4.3 Life Cycle Impact Assessment

In the LCIA section, the environmental impacts associated with the production of battery-grade cobalt sulfate are presented and analysed using the ReCiPe 2016 (H) midpoint impact categories. To facilitate comparison and discussion, the impact categories have been grouped into relevant clusters, allowing for a clearer understanding of the various environmental effects. The impact categories have been grouped into related themes, including air pollution, ecotoxicity and eutrophication, human toxicity, resource scarcity, ozone formation and depletion, and water and land use. Ionizing radiation has been excluded due to its low relevance to the cobalt sulfate production process. The environmental impacts have been divided into concentration plant, hydrometallurgy plant and refining plant. Table 16 presents the environmental impacts associated with the production of 1 kg of battery-grade cobalt sulfate using the ReCiPe assessment method.

Table 15: Environmental Impacts of Producing 1 Kg of Battery grade cobalt sulfate based on the ReCiPe Impact Assessment Method

Impact Category	**Unit**	**Concentration plant**	**Hydro-metallurgy plant**	**Refining Plant**	**Total**
Global Warming	kg CO2 Eq	1.898	9.142	1.067	12.107
Fine Particulate Matter Formation	kg PM 2.5 eq	0.018	0.056	0.004	0.078
Terrestrial Acidification	kg SO2 Eq	0.057	0.173	0.013	0.243
Fresh Water Ecotoxicity	kg 1,4 DCB eq	2.671	2.034	0.114	4.819
Terrestrial Ecotoxicity	kg 1,4 DCB eq	20.178	33.455	23.012	76.645
Marine Ecotoxicity	kg 1,4 DCB eq	3.321	2.554	0.156	6.031
Fresh water Eutrophication	kg P eq	0.003	0.005	0.000	0.009
Marine Eutrophication	kg N eq	0.000	0.005	0.000	0.006
Human Carcinogenic Toxicity	kg 1,4 DCB	0.569	0.737	0.071	1.377
Human Non-Carcinogenic Toxicity	kg 1,4 DCB	26.421	25.244	2.513	54.179

Mineral Resource Scarcity	kg Cu eq	1.068	0.037	0.009	1.113
Fossil Resource Scarcity	kg Oil Eq	0.441	2.451	0.347	3.239
Land Use	m2a crop Eq	0.034	0.143	0.041	0.218
Water Consumption	m3	0.046	0.226	0.088	0.359
Ionizing Radiation	kBq Co-60-eq	0.039	0.411	0.621	1.051
Ozone Depletion	kg CFC Eq	0.000009	0.000005	0.00000083	0.00001
Ozone Formation, Human Health	kg NOx Eq	0.075	0.023	0.006	0.103
Ozone Formation Terrestrial Ecosystems	kg NOx Eq	0.077	0.022	0.006	0.105

4.3.1 Impact Categories Associated with Affecting Air Quality

Global warming potential (GWP), fine particulate matter formation (FPMF), and terrestrial acidification have been grouped together as they are all primarily driven by the release of airborne pollutants. Climate change is influenced by greenhouse gases like CO2, acidification is caused by sulphur dioxide (SO2) and nitrogen oxides (NOx), and fine particulate matter formation results from the combustion of fossil fuels and industrial emissions. The contribution analyses of global warming potential, fine particulate matter formation, and terrestrial acidification are shown in Figure 21.

The global warming potential of one kilogram of battery grade cobalt sulphate is 12.1 kg CO2 Eq. The highest overall contributions are from the processes 'market for sodium hydroxide' and 'market for lime, hydrated' and 'market for electricity, medium voltage' respectively. Approximately sixteen percent of the impacts are from the concentrator plant, seventy five percent are from hydrometallurgical plant and nine percent are from refining. Both lime and sodium hydroxide are used in hydrometallurgical processing. In the concentration plant, the highest impacts are from 'market for blasting' and 'diesel, burned in building machine' respectively. In the refining plant, the highest impacts are attributed to the transport of impure cobalt hydroxide from the plant to the port.

The total impact for fine particulate matter formation is 0.078 kg PM 2.5 eq. Seventy-one percent of the impacts are associated with the hydrometallurgy plant, twenty-three percent with the concentration plant, and six percent with the refining plant. The most significant overall impacts stem from the 'market for blasting' in mineral processing, and 'market for sodium hydroxide' and 'market for medium voltage' in hydrometallurgical processing. Within refining, the highest impacts are linked to the 'market for waste gypsum.' The terrestrial acidification to produce one kilogram of battery grade cobalt sulphate is 0.243 Kg SO2 Eq. The impacts from terrestrial acidification follow the same trend as those of the fine particulate matter formation category, with the same processes contributing most significantly.

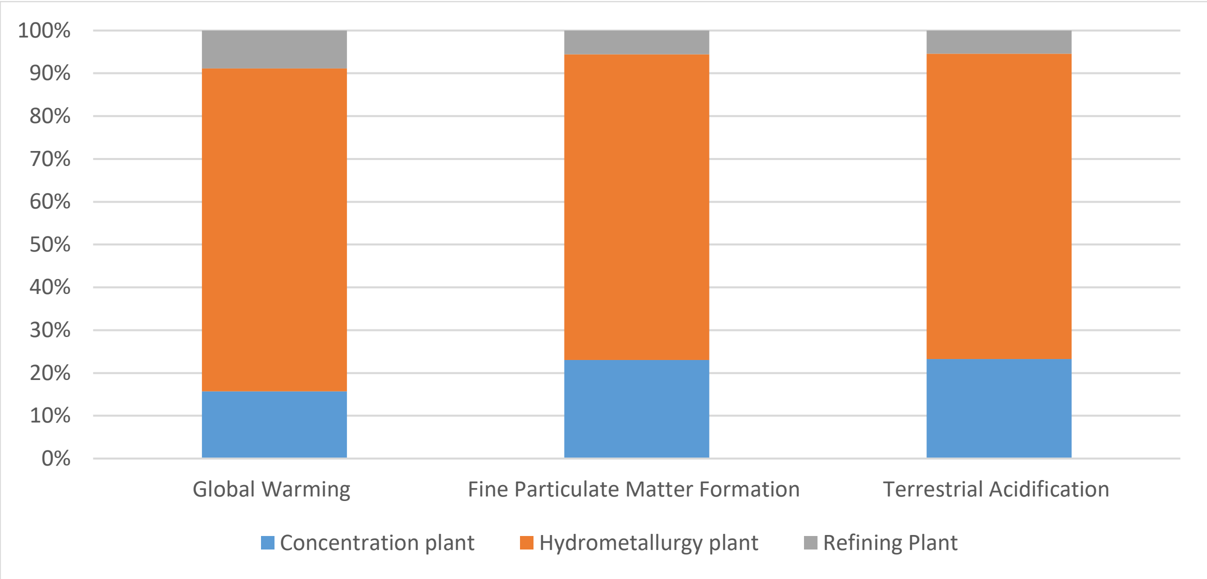

Figure 21: Contribution Analysis of Global warming, Fine particulate Matter formation and Terrestrial Acidification

4.3.2 Ecotoxicity and Eutrophication

The ecotoxicity and eutrophication impact category in ReCiPe assesses the potential harm to aquatic and terrestrial ecosystems due to the release of toxic substances and nutrient enrichment respectively. Ecotoxicity refers to the harm caused by chemical pollutants to ecosystems, affecting biodiversity and disrupting organisms, while eutrophication involves the excessive enrichment of ecosystems with nutrients, leading to issues like algal blooms and oxygen depletion. The unit of ecotoxicity kg 1,4-DCB Eq refers to kilograms of 1,4-dichlorobenzene equivalents. It is used in the context of ecotoxicity to express the potential impact of a substance in relation to the toxicity of 1,4-dichlorobenzene, which is a reference substance. The contribution analyses of fresh water, marine and terrestrial ecotoxicity and freshwater and marine eutrophication are shown in Figure 22.

The total impact for producing 1 kg of cobalt sulfate is 4.819 kg 1,4 DCB eq for fresh water ecotoxicity. 55.5% of the impacts are attributed to mineral processing, 42.2% to hydrometallurgical processing, and 2.4% to refining. The highest impacts come from 'treatment of sulfidic tailings' (52%) in mineral processing and 'market for leach residue' (35%) in the hydrometallurgy plant, while other processes do not significantly contribute to fresh water ecotoxicity. Marine ecotoxicity has a total impact of 6.031 kg 1,4 DCB eq for producing 1 kg of cobalt sulfate. The impacts from marine ecotoxicity follow the same trend as those of the fresh water ecotoxicity category, with the same processes contributing most significantly.

The total impact for producing 1 kg of cobalt sulfate is 76.645 kg 1,4 DCB eq for terrestrial ecotoxicity. The highest contribution of 43.6% comes from the hydrometallurgical plant, followed by 30% from the refining plant and 26.4% from the concentration plant. The processes with the highest contributions are 'market for transport, freight, lorry 16-32 metric tons' and 'market for sulfuric acid' from the refining process, and 'market for sodium hydroxide' from the hydrometallurgical processing respectively.

The total impact for producing 1 kg of cobalt sulfate is 0.009 kg P eq for freshwater eutrophication. The hydrometallurgical plant has the highest contribution of 59.6%, and the concentration plant has a contribution of 37.5%. While the contribution of the refining plant is negligible. The highest contributing process is treatment of sulfidic tailings from mineral processing (31.8%), followed by market for leach residue (21.8%) and market for sodium hydroxide (10.2%) from hydrometallurgical processing. The total impact for producing 1 kg of cobalt sulfate is 0.006 kg N eq for marine eutrophication. The contributions to marine eutrophication are predominantly from the process 'market for wastewater average,' which accounts for 91.4% of the total impact. The hydrometallurgical plant is responsible for 87% of the contribution to this process while the rest is from the concentration plant.

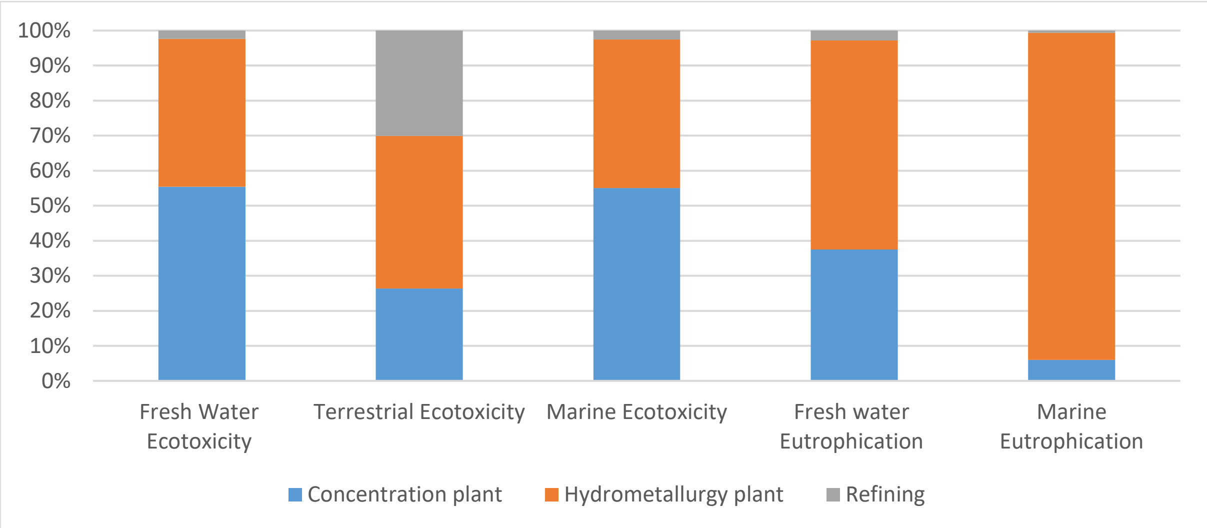

Figure 22: contribution analyses of fresh water, marine and terrestrial ecotoxicity and freshwater and marine eutrophication

4.3.3 Human Carcinogenic and Non-Carcinogenic Toxicity

Human carcinogenic toxicity (HCT) and human non-carcinogenic toxicity (HNCT) impacts are measured in Kg 1,4-DCB eq (kilogram 1,4-dichlorobenzene equivalent) as well. This unit compares the toxicity of various substances to the effect of 1,4-dichlorobenzene, providing a standardized measure for human health risks associated with carcinogenic and non-carcinogenic effects. The contribution analyses of human carcinogenic toxicity and human non carcinogenic toxicity are shown in Figure 23.

The total impact for producing 1 kg of cobalt sulfate is 1.377 kg 1,4 DCB eq for human carcinogenic toxicity. 53.5% of the impacts, are attributed to hydrometallurgical processing, followed by 41.3% from mineral processing, and 5.2% from refining. The highest contributing processes include 'market for chromium steel' in mineral processing, and 'market for wastewater' (11.3%) and 'market for sodium hydroxide' (9.3%) from hydrometallurgical processing.

For human non-carcinogenic toxicity, the total impact is 54.179 kg 1,4 DCB eq. The contributions from mineral processing and hydrometallurgical processing are nearly equal at 47.5% each, with refining contributing 5%. The most significant processes include 'treatment of sulfidic tailings' (43.5%) from mineral concentration, and 'market for leach residue' (29%) and 'market for wastewater' (4.6%) from hydrometallurgical processing.

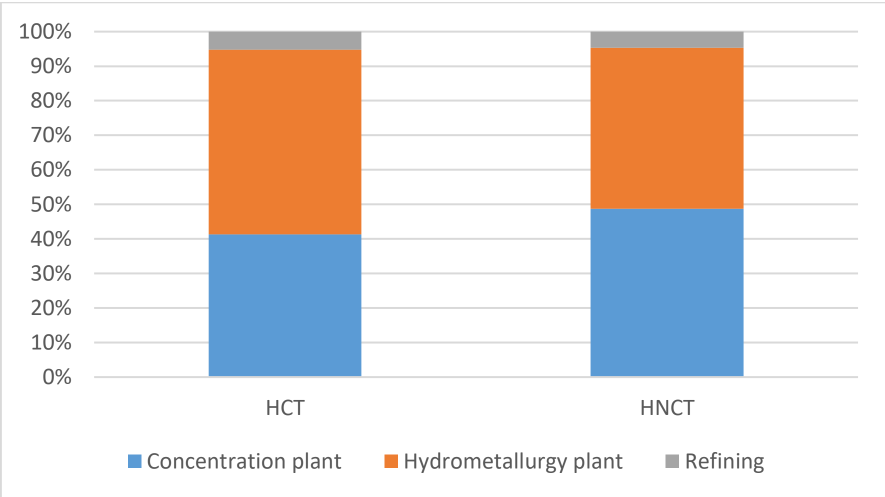

Figure 23: contribution analyses of human carcinogenic toxicity and human non carcinogenic toxicity

4.3.4 Mineral and Fossil Resource Scarcity

Mineral resource scarcity measures the depletion of mineral resources, reflecting the environmental impact of extracting non-renewable metals and minerals. It is expressed in kg Cu eq (kilograms of copper equivalent), representing the scarcity-weighted extraction of resources. The production of 1 kg of cobalt sulfate results in a mineral resource scarcity impact of 1.113 kg Cu eq. Mining is the primary contributor, directly accounting for 1.04 kg Cu eq due to the extraction of minerals from the ground. The mineral concentration plant is responsible for 96% of the total impact.

Fossil resource scarcity quantifies the depletion of fossil fuels such as coal, oil, and natural gas, assessing their long-term availability and environmental impact. It is measured in kg oil eq (kilograms of oil equivalent), indicating the energy content of the extracted fossil resources. The production of 1 kg of cobalt sulfate results in a fossil resource scarcity impact of 3.239 kg oil eq. The hydrometallurgical plant is the largest contributor, responsible for 75.7% of the impact, followed by the mineral concentration plant at 13.6% and the refining plant at 10.7%.

Key contributing processes in the hydrometallurgical stage include ‘market for kerosene,’ ‘market for sodium hydroxide,’ and ‘market for electricity, medium voltage.’ In refining, the primary impact stems from ‘market for transport, freight, lorry,’ while in mineral processing, ‘market for blasting’ is the highest contributor. The contribution analyses of mineral resource scarcity and fossil resource scarcity are shown in Figure 24.

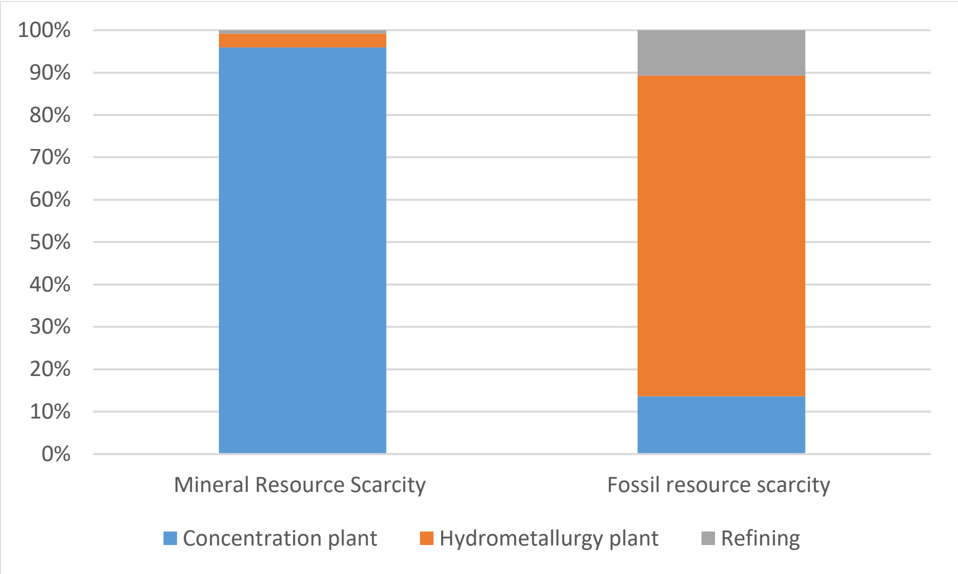

Figure 24: contribution analyses of mineral resource scarcity and fossil resource scarcity

4.3.5 Water and Land Use

In the ReCiPe method, land use is measured in m^2a crop eq, representing the area occupied for one year with its impact on ecosystem quality. It considers both land occupation and transformation, reflecting environmental pressures like habitat destruction and soil degradation. The total land use impact for producing 1 kg of cobalt sulfate is 0.218 m^2a crop eq. The hydrometallurgical plant contributes the most at 65.9%, followed by refining (18.6%) and the concentration plant (15.5%). The key contributing processes include ‘treatment of hazardous waste, underground deposit’ (18.5%) and ‘market for sodium hydroxide’ (14%) from hydrometallurgical processing, as well as ‘market for transport, freight, lorry’ from refining. The most significant process in the mineral concentration plant is ‘market for blasting’ with an overall contribution of 8%.

The total water consumption impact for producing 1 kg of cobalt sulfate is 0.359 m^3. The hydrometallurgical plant has the largest contribution at 62.7%, followed by refining (24.6%) and mineral processing (12.7%). The primary contributing processes overall are ‘market for water, decarbonised’, ‘market for water, deionised’, and ‘market for sodium hydroxide’ from the hydrometallurgical plant. In the refining plant, ‘market for water, deionised’ is the most significant, while in mineral processing, the contribution comes from direct emissions of naturally sourced water used in mining. The contribution analyses of water and land use are shown in Figure 25.

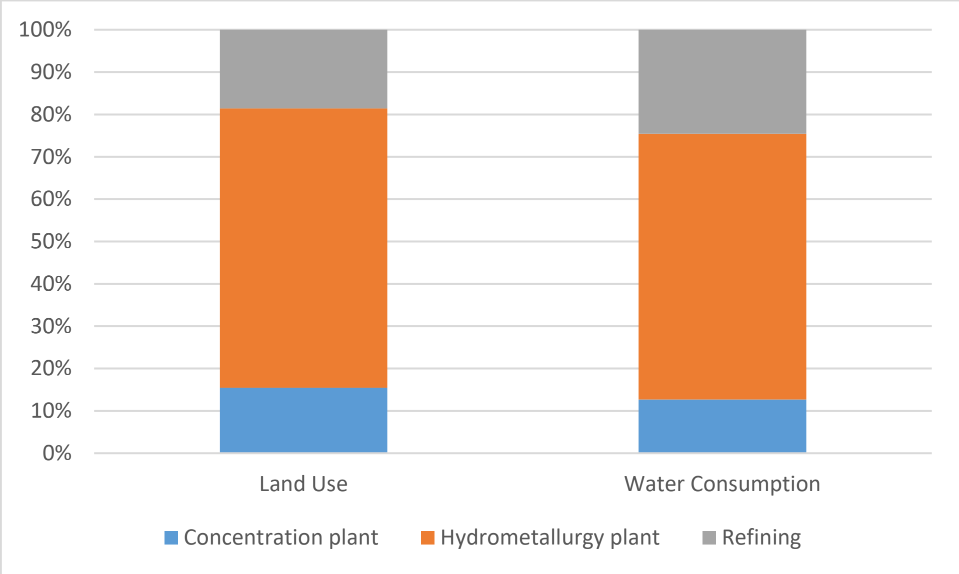

Figure 25: The contribution analyses of water and land use

4.3.6 Stratospheric Ozone Depletion and Ozone Formation

Stratospheric ozone depletion measures the potential degradation of the ozone layer due to emissions of substances like CFCs and halons, leading to increased UV radiation exposure. Ozone formation, on the other hand, evaluates the contribution of precursor emissions (e.g., NO_x and volatile organic compounds) to tropospheric ozone formation, which impacts air quality and human health.

The total impact for producing 1 kg of cobalt sulfate is 0.00001 kg CFC eq for ozone depletion, 0.103 kg NOx eq for ozone formation, human health and 0.105 kg NOx eq for ozone formation, terrestrial ecosystems. In all categories, the concentration plant has highest contribution due to the use of process 'market for blasting'. Figure 26 shows the contribution analyses of stratospheric ozone depletion, ozone formation, human health and ozone formation, terrestrial ecosystems.

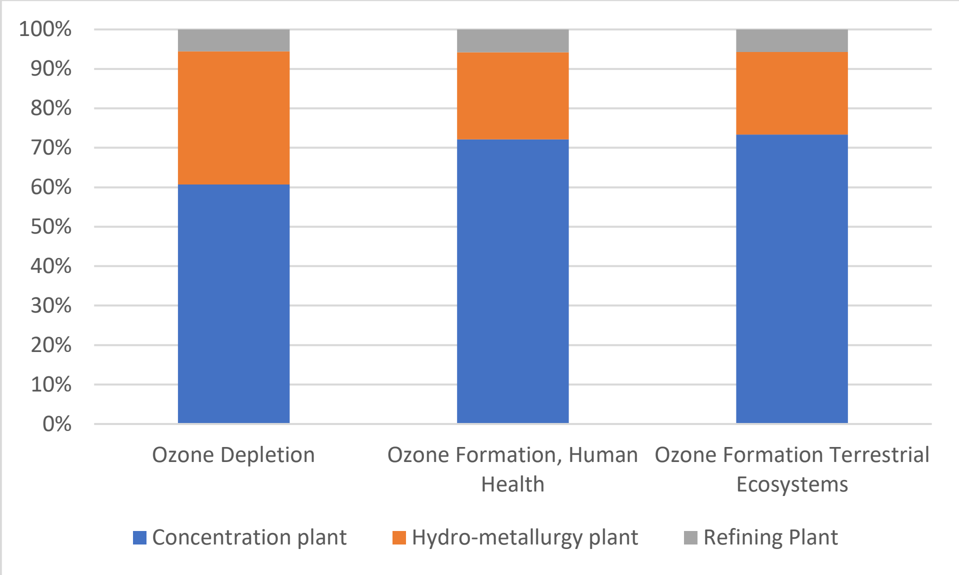

Figure 26: The contribution analyses of stratospheric ozone depletion, ozone formation, human health and ozone formation, terrestrial ecosystems.

4.4 Interpretation

4.4.1 Results and Discussion

Identification of Key Relevant Findings

In Figure 27, which presents the contribution analysis for producing 1 kg of cobalt sulfate across all ReCiPe impact categories, the hydrometallurgy plant is identified as the largest contributor in most impact categories, followed by mineral processing and refining.

The Hydro-metallurgy plant is a significant contributor across multiple environmental impacts, particularly those related to resource depletion, toxic emissions, and eutrophication. This suggests that processes in this plant are likely more resource and energy-intensive, with a higher environmental footprint due to chemical usage, water consumption, and emissions. Hydrometallurgical processing has the highest impacts in global warming (75.5%), fine particulate matter formation (71.8%), terrestrial acidification (71.2%), freshwater ecotoxicity (42.2%), terrestrial ecotoxicity (43.6%), freshwater eutrophication (55.6%), marine eutrophication (83.3%) and fossil resource scarcity (75.7%).

The high environmental impact of the hydrometallurgical process is primarily attributed to the use of sodium hydroxide, which plays a critical role in facilitating sulphur dioxide (SO_2) capture during roasting and its subsequent conversion into sulfuric acid. By considering the molar ratio of sodium sulfate to sulfuric acid (1.5) and treating sulfuric acid as an avoided product, the negative environmental impacts associated with its production help offset both the overall burden of sulfuric acid consumption in hydrometallurgical processing and the direct emissions of sulphur dioxide into the atmosphere.

Among the various impact categories, sodium hydroxide usage emerges as the most significant contributor to global warming potential, particulate matter formation, terrestrial acidification, and terrestrial ecotoxicity. Sulfuric acid would have been the dominant contributor to terrestrial acidification had the avoided burden from its production via sodium hydroxide not been accounted for. Additionally, the market for leach residue generated during leaching and the bleed stream from copper electrowinning represents the highest contributor to freshwater ecotoxicity and freshwater eutrophication. In terms of fossil resource depletion, the primary contributor is kerosene consumption in the solvent extraction process.

The concentration plant has the highest impacts in categories related to mineral resource extraction, stratospheric ozone depletion, and ozone formation, indicating that mineral extraction processes involve ozone-depleting chemicals, contributing to its high environmental burden. It is identified as a hotspot for mineral depletion and atmospheric impacts. The market for blasting process has the overall highest impacts in stratospheric ozone depletion, and ozone formation, terrestrial and human health. Within the concentration plant, the blasting process in mining is the primary contributor to global warming, fine particulate matter formation, fossil resource scarcity, and land use impacts. Blasting process releases NOx gasses, and non-methane volatile organic compounds (NMVOC) resulting in these impacts.

The refining plant has significant contributions in water consumption (24.5%), terrestrial ecotoxicity (30%), land use (18.8%). The high demands in water consumption are primarily due to deionised water required in the leaching and crystallization processes. Significant impacts are associated with transportation from Africa to China, especially road transport by lorry which has the highest contribution to refining in terrestrial ecotoxicity and land use.

The hydrometallurgy plant is the largest contributor to water consumption (63%) and freshwater ecotoxicity (42.2%), emphasizing its high resource intensity in terms of water use and quality impacts. This underscores the need for improved water management strategies and the adoption of sustainable water usage practices to mitigate environmental effects. Hydro-metallurgy plant contributes significantly (83.3%) to marine eutrophication. The process market for wastewater in the Hydro-metallurgy plant has direct emissions of nutrient discharges (such as phosphates and nitrates) during processing. This suggests a need for advanced wastewater treatment or alternative methods to reduce eutrophication.

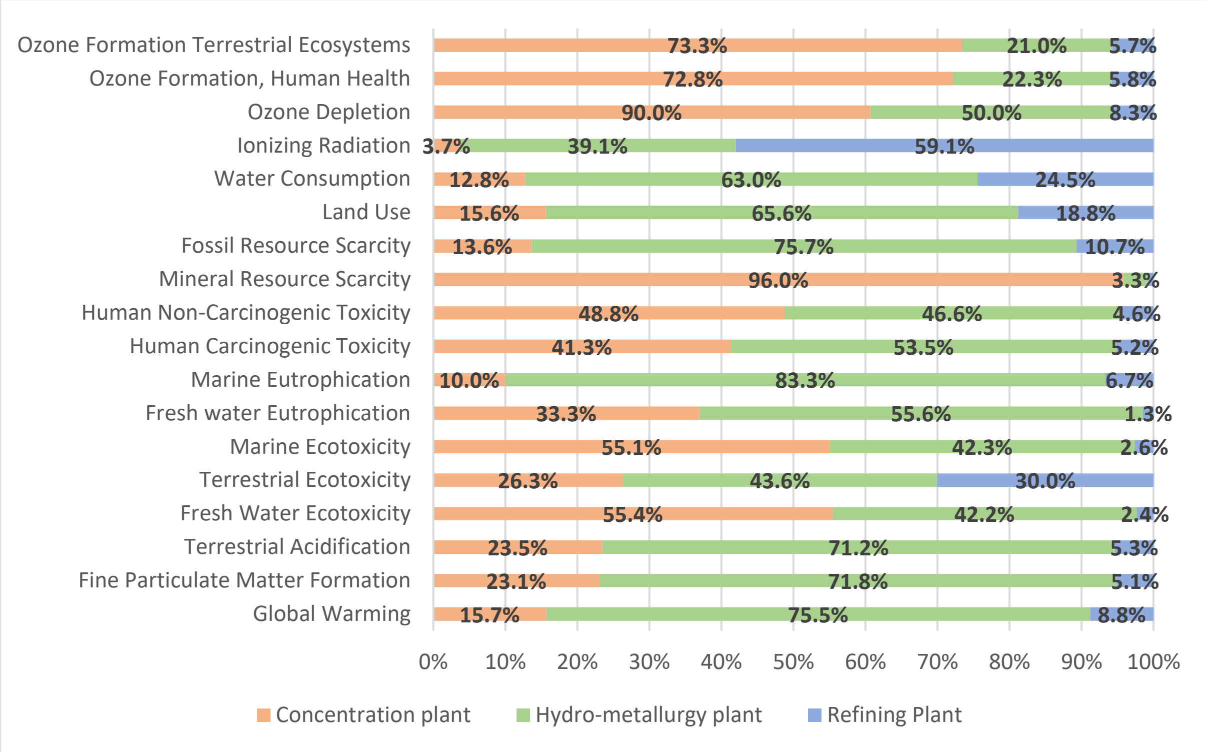

Figure 27: Contribution Analysis for Producing 1 kg of Cobalt Sulfate Across All ReCiPe Impact Categories.

Comparison with other datasets

The ecoinvent model for cobalt sulfate production has a GWP of 24.7 kg CO_2 eq. This dataset integrates the 'market for cobalt hydroxide' model (Cobalt Development Institute, 2016) covering processes from mining to cobalt hydroxide production, followed by the GREET model for conversion to cobalt sulfate (Dai et al., 2018). The cobalt hydroxide dataset aggregates multiple process flows, including extraction from nickel-cobalt lateritic and sulfidic ores via pyrometallurgical and pressure leaching routes. Consequently, while it provides an estimate, it is not directly comparable to the current model, which focuses solely on a defined process flow from copper-cobalt ores. Additionally, since nickel has a higher GWP than copper (Norgate, T., et al., 2000), it can be inferred that cobalt production as a byproduct of nickel processing results in a higher carbon footprint compared to cobalt extraction from copper-cobalt ores.

The obtained value for global warming potential in this study is within range of literature sources. The range for GWP between various cobalt sulphate sources is between 4.0 kg CO_2 Eq (Cobalt institute) and 35.6 kg CO_2 Eq (Zhang et al., 2021). It has three times more than the GWP obtained by the study from cobalt institute. Additionally, hydrometallurgical processing was identified as the key contributor in this study. The study by Rinne et al., (2021), also identifies hydrometallurgical processing as the key contributor. This study also uses process simulation for determining the environmental impacts of cobalt sulphate. In the study by Farjana et al., (2019), the GWP for 1 kg of cobalt was determined as 11.73 kg CO_2 Eq.

The refining step is identified to have the lowest environmental impact in this LCA. The GWP of only the re-leaching and crystallization is 1.07 kg $CO_{2\ Eq.}$ In comparison to the results of refining study done Minviro, (2020) for first cobalt, the refining stage has significantly lesser impacts. The results generated by Minviro had a GWP of 1.58 kg $CO_{2\ Eq}$ for a refinery in Canada which was lower than the value for the refinery in China which had a GWP of 3.25 kg $CO_{2\ Eq.}$

The GREET model by Dai et al. (2018) does not discuss the life cycle assessment results of production of cobalt sulfate heptahydrate. Instead, it provides the life cycle inventory (LCI) for cobalt sulfate production from cobalt hydroxide, reported per ton of cobalt equivalent. Prior to this stage, the LCI is aggregated for both copper and cobalt hydroxide production. The refining process used in the GREET model consumes significantly more energy, water, and reagents compared to the re-leaching and crystallization process analysed in this study. In the GREET model, the refining step involves leaching cobalt hydroxide, followed by two solvent extraction stages. Cobalt is then back extracted using sulfuric acid to produce cobalt sulfate, which subsequently undergoes crystallization and drying. However, due to the lack of detailed process parameters for these steps in the available literature, this process could not be modelled in HSC Sim for this study. As a result, one of the reasons for the lower global warming potential (GWP) in this study is the different approach taken in the refining process.

The ore grade used for modelling in HSC had a significantly higher copper and cobalt content, with 22.8% Cu and 3.2% Co. In comparison, the ore grade used in the GREET model had 2.44% Cu and 0.47% Co. The ore composition for the HSC modelling was obtained from a literature source that provided a 100% weight composition of all the minerals present in the ore. This level of detail was necessary to accurately capture the ore's chemistry within the model. Because of the high ore grade, the impact from the ore concentration plant is low as a lower ore grade would require more mining, beneficiation and froth floatation. This would significantly increase impacts from the concentration plant.

Additionally, the composition of the concentrate obtained after froth flotation differs between low-grade and high-grade ores. A low-grade ore concentrate would contain more impurities and have lower copper and cobalt content compared to a high-grade ore concentrate. Consequently, processing a low-grade concentrate would require higher amounts of reagents and energy in the hydrometallurgical stage. However, the increase in environmental impacts would not be as significant as those from the concentration plant. By increasing the environmental impacts of mining seven times, which is the approximate ratio between copper and cobalt in the ore grades, in the LCA model, the global warming potential (GWP) was found to be 23.5 kg CO_2-eq. The concentration plant accounts for 56.5% of the total emissions in this case.

Furthermore, the ore composition did not consist of nickel and zinc. Zinc has an additional removal process before refining where it is separated either via solvent extraction or precipitation (Crundwell et al., 2020). While nickel is separated during the refining process when crude cobalt sulfate undergoes multiple solvent extraction steps. Not including these additional process steps in the model also contributes to lower environmental impacts.

HSC modelling relies on thermodynamic data and is highly useful for eco-design, as it helps optimize processes for maximum efficiency. However, due to the lack of industrial data, the processes in this study were modelled under ideal conditions, assuming the highest possible efficiency when the yield or efficiency was not known from literature. In real life situations, industrial operations are often less efficient, leading to higher emissions.

4.4.2 Process Optimization

The most significant impact in the study was from the use of sodium hydroxide used in roasting process for gas cleaning and sulfuric acid production. Process simulation has the benefit of pinpointing hotspots within the process flow. By identifying the details relating to the key impacts in a process flow, optimizations can be made in the production process to make the production more sustainable.

4.4.3 Consistency

The functional unit of production of 1 kg of cobalt sulfate remains consistent throughout the LCA. The HSC Sim model ensures mass and energy balances within the model. Data has been normalized accordingly for mining as it was not taken from the HSC Sim model. All assumptions made during the modelling have been documented. Where possible representative datasets have been chosen from ecoinvent database, where it was not available a proxy dataset has been used for sodium isopropyl xanthate used in froth floatation.

4.4.4 Limitations

The acid production plant does not fall within the system boundaries of the LCA model. Because of the interconnectedness of sodium hydroxide for sulphur dioxide gas capture to produce sulfuric acid, the acid production plant plays an important role in understanding the environmental impacts of hydrometallurgical processing.

To better determine the impacts, a sensitivity analysis should be conducted representative of the ore composition of the African Copperbelt. However, using a completely different ore composition would require HSC Sim modelling of all the processes according to its chemistry which is a time-consuming task.

HSC Sim does not have the capability to calculate energy flows for chemical processes. Therefore, energy consumption values were sourced from literature to estimate the energy use within the model. However, these values are generalized and may not accurately reflect the specific conditions of the current model. The applicability of these estimates remains uncertain, as they may not precisely correspond to the actual energy requirements of the modelled processes.

The waste treatment processes modelled in the life cycle assessment (LCA) are based on the composition of the generated waste. However, a more detailed understanding of industrial waste management practices is necessary to determine whether these treatment methods align with real-world scenarios. The lack of specific industrial data introduces uncertainty in the assessment of waste treatment impacts.

The cobalt sulfate heptahydrate obtained from the HSC model serves as the functional unit in this study, as it is assumed to be of high purity without impurities. However, if the same re-leaching and crystallization route were implemented in industrial settings, the resulting purity levels may differ due to variations in process conditions, raw material quality, and operational efficiencies.

The model focuses solely on the technological aspects of production and does not account for additional operational emissions associated with plant activities. Energy and resource consumption related to non-technological aspects, such as office operations, employee commuting, and facility maintenance, are excluded from the energy consumption estimates.

4.4.5 Conclusion

The LCA of cobalt sulphate heptahydrate using process simulation developed to provide a more accurate representation of the environmental impacts associated with cobalt sulfate production. The custom dataset was created using process simulation software HSC Chemistry. Data for the simulation was taken from literature sources. The results reveal that the battery grade cobalt sulfate dataset emissions are within range of other studies relating to cobalt or cobalt sulfate. The environmental impacts of the custom cobalt sulphate dataset are on the lower range of the literature. The value obtained for GWP was 12.1 kg CO_2 Eq. This can be attributed to the alternate approach taken for refining and the high ore grade selected for the study. The highest impacts were associated with hydrometallurgical operations involving roasting, leaching, solvent extraction, copper electrowinning and precipitation.

The key finding from this LCA is that the custom process specific LCI generated via process simulation provides a more regionally specific and process-refined approach to assessing the environmental impact of cobalt sulfate production as compared to other studies. The lower emissions associated with this dataset can be reflected by process optimizations and improved efficiencies that are not captured in other studies or datasets.

Additionally, expanding the analysis to include a broader range of production scenarios and geographical contexts would strengthen the relevance of these findings and improve the accuracy of future LCAs in the field of lithium-ion battery materials.

5 Comparative Life Cycle Assessment of NMC 811 oxide and NMC 111 oxide

5.1 Introduction

Lithium-ion batteries (LIBs) are widely used in electric vehicles (EVs), consumer electronics, and energy storage systems due to their high energy density, long cycle life, and efficiency. One of the key components of a lithium-ion battery is the cathode active material (CAM), which plays a crucial role in determining the battery's performance, capacity, and stability. In nickel-manganese-cobalt (NMC) batteries, the cathode active material is typically a lithium metal oxide derived from precursor materials.

NMC precursor materials are intermediate compounds, usually in the form of hydroxides or carbonates, that undergo calcination with lithium salts to form the final cathode material (Zhang, X., Belharouak, I., Lei, D., et al., 2019). These precursors are essential in determining the chemical composition, particle morphology, and electrochemical properties of the cathode material. Two common types of NMC oxides are NMC 111 and NMC 811, which differ in their nickel (Ni), manganese (Mn), and cobalt (Co) ratios.

NMC 111 oxide refers to $LiNi_{1/3}Mn_{1/3}Co_{1/3}O_2$, where nickel, manganese, and cobalt are present in equal proportions. This composition offers a balance between thermal stability, cycle life, and electrochemical performance. However, due to the relatively high cobalt content, it is more expensive and associated with supply chain concerns. NMC 811 oxide, $LiNi_{0.8}Mn_{0.1}Co_{0.1}O_2$, has a much higher nickel content while reducing cobalt dependency. This leads to higher energy density and improved specific capacity, making it more suitable for next-generation lithium-ion batteries. However, the increased nickel content results in reduced structural stability and has a greater sensitivity to moisture and thermal degradations (Manthiram, A., 2020, Xu, G., Zhang, X., Li, X., et al., 2021). Understanding the environmental impacts and efficiency of different synthesis routes is critical for optimizing battery production and ensuring sustainable material sourcing.

5.1.1 The NMC Production Process

The production of these cathode materials involves hydrometallurgical processing, where cobalt, nickel, and manganese are extracted, purified, and combined in controlled ratios to form the precursor. The production of the desired oxide ($Li_aNi_xMn_yCo_zO2$) begins with the reaction of substrate solutions, such as MSO4 (where M = Ni, Mn, or Co), with a carbonate or hydroxide to form the corresponding carbonate or hydroxide coprecipitates (Wang et al., 2004). In the reactions, M stands for metal.

$$MSO_4 + Na_2CO_3 \rightarrow MCO_3\downarrow + Na_2SO_4 \quad (39)$$
$$MSO_4 + 2NaOH \rightarrow M(OH)_2\downarrow + Na_2SO_4 \quad (40)$$

After drying, the carbonate powder is mixed with lithium carbonate or hydroxide and calcined to produce the desired oxide, as shown in the following reaction:

$$xNiCO_3 + yMnCO_3 + zCoCO_3 + a/2Li_2CO_3 \rightarrow Li_aNi_xMn_yCo_zO_2 + (x+y+z+a/2)\ CO_2 \qquad (41)$$

Li_2CO_3 is used in the production of NMC111, while LiOH is used in the production of NMC811. Li_2CO_3 is used for LCO, NMC 111, and NMC 622 because these materials can withstand higher sintering temperatures (≥850°C). In contrast, LiOH is preferred for NMC 811 and NCA as it allows for lower synthesis temperatures (~750°C), which helps stabilize nickel-rich structures and reduces lithium loss during calcination. Nickel-rich compositions are more sensitive to high temperatures, making LiOH the better choice for ensuring proper phase formation and electrochemical performance (Xu *et al.*, 2012).

5.2 Goal and Scope

5.2.1 Goal

The Life Cycle Assessment of NMC oxide 111 and NMC oxide 811 analyses the environmental impacts of the production of the cathode active material in various NMC compositions. The objective aims to evaluate and compare the environmental footprints of various NMC CAM compositions with various cobalt content, with a focus on global warming potential. The cobalt sulfate heptahydrate dataset obtained from the previous LCA is used in pre-existing datasets of NMC811oxide and NMC111 oxide to form a comparison of differing amounts of cobalt sulphate concentration in the CAMs. The NMC 111 contains approximately 33.3% cobalt, 33.3% nickel, and 33.3% manganese, while NMC 811 contains 80% nickel, 10% manganese, and 10% cobalt. The difference in cobalt concentrations between these two compositions is especially significant, making them ideal for evaluating the environmental impacts related to cobalt content reduction in battery production. The LCA offers insights and recommendations to shape sustainable battery design and production processes.

This comparative LCA primarily targets researchers, academics, and professionals in fields related to battery technology, sustainability, and materials science and engineering. Key audiences include battery manufacturers, material suppliers, and companies involved in cobalt sourcing and recycling. Additionally, the study targets policymakers and regulatory bodies focused on the environmental impacts of electric vehicle (EV) batteries, as well as investors and stakeholders in the EV and renewable energy sectors.

The target audience also includes eco-design professionals seeking to develop more sustainable battery technologies and sustainability experts evaluating the lifecycle impacts of materials used in energy storage systems. By examining the environmental implications of different NMC oxide chemistries, this research provides valuable insights for stakeholders aiming to reduce the environmental footprint of battery production and enhance the sustainability of electric vehicle technologies.

5.2.2 Scope of the Study

The scope of the study gives information on the choices of functional unit, system boundaries, allocation, impact methodology and categories, made to define the study.

Functional Unit

The functional unit serves as the reference basis for quantifying environmental impacts, ensuring consistency in system boundary definition and comparability of results (ISO 14040, 2006). The functional unit of the study is defined as, “Production of 1 kg of NMC oxide with varying cobalt concentrations in China.” These environmental impacts are calculated based on the declared unit wherein each flow related to material consumption, energy consumption, emissions, effluent and waste is scaled to the reference flow.

System Boundaries

The LCA study follows a cradle-to-gate approach, covering all stages from resource extraction to the production of NMC oxide. The system includes the mining and refining of key battery materials such as cobalt, nickel, manganese, and lithium. Cobalt, nickel, and manganese are refined into their respective sulphate salts. These compounds, along with lithium hydroxide or carbonate, are then mixed to form a stable precursor material (e.g., nickel cobalt manganese hydroxide). The precursors are then subjected to high-temperature calcination and milling to produce the final NMC oxide material. This stage involves energy inputs, including natural gas and electricity, as well as emissions associated with the heat treatment processes.

The transportation of raw materials (cobalt, nickel, manganese, lithium) from extraction sites to processing and refining locations is included in the study. However, downstream processes such as battery assembly, use, and end-of-life are excluded. The final production of NMC oxide materials, NMC 111 and NMC 811, is the point where the material is ready for use in battery manufacturing. The energy mix in China is considered throughout the study, reflecting the regional energy profile's impact on the production process.

The geographical scope of the comparative LCA study of NMC oxide chemistries is placed in China as China is the world's largest producer and processor of key battery materials, including cobalt, nickel, manganese, and lithium. Most of the NMC cathode active materials are manufactured in China. Additionally, the cobalt sulphate dataset developed in this study is also refined in China. Using China as a geographical basis reflects real-world supply chain impacts as China dominates the global battery supply chain. Thus, LCA conclusions drawn from this study are relevant to international stakeholders, including automakers, policymakers, and sustainability researchers. Fig 28 shows the system boundaries of the NMC oxide production process.

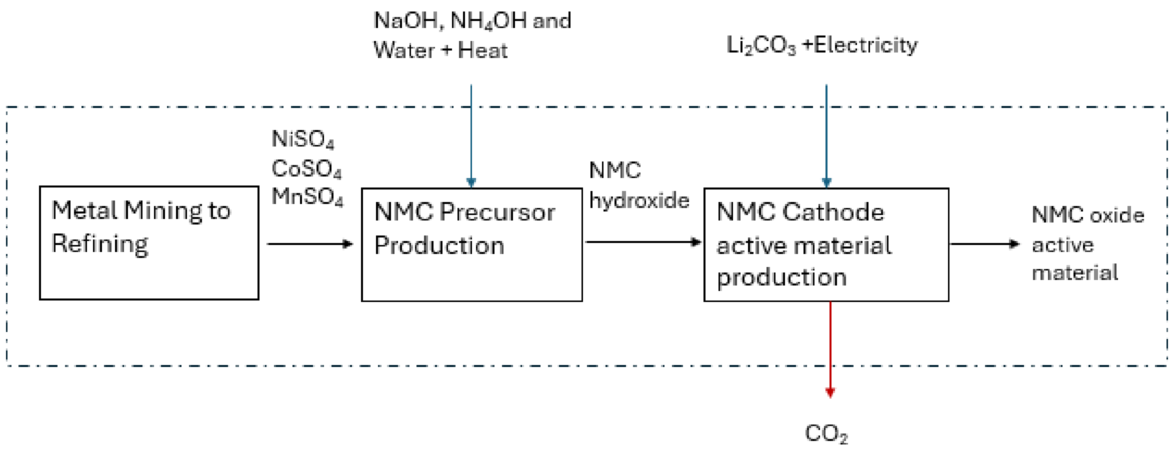

Figure 28: System boundaries of NMC oxide production

Selection of Impact Assessment Method and Categories

The ReCiPe 2016 v1.03 method has been chosen for this study to evaluate the potential environmental impacts associated with the production of NMC 811 oxide and NMC 111 oxide. Refer to section 4.1.2 on the introduction of the ReCiPe method.

Software and Database

The LCA model is conducted using OpenLCA 2.3.0 software. The software supports various LCIA methods, including ReCiPe 2016 v1.03, allowing for a comprehensive assessment of environmental impacts. For the background data, ecoinvent 3.8 cutoff is being used, as ecoinvent provides high-quality, peer-reviewed inventory data covering a broad range of sectors, including energy, materials, chemicals, transportation, and industrial processes.

5.3 Life Cycle Inventory

For this study, a custom cobalt sulphate dataset was integrated into the Ecoinvent 3.8. database to evaluate the environmental impacts of NMC 111 oxide and NMC 811 oxide. The LCI was constructed by modifying the default datasets for cobalt sulphate and incorporating the custom generated cobalt sulphate dataset in the ecoinvent 3.8 dataset for NMC oxide 111 and NMC oxide 811. This dataset was tailored to accurately represent the actual supply chain conditions, particularly focusing on the refining process that occurs in China. Further details on the custom cobalt sulphate dataset can be found in section 4. The ecoinvent dataset has been adopted from the GREET model by Dai, Q, et al., (2018).

For NMC 111 oxide, the composition consists of 33.3% cobalt, 33.3% nickel, and 33.3% manganese. The updated cobalt sulphate data was applied to calculate the environmental impacts associated with cobalt extraction and processing in this chemistry. For NMC 811, the composition consists of 10% cobalt, 80% nickel, and 10% manganese. The same cobalt sulphate dataset was used to account for the reduced cobalt content and its associated impact on the overall environmental footprint. NMC 111 uses lithium carbonate as a precursor while NMC 811 uses lithium hydroxide as a precursor. The lithium content in both precursors is comparable with lithium hydroxide having 16.54% of Li content while lithium carbonate has a lithium concentration of 18.8%.

This LCI framework enables a detailed comparison of the environmental impacts of NMC 111 oxide and NMC 811 oxide, particularly with respect to cobalt concentration, and provides an accurate basis for assessing the implications of using lower-cobalt chemistries in lithium-ion battery production. Tables 17 and 18 depict the Life Cycle Inventory (LCI) results obtained by incorporating the custom cobalt sulphate dataset into the Ecoinvent NMC 811 oxide and NMC 111 oxide datasets, respectively. These tables show the environmental impacts associated with the production of NMC 811 oxide and NMC 111 oxide.

Table 16: Life Cycle Inventory for NMC oxide 811

Input Flow	**Amount**	**Unit**
ammonia, anhydrous, liquid	5.51E-03	kg
chemical factory, organics	1.42E-09	Item(s)
electricity, medium voltage	7.26E+00	kWh
heat, district or industrial, natural gas	3.71E+01	MJ
lithium hydroxide	2.46E-01	kg
manganese sulfate	1.49E-01	kg
nickel sulfate	1.22E+00	kg
sodium hydroxide	8.10E-01	kg
transport, freight train	3.62E-02	t*km
transport, freight, inland waterways, barge	2.93E-03	t*km
transport, freight, lorry, unspecified	2.45E-02	t*km
transport, freight, sea, container ship	7.02E-02	t*km
Water, cooling, unspecified natural origin	5.81E-04	m3
Cobalt sulfate heptahydrate	1.58E-01	kg
Output Flow	**Amount**	**Unit**
NMC811 oxide	1.00E+00	kg
wastewater, average	5.81E-04	m3
Ammonia	5.51E-03	kg
Water	1.96E-04	m3

Table 17: Life Cycle Inventory for NMC oxide 111

Input Flow	**Amount**	**Unit**
ammonia, anhydrous, liquid	5.58E-03	kg
chemical factory, organics	1.42E-09	Item(s)
electricity, medium voltage	6.87E+00	kWh

heat, district or industrial, natural gas	3.75E+01	MJ
lithium carbonate	3.83E-01	kg
manganese sulfate	5.07E-01	kg
nickel sulfate	5.19E-01	kg
sodium hydroxide	8.20E-01	kg
transport, freight train	4.83E-02	t*km
transport, freight, inland waterways, barge	3.90E-03	t*km
transport, freight, lorry, unspecified	1.37E-01	t*km
transport, freight, sea, container ship	9.36E-02	t*km
Water, cooling, unspecified natural origin	6.03E-04	m3
Cobalt sulfate heptahydrate	5.20E-01	kg
Output Flow	**Amount**	**Unit**
NMC111 oxide	1	kg
wastewater, average	5.90E-04	m3
Ammonia	0.005426	kg
Carbon dioxide, fossil	0.207	kg
Water	1.25E-04	m3

5.4 Life Cycle Impact Assessment

In the LCIA section, the environmental impacts associated with the production of battery-grade cobalt sulfate are presented and analysed using the ReCiPe 2016 (H) midpoint impact categories. For this study the focus is solely on the global warming potential of NMC cathode active materials. Table 19 shows the environmental impacts associated with the production of 1 kg of battery-grade cobalt sulfate using the ReCiPe assessment method.

Table 18: Environmental Impacts of Producing 1 kg of Battery grade cobalt sulfate based on the ReCiPe Impact Assessment Method

Impact Category	Unit	NMC 811	NMC 111
Global Warming	kg CO2 Eq	21.85705	22.39697
Fine Particulate Matter Formation	kg PM 2.5 eq	0.07116	0.08156
Terrestrial Acidification	kg SO2 Eq	0.20976	0.24329
Fresh Water Ecotoxicity	kg 1,4 DCB eq	2.88145	3.73340
Terrestrial Ecotoxicity	kg 1,4 DCB eq	417.73481	240.11254
Marine Ecotoxicity	kg 1,4 DCB eq	3.79746	4.77414
Fresh water Eutrophication	kg P eq	0.00815	0.00983
Marine Eutrophication	kg N eq	0.00501	0.00601

Human Carcinogenic Toxicity	kg 1,4 DCB	1.50060	1.62045
Human Non-Carcinogenic Toxicity	kg 1,4 DCB	61.82493	58.10165
Mineral Resource Scarcity	kg Cu eq	2.86653	1.86408
Fossil Resource Scarcity	kg Oil Eq	5.85197	5.75241
Land Use	m2a crop Eq	0.17748	0.22097
Water Consumption	m3	1.56794	0.88521
Ionizing Radiation	kBq Co-60-eq	2.53488	1.79188
Ozone Depletion	kg CFC Eq	0.00001	0.00001
Ozone Formation, Human Health	kg NOx Eq	0.07038	0.09739
Ozone Formation Terrestrial Ecosystems	kg NOx Eq	0.07135	0.09888

5.4.1 Global Warming Potential

To compare the Global Warming Potential (GWP) between NMC 111 oxide and NMC 811 oxide, raw materials and energy flows were categorized into two distinct groups. In the LCIA analysis, cobalt sulfate heptahydrate, nickel sulfate, lithium hydroxide ($LiOH.H_2O$), lithium carbonate, sodium hydroxide (NaOH), manganese sulfate, and ammonia are grouped under "Raw Materials", as they represent the primary precursors used in NMC oxide production. Electricity and heat are grouped under "Energy", as they are the key inputs driving the manufacturing processes. Additionally, transport emissions, chemical factory emissions, and wastewater treatment contributions are considered separately to capture their specific environmental impacts. Figure 29 shows the GWP of NMC 111 and NMC 811 as grouped categories. The total CO_2 equivalent emissions for NMC 111 oxide are 22.4 kg CO_2 Eq, while for NMC 811 oxide, the emissions are 21.8 kg CO_2 Eq. The emissions are primarily driven by raw material production and energy consumption, which together account for over 95% of the total emissions. The contribution of raw materials to the carbon footprint is slightly higher for NMC 111 (59.7%) compared to NMC 811 (57.4%), whereas the energy contribution is higher for NMC 811 (41.7%) than for NMC 111 (39.2%). The overall energy consumption for both NMC chemistries is comparable. Transport, waste treatment, and other process-related emissions are negligible in comparison.

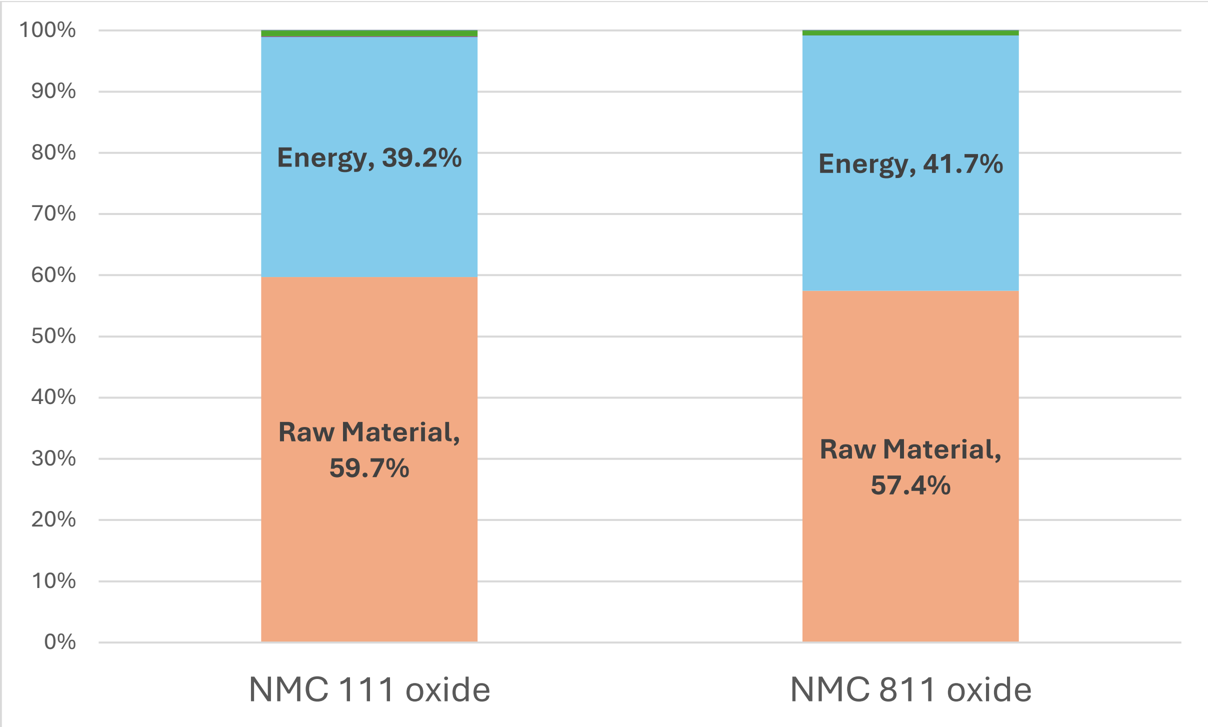

Figure 29: Global Warming Potential (kg CO_2eq) for NMC 111 and NMC 811 Oxide Production respectively - Grouped Contributions

Figure 30 specifically focuses on the emissions from raw materials used in the cathode active material to highlight the difference of having different concentrations of cobalt in the NMC oxide chemistries. There are significant differences between NMC 111 and NMC 811 oxide chemistries in terms of individual material contributions. Cobalt sulfate heptahydrate is the largest contributor to emissions in NMC 111 oxide, accounting for 47.5% of total raw material emissions, whereas its contribution is significantly lower in NMC 811 oxide (14.8%). Conversely, nickel sulfate emissions are much higher in NMC 811 oxide (46.4%) compared to NMC 111 oxide (22.4%), reflecting the higher nickel content in NMC 811 compositions. Lithium precursor emissions also increase from 18.7% in NMC 111 oxide to 29.3% in NMC 811 oxide. Although the NMC 111 composition requires a larger amount of lithium precursor (0.383 kg of lithium carbonate), its overall global warming potential (GWP) remains lower than that of NMC 811, which uses a smaller quantity (0.246 kg of lithium hydroxide). This disparity is because lithium hydroxide has a significantly higher GWP than lithium carbonate. According to the ecoinvent database, the GWP of lithium hydroxide (14.85 kg CO_2-eq) is nearly double that of lithium carbonate (7.75 kg CO_2-eq), leading to a greater environmental impact despite the lower material requirement in NMC 811. The contributions from sodium hydroxide (NaOH) and manganese sulfate are relatively small, with manganese sulphate's share being lower in NMC 811 (1.0%) compared to NMC 111 (3.1%), consistent with the lower manganese content in NMC 811.

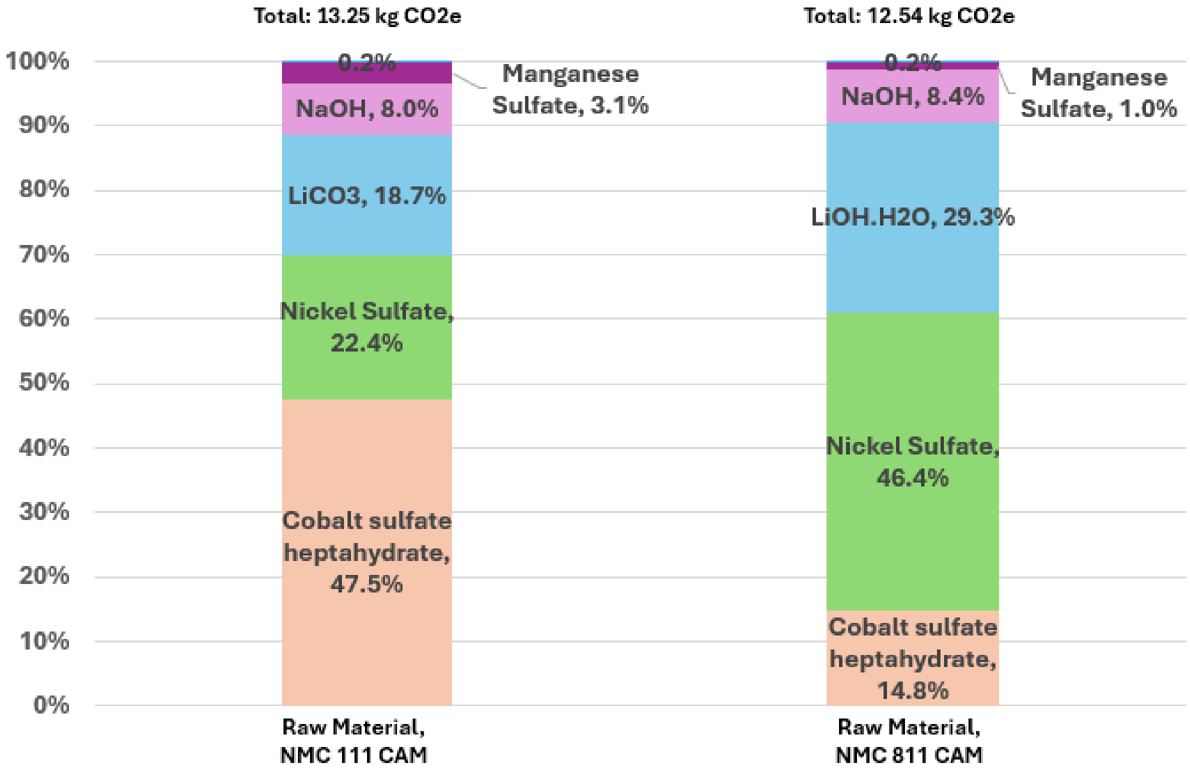

Figure 30: Raw Material Contribution to Global Warming Potential (kg CO_2 Eq) for NMC 111 and NMC 811 Oxide Production respectively

5.5 Interpretation

5.5.1 Identification of Key Findings

The results of the LCA of global warming potential suggest that cobalt sulfate heptahydrate is a significant contributor to the overall environmental impact in both NMC 111 and NMC 811 chemistries. However, due to its higher cobalt content, NMC 111 oxide relies more heavily on cobalt sulfate (47.5%) compared to NMC 811 oxide (14.8%). Conversely, nickel sulfate plays a more dominant role in NMC 811 oxide, accounting for 46.4% of the impact, compared to 22.4% in NMC 111 oxide, reflecting the shift in composition towards higher nickel content. Additionally, impacts from lithium hydroxide are more pronounced in NMC 811 oxide (29.3%) as compared to lithium carbonate emissions in NMC 111 oxide (18.7%), indicating high carbon footprint of lithium hydroxide. Manganese sulfate and sodium hydroxide contribute minimally to the total impact, with manganese sulfate emissions being notably lower in NMC 811, due to its lower manganese content.

The total carbon footprint of NMC 111 oxide production is 22.4 kg CO_2 eq, while NMC 811 oxide has a slightly lower impact at 21.8 kg CO_2 eq. Raw material extraction, processing, and refining account for the largest share of emissions, contributing 59.7% in NMC 111 oxide and 57.4% in NMC 811 oxide. Energy consumption is another major factor, with a slightly higher contribution in NMC 811 oxide (41.7%) compared to NMC 111 oxide (39.2%), indicating that despite its lower cobalt content, NMC 811 oxide's production process remains energy intensive. Though it NMC 811 oxide uses less heat in its production, but it consumes more electricity. Transport and other process-related emissions are negligible in comparison, reinforcing the dominance of material inputs and energy consumption in the overall environmental footprint of NMC cathode active material production.

The ecoinvent dataset for the production of NMC 111 oxide in China has a Global Warming Potential of 28.94 kg CO_2 Eq, while the GWP for NMC 811 oxide is 23.78 kg CO_2 Eq. This difference is primarily due to the higher emissions associated with the default ecoinvent cobalt sulfate dataset compared to the custom cobalt sulfate dataset used in this study. Since the other datasets used in the LCA were identical, this difference in GWP is directly linked to the cobalt sulfate dataset's emissions.

5.5.2 Consistency

The functional unit of production of 1 kg of NMC oxide precursor from cradle to gate remains consistent throughout the LCA. Ecoinvent datasets were used for modelling with the exception of the custom cobalt sulphate dataset. The custom cobalt sulfate dataset used in the LCA study has been developed using process simulation techniques and details on the dataset can be found in section 3 and section 4. The geographical scope of this LCA is consistent with the geographical scope of the custom cobalt dataset. The primary impact category analysed in this study is Global Warming Potential (GWP). While the IPCC method is commonly used to assess GWP, this study uses the ReCiPe method, as the previous LCA study for battery grade cobalt sulphate, also utilizes ReCiPe for impact assessment.

5.5.3 Limitations

The current LCA study focuses on a specific geographical scope, namely China. While China dominates the global production of NMC cathode materials, it would be beneficial to conduct a sensitivity analysis involving other regions to assess how the environmental impacts of NMC production vary across different geographical contexts. Given that China's energy mix is heavily reliant on fossil fuels, incorporating energy sources from regions with lower carbon intensities would provide a more comprehensive view of the global environmental impacts.

Furthermore, the study could benefit from a scenario analysis that examines various datasets for the metal precursors used in cathode active materials. This would offer a more detailed understanding of how the production processes for nickel, cobalt, manganese, and lithium derived from different process routes affect emissions and environmental impacts.

Expanding the study to include other NMC chemistries, such as NMC 532 or NMC 622, would offer a more complete picture of how varying concentrations of metals influence the environmental outcomes associated with cathode production.

Lastly, the study focuses solely on Global Warming Potential (GWP), and other important impact categories, such as human toxicity, resource depletion, and ecosystem quality, should be considered to obtain a more comprehensive assessment of the environmental performance of NMC chemistries across several environmental dimensions.

5.5.4 Conclusion

This study provides a comparative Life Cycle Assessment of NMC 111 and NMC 811 oxide chemistries, with a primary focus on their Global Warming Potential impacts. The total CO_2 equivalent emissions for NMC 111 oxide are 22.4 kg CO_2 Eq, while for NMC 811 oxide, the emissions are 21.8 kg CO_2 Eq. By utilizing custom dataset for cobalt sulfate production, this study offers valuable insights into the environmental implications of these two widely used cathode active materials and their dependence on varying cobalt concentrations. The findings highlight the significant contribution of cobalt sulfate to the overall GWP, with NMC 111 exhibiting a higher GWP due to its greater reliance on cobalt compared to NMC 811, which, despite using a lower quantity of lithium precursor, has a higher GWP contribution from lithium hydroxide.

While the results emphasize the importance of cobalt sulfate in both chemistries, further research is needed to explore other NMC chemistries, as well as the impacts of various metal precursor sourcing and process routes. Additionally, expanding the scope to include additional impact categories such as resource depletion, human toxicity, and ecosystem quality would provide a more complete view of the environmental performance of NMC-based lithium-ion battery materials. The study also highlights the need for a broader geographical perspective, including a sensitivity analysis across different regions, to fully understand the global implications of NMC production. The LCA emphasizes the critical role of material sourcing and process routes in minimizing the environmental footprint of future battery technologies.

6 Conclusions, Recommendations and Future Work

6.1 Synergistic Effect of Process simulation and LCA for Development of Sustainable Materials

This study demonstrates the advantages of using process simulation to develop a more accurate and region-specific LCA of cobalt sulfate heptahydrate production. By leveraging HSC Chemistry to create a custom life cycle inventory, the analysis provides a refined representation of environmental impacts compared to existing literature. The results indicate that the global warming potential of battery-grade cobalt sulfate in this study is 12.1 kg CO_2 eq, placing it at the lower end of reported values. This reduction can be attributed to the selection of high-grade ore and an alternative refining approach. The highest environmental impacts were linked to hydrometallurgical operations, including roasting, leaching, solvent extraction, copper electrowinning, and precipitation.

This study provides a comparative LCA of NMC 111 and NMC 811 cathode chemistries, focusing on their GWP impacts. The results indicate that NMC 111 has a higher GWP (22.4 kg CO_2 eq) compared to NMC 811 (21.8 kg CO_2 eq), primarily due to its greater cobalt content. While NMC 811 reduces cobalt dependency, its environmental advantage is offset by the higher GWP contribution of lithium hydroxide. These findings highlight the significant role of cobalt sulfate in the overall impact of lithium-ion batteries and emphasize the need for continued research into alternative chemistries and process improvements.

The use of HSC Chemistry for process-specific data generation provides key advantages in ensuring accurate mass and energy balances through detailed thermodynamic calculations. By simulating precise process conditions such as reaction stoichiometry, temperature, pressure, and material properties HSC Chemistry delivers reliable data on resource consumption, emissions, and energy use, which is critical for robust LCAs. Additionally, it enables the identification of inefficiencies and optimization of process parameters, leading to more sustainable and cost-effective production methods. When integrated with LCA, this approach enhances process optimization by combining macro-level environmental assessments with detailed simulations that refine production parameters. While LCA identifies key emission sources and resource-intensive stages, HSC Chemistry allows for targeted modifications to process conditions, enabling the evaluation of alternative, lower-impact production routes. This combined methodology improves efficiency, reduces environmental footprints, and ensures that sustainability is incorporated into process development and material selection.

In material science, this methodology is particularly valuable for developing advanced materials that balance performance with sustainability. Early-stage integration of LCA and process modelling ensures that new materials and production methods minimize environmental and societal impacts while maintaining functionality. Furthermore, this approach promotes the use of low-impact raw materials and supports the continuous optimization of existing technologies, reinforcing its role in advancing sustainable manufacturing.

6.2 Future Work and Recommendations

Future studies should consider conducting sensitivity analyses by expanding the geographical scope beyond China. While China is a dominant producer of NMC materials, different regions with varying energy mixes, raw material extraction methods, and processing techniques could result in significant differences in environmental impacts. A more global perspective will help provide a broader understanding of how geographical factors influence the sustainability of cobalt sulfate and NMC oxide production.

Additionally, scenario analysis comparing different production routes for cobalt, nickel, manganese, and lithium should be considered. This would involve assessing alternative refining processes, such as those that utilize renewable energy sources or innovative technologies, to determine how these alternatives affect the overall environmental footprint. Such comparisons could reveal pathways for reducing emissions, energy consumption, and resource depletion.

The current study focused on NMC 111 and NMC 811, but other chemistries, such as NMC 532, NMC 622, and NCA, should also be considered in future research. By examining a wider range of cathode materials with different metal compositions, the study could provide a more complete picture of how variations in metal concentrations impact the environmental footprint of battery production.

Moreover, collaborations should be made with industry partners to gather real-life data on material production, energy use, and emissions for modelling in process simulation software. This would provide valuable insights into actual production practices, making the resulting LCA from process simulation data more representative of current industry conditions and improving the accuracy of environmental impact assessments.

Furthermore, the development of more detailed and region-specific datasets, such as the custom cobalt sulfate dataset used in this study, should be extended to other materials used in battery production. This could include refining datasets for nickel sulfate, lithium hydroxide, and manganese sulfate, further improving the accuracy of the environmental impact assessment and enabling more precise optimization of production processes.

Finally, future studies should include a geopolitical analysis to assess the supply chain risks and sustainability implications of critical materials, such as cobalt, nickel, and lithium. The concentration of these materials in specific regions, such as cobalt in the Democratic Republic of Congo, raises concerns about supply security, ethical sourcing, and environmental degradation. A comprehensive sustainability assessment that incorporates geopolitical factors such as mining practices, labour conditions, and trade policies, would provide a more robust understanding of the environmental and social impacts of critical material sourcing. This analysis could also identify opportunities for improving the resilience and sustainability of supply chains, fostering more responsible sourcing practices, and reducing dependence on high-risk regions.

By addressing these areas, future work can further enhance our understanding of the environmental impacts associated with battery material production, contribute to the development of more sustainable materials, and inform the transition to more sustainable manufacturing practices in the battery industry.

7 Appendices

7.1 Parameters for Beneficiation used in HSC Sim

Beneficiation Parameters			
Parameters	**Value**	**Reason**	**Reference**
Starting feed	1000 t/h	standard value for a small plant	
moisture content	3%	Ranges from 2-5%	(Bleiwas, 2012)
passing size	99.999% passes 24,999 micrometers	Ore less than 0.25 m	(Crundwell, 2011)
Distribution	Swerbec Distribution	can be used where size variability is large	
100 mm screen for primary crushing	100 mm		(Crundwell, 2011)
CSS for primary crushing	100	should be less than 100	
20 mm screen for secondary crushing	20 mm		(Crundwell, 2011)
CSS for secondary crushing	20	should be less than 20	
SAG Mill		seen in flow sheet but no values in literature	(Moats, Alagha and Awuah-Offei, 2021)
Ball Mill		seen in flow sheet but no values in literature	(Moats, Alagha and Awuah-Offei, 2021)
Hydro cyclone		seen in flow sheet but no values in literature	(Moats, Alagha and Awuah-Offei, 2021)
Range for input size for floatation		Floatation occurs in the range from 30- 100 micrometres, so parameters for SAG Mill and Hydro cyclone are estimated to	(Dehaine *et al.*, 2024)

		resize from 20 mm to 75 micrometres.	
Ball Mill	P80 80 micro-meter	Ball milling resizes in the range of 75 - 200 micrometres but a regrinding step may be required afterwards. So, it is better to stick to the lower range of 80 micrometres as an additional regrinding step has not been added in floatation.	(Bleiwas, 2012)
SAG Mill	Fixed P80 set to 3 mm	Used as an estimate. Value chosen which would avoid giving errors.	
Hydro cyclone	d50 c set as 110 micrometres	Hydro cyclones are used to crush into fine particles. It would resize the SAG mill product from 3mm to somewhere above 80 micrometres as the Ball Mill output size is already 80 micrometres. So, a range can be defined from 80 - 150 micrometres.	
Ball Mill Water stream	50% solids - 1000 t/h	ranges from 20- 55% solids	(Bleiwas, 2012)
SAG Mill Water stream	60% solids - 700 t/h	Usually SAG Mills have higher solid content than Ball Mills	
Bond Work Index	12 kWh/t	Range between 12 - 14 kWh/t for the main mineral bornite. Default setting was 12.	911 metallurgist

7.2 Parameters for Froth Floatation used in HSC Sim

Froth Floatation			
Parameters	**Value**	**Reason**	**Reference**
floatation launder water solids %	31%	25-40% solids in floatation pulp	(Bleiwas, 2012)
No of cells	6	industrial cell can process 200 - 300 m^3 of volume	
Water for conditioner	set by controls	to satisfy 31% solids in floatation circuit	
Launder water for rougher	set by controls	30.8% solids	

Launder water for cleaner	set by controls	29.50% solids	
Launder water for scavenger	set by controls	To satisfy the 29% solids target.	
solid % in scavenger	29%	It is less than 30%	(Bleiwas, 2012)
solids % in concentrator	95%	Only 4-8% moisture in sulphide concentrate	(Bleiwas, 2012)
solids % in tailings	60%	In the 40-60% solids range	(Bleiwas, 2012)
Sodium Isopropyl Xanthate (SIPX)	0.2 ton	200 g/t	(Mpongo and Siame, 2006; Crundwell, du Preez and Knights, 2020)
1,1,3-triethoxybutane (TEB)	0.02 ton	20 g/t	(Crundwell, du Preez and Knights, 2020)

7.3 Parameters for Roasting used in HSC Sim

Roasting Parameters	**Value**	**Reason**	**Reference**
Input feed	500 tons feed and 50 ton sulphur additional	In between 480 - 600 tons	(Crundwell, 2011)
Input gas	33 wt% oxygen, 67 wt% nitrogen (oxygen enriched air)	30 vol % O_2, 70 vol % N_2. Calculation from volume % to weight % gives the value	(Crundwell, 2011)
Temperature of calcine	700 °C	695 - 705 °C	(Crundwell, 2011; Crundwell, du Preez and Knights, 2020)
Dust removed from off gas	90%	90% dust removed from roaster offgas: 10% as bed overflow	(Crundwell, 2011)
Dust weight %	2% of all the products becomes dust	Generally, dust in roasting is from 0.5 - 5%. Usually it is between 1-3% for copper sulphide roasting	911 Metallurgist
Yield of SO_2 capture in gas cleaning	90%	estimate	

Weight % of water evaporating in scrubber for quenching	set from controls to balance enthalpy		
Water used for capturing gasses	To get 5 wt % solution of NaOH in water		
NaOH used for capturing SO_2	calculated by software	Assuming that 90% of SO_2 is captured so this is required NaOH needed.	
Weight % of water evaporating in quenching chamber for quenching	set in proportion of the NaOH amount added for SO_2 capture		
Heat loss		Assuming that the roasting furnace loses 5000 kW energy as heat dissipation	

7.4 Parameters of Leaching used in HSC Sim

Leaching Parameters	**Value**	**Reason**	**Reference**
Yield for Co	80%		(Dai, Kelly and Elgowainy, 2018)
Yield for Cu	95%		(Dai, Kelly and Elgowainy, 2018)
acid input	set from controls	pH 1.5	(Crundwell, 2011)
water input for leach tank	set from controls	to get 30g/l input slurry density. Values from 15g/l to 30 g/l found in literature sources.	(Baisui, Batnasan and Haga, 2024)
distribution of thickener	all of the solids go to LG SX feed and 60% of the ions stay in overflow water while 40% remain in the underflow	All of the solids would settle down in a thickener and make the lower part of the solution denser. Hence, the aqueous ions would not be exactly	(Crundwell, du Preez and Knights, 2020)

		uniformly distributed. This is also supported by the concentrations in Crundwell (2021).	
distribution of organic phase in thickener	100% of the organic phase goes to the HG Cu SX	100% of the organic phase goes to the HG Cu SX because it is lighter, and it floats on the aqueous phase	assumption

7.5 Power Calculations from Using HSC Sim data

7.5.1 Concentrator Plant

In the concentrator plant, HSC sim software can calculate the power consumption for the machines used in beneficiation and froth floatation. However, a large amount of slurry is being pumped from several connected machines and these calculations must be taken into account. These include the calculations of power required for the pumping of various streams and the hydrocyclone. The formula for calculating the power required for the flow of liquids and slurries was adopted from White (2011), as it provides a simple yet effective approach for determining flow-related power consumption. Since HSC Sim provides data on mass flow and volume flow, key parameters such as fluid density and flow rate can be derived directly. Estimates have been used for pump efficiency and pump head values. The pump head (H) in the power equation represents the energy per unit weight of fluid imparted by the pump to move the liquid or slurry through a system. It can typically have a value ranging from 10 to 80 meters for industrial applications (*Orion Series Horizontal slurry pumps*, no date). For the calculations a value of 50m has been used.

$$P = \frac{\rho g Q H}{\eta * 1000}$$

P= power required

ρ= fluid density (kg/m^3)

g= gravitational constant (9.81 m/s^2)

Q= flow rate (m^3/s)

H= pump head (m)

η= pump efficiency.

Variable	value	units
Pump head	50	m
Acceleration due to gravity	9.8	m/s^2
Efficiency	0.7	
Pumping of SAG water		
Mass	700.00	ton
Volume	702.10	m^3
Density	997.01	kg/m^3
Flow rate	0.20	m^3/s
Power	136.11	kW
Pumping of SAG mill product		
Mass	1731.00	ton
Volume	1021.85	m^3
Density	1693.97	kg/m^3
Flow rate	0.28	m^3/s
Power	336.58	kW
Pumping of Ball mill product		
Mass	2941.50	ton
Volume	1872.10	m^3
Density	1571.23	kg/m^3
Flow rate	0.52	m^3/s
Power	571.96	kW
Pumping of BM water		
Mass	1000.00	ton
Volume	1003.00	m^3
Density	997.01	kg/m^3
Flow rate	0.28	m^3/s
Power	194.44	kW

Pumping of Cyclone Feed		
Mass	4672.40	ton
Volume	2893.90	m^3
Density	1614.57	kg/m^3
Flow rate	0.80	m^3/s
Power	908.52	kW
Pumping of Cyclone UF		
Mass	1941.47	ton
Volume	869.10	m^3
Density	2233.88	kg/m^3
Flow rate	0.24	m^3/s
Power	377.51	kW
Pumping of Cyclone OF		
Mass	2730.93	ton
Volume	2024.80	m^3
Density	1348.74	kg/m^3
Flow rate	0.56	m^3/s
Power	531.01	kW

Pumping of Conditioner Water		
Mass	494.17	ton
Volume	431.29	m^3
Density	1145.79	kg/m^3
Flow rate	0.12	m^3/s
Power	96.09	kW
Pumping of Floatation Feed		
Mass	3129.20	ton
Volume	2456.09	m^3
Density	1273.98	kg/m^3

Flow rate	0.68	m^3/s
Power	608.42	kW
Pumping of Launder Water for Floatation		
Mass	20.32	ton
Volume	20.06	m^3
Density	1012.96	kg/m^3
Flow rate	0.01	m^3/s
Power	3.95	kW
Pumping of Tails Feed		
Mass	80.32	ton
Volume	66.34	m^3
Density	1212.12	kg/m^3
Flow rate	0.02	m^3/s
Power	15.55	kW
Pumping of Cleaner Tails		
Mass	393.71	ton
Volume	60.55	m^3
Density	6502.23	kg/m^3
Flow rate	0.02	m^3/s
Power	76.55	kW
Pumping of Rougher Concentrate		
Mass	3069.34	ton
Volume	2475.46	m^3
Density	1239.77	kg/m^3
Flow rate	0.69	m^3/s
Power	596.75	kW
Pumping of Scavenger tails		
Mass	98.65	ton
Volume	69.08	m^3
Density	1428.05	kg/m^3
Flow rate	0.02	m^3/s
Power	19.18	kW
Pumping of Final tails		

Mass	84.31	ton
Volume	48.43	m^3
Density	1740.86	kg/m^3
Flow rate	0.01	m^3/s
Power	16.39	kW
Pumping of Recirculating water tails		
Mass	12.78	ton
Volume	12.81	m^3
Density	997.66	kg/m^3
Flow rate	0.004	m^3/s
Power	2.49	kW
Pumping of Cleaner Feed		
Mass	3249	ton
Volume	2544.54	m^3
Density	1276.85	kg/m^3
Flow rate	0.71	m^3/s
Power	631.75	kW
Pumping Cleaner Launder Water		
Mass	149.91	ton
Volume	150	m^3
Density	999.42	kg/m^3
Flow rate	0.042	m^3/s
Power	29.15	kW
Pumping of Cleaner Concentrate		
Mass	3005.23	ton
Volume	2499.03	m^3
Density	1202.47	kg/m^3
Flow rate	0.69	m^3/s
Power	584.31	kW
Pumping of Scavenger Launder water		
Mass	207.22	ton
Volume	208.89	m^3
Density	996.25	kg/m^3
Flow rate	0.06	m^3/s
Power	40.29	kW
Scavenger feed		
Mass	3197.49	ton
Volume	2499.03	m^3
Density	1279.49	kg/m^3

Flow rate	0.69	m^3/s
Power	621.73	kW
Pumping of Scavenger concentrate & Conc. Thickener feed		
Mass	3273.84	ton
Volume	2605.48	m^3
Density	1256.52	kg/m^3
Flow rate	0.72	m^3/s
Power	636.58	kW
Pumping of Thickener underflow & filter feed		
Mass	1582.36	ton
Volume	908.92	m^3
Density	1740.92	kg/m^3
Flow rate	0.25	m^3/s
Power	307.68	kW
Pumping of Filtrate		
Mass	582.97	ton
Volume	584.72	m^3
Density	997.01	kg/m^3
Flow rate	0.16	m^3/s
Power	113.35	kW
Pumping of conc. recirculating water		
Mass	2274.46	ton
Volume	2281.28	m^3
Density	997.01	kg/m^3
Flow rate	0.63	m^3/s
Power	442.26	kW

Hydrocyclone Energy Consumption

The formula for calculating electricity of the hydrocyclone has been taken from (White, 2011) and is used to calculate the power required for fluid flow. This equation represents the relationship between power consumption, fluid flow rate, and pressure loss across a system, while also considering the efficiency of the pump used.

$$P = \frac{Q \cdot \Delta P}{\eta}$$

Q= flow rate (m^3/s)

ΔP= pressure drop across the hydrocyclone (pa)

η= pump efficiency

Estimates have been made regarding the pressure drop and efficiency in the system. While the volumetric flow value has been taken from the HSC model.

Pressure drop = 1.5 bar or 150,000 Pa.
Efficiency = 70%.
Volumetric flow = 3036.89 m^3/h
Power = 180.77 kW

Calculation of conveyer belt distance into mass for concentration plant

Transportation of solid ore via conveyor belts	**mass in tons**	**Distance (km)**	**Product (tons x km)**
Transport of ore	1000	0.1	100
Primary crushing feed	1000	0.1	100
Primary crushing oversize feed	203	0.1	20.3
Primary crushing undersize	707	0.1	70.7
Primary crushing product	203	0.1	20.3
Secondary crushing oversize feed	981	0.1	98.1
Secondary crushing undersize feed	19	0.1	1.9
Secondary crushing product	981	0.1	98.1
SAG feed	1000	0.1	100
Transport of concentrate	285	0.1	28.5
Transport of tails	850	0.1	85
Total			722.9

7.5.2 Hydrometallurgical Plant

The formulas mentioned in the previous section have been applied to determine the power requirements for cyclones, scrubbers, and the pumping of slurries or solutions.

Power Calculation for Roasting and Gas Cleaning Model		
Variable	**value**	**units**

Pump head	50	m
Acceleration due to gravity	9.8	m/s^2
Efficiency	0.7	
Pumping of Water for Temperature Control		
Mass	481.81	ton
Volume	484.34	m^3
Density	999.58	kg/m^3
Flow rate	0.13	m^3/s
Power	93.68	kW
Pumping of Scrubbing Water		
Mass	3297.45	ton
Volume	3000.32	m^3
Density	1099	kg/m^3
Flow rate	0.83	m^3/s
Power	641.08	kW
Pumping of Na2SO4 solution		
Mass	2865	ton
Volume	2500	m^3
Density	1146	kg/m^3
Flow rate	0.69	m^3/s
Power	557.08	kW
Pumping of Quenching water		
Mass	1118.92	ton
Volume	1120	m^3
Density	999.04	kg/m^3
Flow rate	0.31	m^3/s
Power	217.57	kW
Pumping of Leach Feed		
Mass	1721.23	ton
Volume	1097.85	m^3
Density	1784.32	kg/m^3
Flow rate	0.43	m^3/s
Power	334.67	kW
Pump used in Venturi Gas Scrubber		
Density	1000.80	kg/m^3
Flow rate	0.92	m^3/s
Power	385.04	kWh

Power Calculations for Cyclone

Estimates have been made regarding the pressure drop and efficiency in the system. While the volumetric flow value has been taken from the HSC model.

Volumetric flow rate = 1244569.55 m^3/h
The pressure drop = 1.5 bar or 150,000 Pa
The efficiency 70%.
Power = 740.82 kW

Power Calculations for Leaching		
Pumping of H_2SO_4 + Water		
Mass	19840	ton
Volume	20000	m^3
Density	992	kg/m^3
Flow rate	5.56	m^3/s
Power	3857.78	kW
Pumping of Reactor Feed Raffinate		
Mass	4438	ton
Volume	5093	m^3
Density	871.39	kg/m^3
Flow rate	1.41	m^3/s
Power	862.94	kW
Pumping of Leach Solution		
Mass	22477.58	ton
Volume	21873.14	m^3
Density	1027.63	kg/m^3
Flow rate	6.08	m^3/s
Power	4370.64	kW

Pumping of Mixer Feed		
Mass	10555.51	ton
Volume	10262.98	m^3
Density	1028.50	kg/m^3
Flow rate	2.85	m^3/s
Power	2052.46	kW
Pumping of Filter Feed		
Mass	13037.26	ton
Volume	12749.34	m^3
Density	1022.59	kg/m^3
Flow rate	3.54	m^3/s
Power	2534.97	kW

Pumping of Wash Water Filter		
Mass	196.63	ton
Volume	197.87	m^3
Density	998.12	kg/m^3
Flow rate	0.05	m^3/s
Power	38.23	kW
Pumping of Counter Current Decantation		
Mass	196.63	ton
Volume	197.94	m^3
Density	998.12	kg/m^3
Flow rate	0.05	m^3/s
Power	38.23	kW
Pumping of Residue Tailings		
Mass	174.78	ton
Volume	80.03	m^3
Density	2184.75	kg/m^3
Flow rate	0.02	m^3/s
Power	33.985	kW

Power Calculation for Leaching Reactor

An agitating leaching tank has a power consumption of up to 0.1 - 0.6 kW per m^3 of slurry (Glencore Technology, n.d.). Using this information, the energy consumption of a leaching reactor is calculated.) The upper value in the range, 0.6 kW per m3 used, as slurry has a higher density than typical leaching operations.

Volume of slurry = 26328.87 m^3 (from HSC Sim)
Power Consumption of leaching reactor =15797.32 kW

Power Calculation for Thickener Use

Total power used by thickener = Power of rake + Power of pump for underflow and overflow
The power of pumping is calculated in the tables. This formula calculates the power required for a rake arm in a thickener or similar equipment based on the applied torque and rotational speed, adjusted for efficiency losses.

$$P_{rake}(KW) = \frac{T * 2\pi * N}{60 * \eta}$$

T=Torque
N=rake speed
η =motor efficiency

The low solids concentration (0.75%) indicates a dilute slurry. The resistance against the rake movement is relatively low due to the predominance of the liquid phase. Based on this, the torque value is taken as 50,000 which is average for when mostly liquid phase is there. The speed is also taken from average data.

Variable	**Value**	**Units**
Torque	500000	Nm
Speed	0.3	rpm
Efficiency	0.8	
Power of rake	19.63	kW

Power Calculations for Solvent Extraction		
Pumping of High Grade SX		
Mass	13390.1	ton
Volume	12651	m^3
Density	1058.42	kg/m^3
Flow rate	3.51	m^3/s
Power	2603.63	kW
Pumping of Low Grade SX		
Mass	13510.61	ton
Volume	12865	m^3
Density	1050.18	kg/m^3
Flow rate	3.57	m^3/s
Power	2627.06	kW
Pumping of LIX 984 +Kerosense for HG SX		
Mass	7500	ton
Volume	10243	m^3
Density	732.20	kg/m^3
Flow rate	2.84	m^3/s
Power	1458.33	kW
Pumping of LIX 984 +Kerosense for LG SX		
Mass	7500	ton
Volume	10273	m^3
Density	730.06	kg/m^3
Flow rate	2.85	m^3/s
Power	1458.33	kW
Pumping of HG Raffinate		
Mass	12860.77	ton
Volume	12733	m^3

Density	1010.03	kg/m^3
Flow rate	3.54	m^3/s
Power	2500.71	kW
Pumping of Precipitation Feed Raffinate		
Mass	7716.46	ton
Volume	7639	m^3
Density	1010.14	kg/m^3
Flow rate	2.12	m^3/s
Power	1500.42	kW
Pumping of LG raffinate		
Mass	13019.46	ton
Volume	10445.99	m^3
Density	1246.35	kg/m^3
Flow rate	2.90	m^3/s
Power	2531.56	kW

Power Calculations for Precipitation		
Pumping of Dissolved Calcium Hydroxide		
Mass	61081.28	ton
Volume	61930	m^3
Density	986.29	kg/m^3
Flow rate	17.20	m^3/s
Power	11876.91	kW
Pumping of pH 3.5 solution		
Mass	82568.16	ton
Volume	79590.26	m^3
Density	1037.41	kg/m^3
Flow rate	22.10	m^3/s
Power	16054.92	kW
Pumping of Input Wash Water AF filter		
Mass	738.67	ton
Volume	79590.26	m^3
Density	9.29	kg/m^3
Flow rate	22.11	m^3/s
Power	143.63	kW
Pumping of Al Fe Residue		
Mass	656.62	ton
Volume	376.34	m^3
Density	1746.27	kg/m^3

Flow rate	0.10	m^3/s
Power	127.67	kW
Pumping of Output Wash Water AF		
Mass	738	ton
Volume	740	m^3
Density	997.29	kg/m^3
Flow rate	0.21	m^3/s
Power	143.5	kW
Pumping of Filtrate Precipitation 2		
Mass	81911.57	ton
Volume	82127	m^3
Density	997.37	kg/m^3
Flow rate	22.81	m^3/s
Power	15927.25	kW
Pumping of pH 6.7 solution		
Mass	82674.41	ton
Volume	82860.93	m^3
Density	997.76	kg/m^3
Flow rate	23.01	m^3/s
Power	16075.58	kW
Pumping of wash water in FC filter		
Mass	154.50	ton
Volume	260.27	m^3
Density	593.6143236	kg/m^3
Flow rate	0.07	m^3/s
Power	30.04	kW
Pumping of wash water out FC		
Mass	154.5	ton
Volume	260.27	m^3
Density	593.61	kg/m^3
Flow rate	0.07	m^3/s
Power	30.04	kW
Pumping of Fe Cu Al Residue		
Mass	137.33	ton
Volume	126.02	m^3
Density	1089.74	kg/m^3
Flow rate	0.035	m^3/s
Power	26.70	kW
Pumping of Filtrate precipitation 3		
Mass	82537.73	ton
Volume	79794.41	m^3

Density	1034.37	kg/m^3
Flow rate	22.16	m^3/s
Power	16048.86	kW
Pumping of 8.8 solution		
Mass	82723.08	ton
Volume	80072.37	m^3
Density	1033.10	kg/m^3
Flow rate	22.24	m^3/s
Power	16085.04	kW
Pumping of Wash Water in Filter Co		
Mass	171.41	ton
Volume	206.92	m^3
Density	828.38	kg/m^3
Flow rate	0.057	m^3/s
Power	33.33	kW
Pumping of Wash Water Out Co		
Mass	171.41	ton
Volume	206.92	m^3
Density	828.38	kg/m^3
Flow rate	0.05	m^3/s
Power	33.33	kW
Pumping of $Co(OH)_2$ cake		
Mass	152.36	ton
Volume	99.03	m^3
Density	1538.52	kg/m^3
Flow rate	0.027	m^3/s
Power	29.62	kW
Pumping of Filtrate Basic Solution		
Mass	82570.72	ton
Volume	79973.34	m^3
Density	1032.47	kg/m^3
Flow rate	22.21	m^3/s
Power	16055.41	kW

7.5.3 Refining Plant

Power Calculations for Re-leaching and Crystallization		
Pumping of Reactor Input Diluted H_2SO_4		
Mass	2540.36	ton
Volume	1017	m^3
Density	2497.89	kg/m^3
Flow rate	0.28	m^3/s

Power	493.96	kW
Pumping of Cobalt Re-leach Solution		
Mass	2654.63	ton
Volume	1167.94	m^3
Density	2274.74	kg/m^3
Flow rate	0.32	m^3/s
Power	516.18	kW
Pumping of Input Wash Water for Filter 2		
Mass	114.04	ton
Volume	129.77	m^3
Density	878.78	kg/m^3
Flow rate	0.03	m^3/s
Power	22.17	kW
Pumping of Output Wash Water Filter 2		
Mass	114.04	ton
Volume	129.77	m^3
Density	878.78	kg/m^3
Flow rate	0.036	m^3/s
Power	22.17	kW
Pumping of Filter Cake CoSO4		
Mass	101.37	ton
Volume	65.83	m^3
Density	1539.87	kg/m^3
Flow rate	0.018	m^3/s
Power	19.71	kW
Pumping of Cobalt Sulphate Filtrate		
Mass	2553.26	ton
Volume	1101.67	m^3
Density	2317.62	kg/m^3
Flow rate	0.30	m^3/s
Power	496.46	kW
Pumping of Crystallized CoSO4 + water		
Mass	1008750	ton
Volume	1040166	m^3
Density	969.79	kg/m^3
Flow rate	288.94	m^3/s
Power	196145.83	kW
Pumping of Input Wash Water CF		
Mass	173.42	ton
Volume	1035658.04	m^3
Density	0.17	kg/m^3
Flow rate	287.68	m^3/s

Power	33.72	kW
Pumping of Output Wash water CF		
Mass	173.42	ton
Volume	1035658.04	m^3
Density	0.17	kg/m^3
Flow rate	287.68	m^3/s
Power	33.72	kW
Pumping of Uncrystallized CoSO4		
Mass	1006083.54	ton
Volume	1010517	m^3
Density	995.61	kg/m^3
Flow rate	280.70	m^3/s
Power	195627.36	kW
Pumping of Wet CoSO4 Crystals		
Mass	154.16	ton
Volume	99.81	m^3
Density	1544.53	kg/m^3
Flow rate	0.027	m^3/s
Power	29.98	kW

Power Calculation for Leaching Reactor

An agitating leaching tank has a power consumption of up to 0.1 - 0.6 kW per m^3 of slurry (Glencore Technology, n.d.). Using this information, the energy consumption of a leaching reactor is calculated.) The upper value in the range, 0.6 kW per m^3 used, as slurry has a higher density than typical leaching operations.

Volume of slurry = 4132.72 m^3 (from HSC Sim)
Power Consumption of leaching reactor = 2479.63 kW

7.6 Economic Allocation Applied in the Cobalt Sulphate Production LCA

Allocation $factor_{Co}$ = $Price_{Co}$ x $Quantity_{Co}$/ ($Price_{Co}$ x $Quantity_{Co}$ + $Price_{Cu}$ x $Quantity_{Cu}$)

Allocation for cobalt hydroxide was based on the amount of cobalt content in impure cobalt hydroxide. This was obtained via the HSC Sim model. The average of the prices of the last ten years from 2016 to 2024, were used for economic allocation using data via London Metal Exchange (LME). The annual average prices were then converted into prices in 2025 dollars to account for inflation, using the consumer price index inflation calculator provided by the Bureau of Labor Statistics.

	Dollars per ton			
	Cu price	**Co price**	**Cu price (inflated)**	**Co price (inflated)**
2015	5494	29233	7378.86	39262.13
2016	4863	26433	6398.63	34779.97
2017	6166	55,000	7945.51	70,873.04
2018	6530	80,000	8029.24	101,155.82
2019	6000	35000	7417.19	43266.96
2020	6170	30000	7524.86	36587.64
2021	9317	52000	10,615.92	59,249.55
2022	8800	70000	9418.91	74,923.16
2023	8490	36,000	8792.38	37282.17
2024	8912	25,000	8970	25163.65
10 year Average	7074.2	43866.6	8249.15	52254.409

Literature Sources

Baisui, H., Batnasan, A. and Haga, K. (2024) ‘Copper Recovery from Silicate-Containing Low-Grade Copper Ore Using Flotation Followed by High-Pressure Oxidative Leaching’, *ResearchGate* [Preprint]. Available at: https://doi.org/10.4144/rpsj.64.3.

Balladares, E. *et al.* (2018) ‘Neutralization and co-precipitation of heavy metals by lime addition to effluent from acid plant in a copper smelter’, *Minerals Engineering*, 122, pp. 122–129. Available at: https://doi.org/10.1016/j.mineng.2018.03.028.

Bleiwas, D.I. (2012) ‘Estimated Water Requirements for the Conventional Flotation of Copper Ores’. Available at: https://pubs.usgs.gov/of/2012/1089/ (Accessed: 12 March 2025).

Blengini, G.A. *et al.* (2020) *Study on the EU’s list of critical raw materials (2020): final report*. Publications Office of the European Union. Available at: https://data.europa.eu/doi/10.2873/11619 (Accessed: 12 March 2025).

van den Brink, S. *et al.* (2020) ‘Identifying supply risks by mapping the cobalt supply chain’, *Resources, Conservation and Recycling*, 156, p. 104743. Available at: https://doi.org/10.1016/j.resconrec.2020.104743.

Broughton, D.W. (2014) ‘Geology and ore deposits of the Central African Copperbelt’. Available at: https://hdl.handle.net/11124/251.

de Bruijn, H. *et al.* (2002) ‘Management of LCA projects: procedures’, in H. de Bruijn et al. (eds) *Handbook on Life Cycle Assessment: Operational Guide to the ISO Standards*. Dordrecht: Springer Netherlands, pp. 21–29. Available at: https://doi.org/10.1007/0-306-48055-7_6.

‘Cobalt Value Chain Mapping | Cobalt Institute’ (2022), 17 March. Available at: https://www.cobaltinstitute.org/cobalt-sourcing-responsability/cobalt-value-chain/ (Accessed: 12 March 2025).

‘Cobalt-Market-Report-2023’ (no date). Available at: https://www.cobaltinstitute.org/wp-content/uploads/2024/05/Cobalt-Market-Report-2023_FINAL.pdf (Accessed: 12 March 2025).

‘Copper Recovery by Solvent Extraction Techniques - 911Metallurgist’ (2017), 2 February. Available at: https://www.911metallurgist.com/blog/solvent-extraction-techniques-copper-recovery/ (Accessed: 13 March 2025).

Critical raw materials - European Commission (no date). Available at: https://single-market-economy.ec.europa.eu/sectors/raw-materials/areas-specific-interest/critical-raw-materials_en (Accessed: 12 March 2025).

Crundwell, F. (2011) *Extractive Metallurgy of Nickel, Cobalt and Platinum Group Metals*. Elsevier.

Crundwell, F.K., du Preez, N.B. and Knights, B.D.H. (2020) ‘Production of cobalt from copper-cobalt ores on the African Copperbelt – An overview’, *Minerals Engineering*, 156, p. 106450. Available at: https://doi.org/10.1016/j.mineng.2020.106450.

Dai, Q., Kelly, J.C. and Elgowainy, A. (2018) 'Cobalt Life Cycle Analysis Update for the GREET Model'. Available at: https://greet.es.anl.gov/files/update_cobalt.

Das, J. *et al.* (2024) 'The Cobalt Supply Chain and Environmental Life Cycle Impacts of Lithium-Ion Battery Energy Storage Systems', *Sustainability*, 16(5), p. 1910. Available at: https://doi.org/10.3390/su16051910.

Davenport, W.G. *et al.* (2002) 'Chapter 3 - Concentrating Copper Ores', in W.G. Davenport et al. (eds) *Extractive Metallurgy of Copper (Fourth Edition)*. Oxford: Pergamon, pp. 31–55. Available at: https://doi.org/10.1016/B978-008044029-3/50006-X.

Dean, J.A. and Lange, N.A. (1999) *Lange's Handbook of Chemistry*. McGraw-Hill.

Dehaine, Q. *et al.* (2021) 'Geometallurgy of cobalt ores: A review', *Minerals Engineering*, 160, p. 106656. Available at: https://doi.org/10.1016/j.mineng.2020.106656.

Dehaine, Q. *et al.* (2024) 'Flotation of a copper-cobalt sulphide ore: Quantitative insights into the role of mineralogy', *Minerals Engineering*, 218, p. 108958. Available at: https://doi.org/10.1016/j.mineng.2024.108958.

'Electric Vehicle Batteries.pdf' (no date). Available at: https://www.ucs.org/sites/default/files/2021-02/ev-battery-recycling-fact-sheet.pdf?_gl=1*qr3pf2*_gcl_au*MjQ0MjYyNTA0LjE3NDE3ODA2NTM.*_ga*NDE5NjUzNTE4LjE3NDE3ODA2NTM.*_ga_VB9DKE4V36*MTc0MTc4MDY1My4xLjEuMTc0MTc4MDY4NS4yOC4wLjA. (Accessed: 12 March 2025).

'Electrowinning - 911Metallurgist' (2020), 17 November. Available at: https://www.911metallurgist.com/blog/electrowinning/ (Accessed: 13 March 2025).

Emissions Factors 2023 - Data product (no date) *IEA*. Available at: https://www.iea.org/data-and-statistics/data-product/emissions-factors-2023 (Accessed: 12 March 2025).

Farjana, S.H., Huda, N. and Mahmud, M.A.P. (2019) 'Life cycle assessment of cobalt extraction process', *Journal of Sustainable Mining*, 18(3), pp. 150–161. Available at: https://doi.org/10.1016/j.jsm.2019.03.002.

Fazio, S. *et al.* (2018) *Supporting information to the characterisation factors of recommended EF Life Cycle Impact Assessment methods*, *JRC Publications Repository*. Available at: https://doi.org/10.2760/002447.

Forner, E.L., Scheepers, J. and Du Toit, A.J. (2024) 'Copper electrowinning circuit design: Optimized costing as a function of cell arrangement, productivity, rectiformer size, and throughput', *ResearchGate* [Preprint]. Available at: https://www.researchgate.net/publication/329889084_Copper_electrowinning_circuit_design_Optimized_costing_as_a_function_of_cell_arrangement_productivity_rectiformer_size_and_throughput (Accessed: 13 March 2025).

Fraser, R.J. *et al.* (2021) 'Process for producing crystallized metal sulfates'. Available at: https://patents.google.com/patent/US10995014B1/en (Accessed: 12 March 2025).

Fusiek, D. (2023) *Charging up France*. Available at: https://www.eib.org/en/stories/france-gigafactory-lithium-battery-mobility (Accessed: 12 March 2025).

Gaughran, W. (2013) *Inside the DRC's Artisinal Mining Industry*, *Amnesty International USA*. Available at: https://www.amnestyusa.org/updates/inside-the-drcs-artisinal-mining-industry/ (Accessed: 12 March 2025).

Greenwood, M., Wentker, M. and Leker, J. (2021) 'A region-specific raw material and lithium-ion battery criticality methodology with an assessment of NMC cathode technology', *Applied Energy*, 302, p. 117512. Available at: https://doi.org/10.1016/j.apenergy.2021.117512.

Guinee, J.B. (2002) 'Handbook on life cycle assessment operational guide to the ISO standards', *The International Journal of Life Cycle Assessment*, 7(5), pp. 311–313. Available at: https://doi.org/10.1007/BF02978897.

HSC Chemistry (no date) *Metso*. Available at: https://www.metso.com/portfolio/hsc-chemistry/ (Accessed: 13 March 2025).

Huijbregts, M.A.J. *et al.* (2017) 'ReCiPe2016: a harmonised life cycle impact assessment method at midpoint and endpoint level', *The International Journal of Life Cycle Assessment*, 22(2), pp. 138–147. Available at: https://doi.org/10.1007/s11367-016-1246-y.

Kapusta, J.P.T. (2006) 'Cobalt production and markets: A brief overview', *JOM*, 58(10), pp. 33–36. Available at: https://doi.org/10.1007/s11837-006-0198-2.

Kiezebrink & ten Kate (2016) *Responsible Mining: Cobalt*, *SOMO*. Available at: https://www.somo.nl/responsible-mining-cobalt/ (Accessed: 12 March 2025).

Kordesch, K. and Taucher-Mautner, W. (2009) 'CHEMISTRY, ELECTROCHEMISTRY, AND ELECTROCHEMICAL APPLICATIONS | Manganese', in J. Garche (ed.) *Encyclopedia of Electrochemical Power Sources*. Amsterdam: Elsevier, pp. 784–795. Available at: https://doi.org/10.1016/B978-044452745-5.00838-8.

Lantto, C. *et al.* (2022) 'Process for Preparing Battery Grade Metal Sulphate Solutions'.

Lennan, M. and Morgera, E. (2022) 'The Glasgow Climate Conference (COP26)'. Available at: https://doi.org/10.1163/15718085-bja10083.

Mambwe, P. *et al.* (2022a) 'Geometallurgy of Cobalt Black Ores in the Katanga Copperbelt (Ruashi Cu-Co Deposit): A New Proposal for Enhancing Cobalt Recovery', *Minerals*, 12(3), p. 295. Available at: https://doi.org/10.3390/min12030295.

Mambwe, P. *et al.* (2022b) 'Geometallurgy of Cobalt Black Ores in the Katanga Copperbelt (Ruashi Cu-Co Deposit): A New Proposal for Enhancing Cobalt Recovery', *Minerals*, 12(3), p. 295. Available at: https://doi.org/10.3390/min12030295.

Mas-Fons, A. *et al.* (2024) 'Carbon and water footprint of battery-grade lithium from brine and spodumene: A simulation-based LCA', *Journal of Cleaner Production*, 452, p. 142108. Available at: https://doi.org/10.1016/j.jclepro.2024.142108.

'Mathieu Lucien & Mattea Cecilia' (no date). Available at: https://www.transportenvironment.org/uploads/files/2021_02_Battery_raw_materials_report_final.pdf (Accessed: 12 March 2025).

Mizushima, K. *et al.* (1980) ‘LixCoO2 (0<x<-1): A new cathode material for batteries of high energy density’, *Materials Research Bulletin*, 15(6), pp. 783–789. Available at: https://doi.org/10.1016/0025-5408(80)90012-4.

Moats, M., Alagha, L. and Awuah-Offei, K. (2021) ‘Towards resilient and sustainable supply of critical elements from the copper supply chain: A review’, *Journal of Cleaner Production*, 307, p. 127207. Available at: https://doi.org/10.1016/j.jclepro.2021.127207.

Morales-Mendoza, L.F. and Azzaro-Pantel, C. (2017) ‘Bridging LCA data gaps by use of process simulation for energy generation’, *Clean Technologies and Environmental Policy*, 19(5), pp. 1535–1546. Available at: https://doi.org/10.1007/s10098-017-1349-6.

Mpongo, M.K. and Siame, E. (2006) ‘Effect of collector, frother and depressant addition on the copper recovery and concentrate grade of the nchanga underground scavenger circuit of konkola copper mine - Zambia’, *African Journal of Science and Technology*, 7(1). Available at: https://doi.org/10.4314/ajst.v7i1.55186.

Myung, S.-T. *et al.* (2017) ‘Nickel-Rich Layered Cathode Materials for Automotive Lithium-Ion Batteries: Achievements and Perspectives’, *ACS Energy Letters*, 2(1), pp. 196–223. Available at: https://doi.org/10.1021/acsenergylett.6b00594.

Norgate, T. and Haque, N. (2010) ‘Energy and greenhouse gas impacts of mining and mineral processing operations’, *Journal of Cleaner Production*, 18(3), pp. 266–274. Available at: https://doi.org/10.1016/j.jclepro.2009.09.020.

Orion Series Horizontal slurry pumps (no date) *Metso*. Available at: https://www.metso.com/portfolio/orion-series-horizontal-slurry-pumps/ (Accessed: 12 March 2025).

‘Paris Agreement’ (2016) *International Legal Materials*, 55, p. 743.

Rawat, S. *et al.* (2025) ‘Advancements in specialty batteries: Innovations, challenges, and future directions’, *Journal of Alloys and Compounds*, 1020, p. 179387. Available at: https://doi.org/10.1016/j.jallcom.2025.179387.

Reuter, M.A., van Schaik, A. and Gediga, J. (2015) ‘Simulation-based design for resource efficiency of metal production and recycling systems: Cases - copper production and recycling, e-waste (LED lamps) and nickel pig iron’, *The International Journal of Life Cycle Assessment*, 20(5), pp. 671–693. Available at: https://doi.org/10.1007/s11367-015-0860-4.

Rinne, M., Elomaa, H. and Lundström, M. (2021) ‘Life cycle assessment and process simulation of prospective battery-grade cobalt sulfate production from Co-Au ores in Finland’, *The International Journal of Life Cycle Assessment*, 26(11), pp. 2127–2142. Available at: https://doi.org/10.1007/s11367-021-01965-3.

Rinne, M., Elomaa, H. and Lundström, M. (2023) ‘Flowsheet design and environmental impacts of cobalt co-product recovery from complex Au-Co ores’, *Minerals Engineering*, 204, p. 108444. Available at: https://doi.org/10.1016/j.mineng.2023.108444.

‘Roasting Copper Sulfides Chemistry - 911Metallurgist’ (2021), 4 February. Available at: https://www.911metallurgist.com/blog/roasting-copper-sulfides-chemistry/ (Accessed: 13 March 2025).

Savinova, E. *et al.* (2023) ‘Will global cobalt supply meet demand? The geological, mineral processing, production and geographic risk profile of cobalt’, *Resources, Conservation and Recycling*, 190, p. 106855. Available at: https://doi.org/10.1016/j.resconrec.2022.106855.

Scrosati, B., Hassoun, J. and Sun, Y.-K. (2011) ‘Lithium-ion batteries. A look into the future’, *Energy & Environmental Science*, 4(9), pp. 3287–3295. Available at: https://doi.org/10.1039/C1EE01388B.

Segura-Salazar, J., Lima, F.M. and Tavares, L.M. (2019) ‘Life Cycle Assessment in the minerals industry: Current practice, harmonization efforts, and potential improvement through the integration with process simulation’, *Journal of Cleaner Production*, 232, pp. 174–192. Available at: https://doi.org/10.1016/j.jclepro.2019.05.318.

The Paris Agreement | UNFCCC (no date). Available at: https://unfccc.int/process-and-meetings/the-paris-agreement (Accessed: 12 March 2025).

Thoumsin, F.J. and Coussement, R. (1964) ‘Fluid-bed roasting reactions of copper and cobalt sulfide concentrates’, *JOM*, 16(10), pp. 831–834. Available at: https://doi.org/10.1007/BF03378299.

‘Types of Deposits - Cobalt Institute’ (2023), 5 November. Available at: https://www.cobaltinstitute.org/about-cobalt/types-of-deposit/ (Accessed: 12 March 2025).

White, F.M. (2011) *Fluid Mechanics*. McGraw Hill.

Xu, B. *et al.* (2012) ‘Recent progress in cathode materials research for advanced lithium ion batteries’, *Materials Science and Engineering: R: Reports*, 73(5), pp. 51–65. Available at: https://doi.org/10.1016/j.mser.2012.05.003.

‘XVII. On the electricity excited by the mere contact of conducting substances of different kinds. In a letter from Mr. Alexander Volta, F. R. S. Professor of Natural Philosophy in the University of Pavia, to the Rt. Hon. Sir Joseph Banks, Bart. K.B. P. R. S’ (1800) *Philosophical Transactions of the Royal Society of London*, 90, pp. 403–431. Available at: https://doi.org/10.1098/rstl.1800.0018.

Zeng, A. *et al.* (2022) ‘Battery technology and recycling alone will not save the electric mobility transition from future cobalt shortages’, *Nature Communications*, 13(1), p. 1341. Available at: https://doi.org/10.1038/s41467-022-29022-z.

Zhang, J. *et al.* (2022) ‘Semi-batch evaporative crystallization and drying of cobalt sulphate hydrates’, *Hydrometallurgy*, 208, p. 105821. Available at: https://doi.org/10.1016/j.hydromet.2022.105821.

Zhang, T. *et al.* (2021) ‘Cradle-to-gate life cycle assessment of cobalt sulfate production derived from a nickel–copper–cobalt mine in China’, *The International Journal of Life Cycle Assessment*, 26(6), pp. 1198–1210. Available at: https://doi.org/10.1007/s11367-021-01925-x.